NextGEM

Next Generation Integrated Sensing and Analytical System for Monitoring and Assessing Radiofrequency Electromagnetic Field Exposure and Health

D3.5: EMF sensing technologies and measuring equipment - Final version

Document Summary Information

Start Date	01/07/2022	**Duration**	48 months
Project URL	https://www.nextgem.eu/		
Deliverable	D3.5: EMF sensing technologies and measuring equipment - Final version		
Work Package	WP3	**Task**	T3.1
Contractual due date	31/03/2024	**Actual submission date**	31/03/2024
Type	Report	**Dissemination Level**	PU-Public
Lead Beneficiary	THUAS	**Deliverable Editor**	Erdal Korkmaz (THUAS)

This project has received funding from the European Union's Horizon Europe research and innovation programme under the Grant Agreement No 101057527

Contributors and Peer Reviewers

Contributors
Erdal Korkmaz, Sam Aerts, John Bolte, Derek Land (THUAS), Marco Spirito, Richard Coesoij (TUD), Loek Colussi (AT), Maarten Velghe (RIVM), Fulvio Schettino, Marco Donald Migliore (UCAS), Ruben Otin, Eduardo Soudah (CIMNE), Nikolaos Petroulakis, George Stamatakis (FORTH), Stefanos Fafalios (SANL)
Peer Reviewers
Marco Spirito (TUD), Igal Bilik, Yuri Feldman (HUJI), Fulvio Schettino (UCAS)

Revision history (including peer-reviewing and quality control)

Version	Issue Date	Changes	Contributor(s)
v0.1	31/10/2023	Table of Contents provided	Sam Aerts (THUAS)
v0.2	14/11/2023	Sections populated with the Task leaders	Sam Aerts, Erdal Korkmaz (THUAS)
v0.3	28/11/2023	Section defined, assigned and agreed	Erdal Korkmaz (THUAS)
v0.4	18/12/2023	First contributions	All partners
v0.5	06/02/2024	Integration and harmonization	Erdal Korkmaz, Sam Aerts (THUAS)
v0.6	12/03/2024	Second contributions and updates	All partners
v0.7	16/03/2024	Complete version ready for peer review	Erdal Korkmaz (THUAS)
v0.8	25/03/2024	Peer review and comments addressed	Marco Spirito (TUD), Maryse Ledent (SC), Fulvio Schettino (UCAS), Erdal Korkmaz (THUAS)
v0.9	28/03/2024	Technical and quality assurance review and comments addressed	Mats-Olof Mattsson (SPi), Kyriaki Psara (eBOS), Erdal Korkmaz (THUAS)
v1.0	31/03/2024	Final review and submission	Nikolaos Petroulakis (FORTH)

Disclaimer

Copyright message

Table of Contents

List of Figures

List of Tables

Glossary of terms and abbreviations used

Abbreviation / Term	Description
ADC	Analog-to-Digital Convertor
AM	Amplitude Modulation
AWGN	Additive White Gaussian Noise
CI	Confidence Interval
CENELEC	European Committee for Electrotechnical Standardization
CW	Continuous Wave
DANL	Displayed Average Noise Level
dBFS	Decibel Relative to Full Scale
DL	Downlink
DSP	Digital Signal Processor
DTT	Digital Terrestrial Television
DUT	Device Under Test
DVB-T	Digital Video Broadcasting–Terrestrial
EC	European Council
EMF	Electromagnetic Field
FM	Frequency Modulation
FFT	Fast Fourier Transform
GA	Grant Agreement
GTEM	Gigahertz Transverse Electromagnetic
GPS	Global Positioning System
HPM	High Power Microwave
ICNIRP	International Commission on Non-Ionizing Radiation Protection
IEC	International Electrotechnical Commission
IoT	Internet of Things
IQ	In-phase and Quadrature

LNA	Low Noise Amplifier
LUT	Lookup Table
MCU	Microcontroller Unit
NR	New Radio
OATS	Open Area Test Site
OTA	Over the Air
PAPR	Peak to Average Power Ratio
PEM	Personal Exposimeters
PDE	Personal Distributed Exposimeter
RC	Reverberation Chamber
RF	Radiofrequency
RMS	Root Mean Square
RSS	Root Sum of the Squares
RSSI	Received Signal Strength Indicator
RX	Receiving instrument
SA	Spectrum Analyzer
SAR	Specific Absorption Rate
SAW	Surface Acoustic Wave
SBC	Single Board Computer
SCHEER	Scientific Committee on Health, Environmental and Emerging Risks
SDR	Software Defined Radio
SOTA	State of the Art
TDD	Time Division Duplex
T-DRB	Terrestrial Digital Radio Broadcasting
tRMS	true Root Mean Square
TTI	Transmission Time Interval
TX	Transmitting instrument

UE	User Equipment
UL	Uplink
VNA	Vector Network Analyzer
VSG	Vector Signal Generator
WP	Work Package
WSN	Wireless Sensor Network

Executive summary

Deliverable D3.5 provides a comprehensive overview of the state-of-the-art hardware components, the methodologies and the modelling analysis used in the characterization of Electromagnetic Fields (EMF) to quantify the exposure levels to these fields. Hardware devices currently employed in EMF exposure measurement campaigns are grouped into commercially available and lab-built ones to highlight their performance versus portability/cost trade-offs. The various key performance parameters of the instruments and the passive components used in these setups are reviewed and mapped to their different usage cases. The current methodologies used to derive the measurement uncertainties and bias in the exposure assessment are given as a guideline to compare the different experiments and provide a starting point to derive a uniform approach within the consortium to carry out EMF measurement campaigns, i.e., the NextGEM case studies considered in CS3 of WP7. This document is also intended as to provide the key performance metrics of the hardware that will be developed during the NextGEM project in Task 3.3 to support the experimental analysis carried out in the case studies in WP7. Furthermore, some requirements and recommendations for new measurement systems are presented.

1 Introduction

Deliverable D2.2 provided a comprehensive review of the evolution of the exposure patterns across the various telecommunication generations. This provides a basis to understand the requirements of the hardware employed for EMF measurement. This deliverable (D3.5) focuses on the identification and review of the key instruments presented in the literature for measuring 5G EMF exposure. It provides descriptions of the instruments and passive components used in these test benches, categorizing them into commercially available and lab/user-built devices while explaining their mode of operation. Detailed discussions are included on design considerations for lab-built devices at the component level. By presenting this state-of-the-art overview, the document offers insights into the key performance parameters that are considered when developing measurement equipment specifically for 5G exposure assessment such as widely deployable sensing nodes.

Different types of EMF exposure measurement devices can be employed for various purposes, each with its own specific objectives. Moreover, the calibration procedures and the composition of the uncertainty budget are crucial for Radio Frequency (RF) measurement equipment. The total measurement uncertainty is influenced not only by the measurement device itself but also by factors such as methodology, environment, and RF sources.

The document also explores modelling approaches aimed at optimizing the performance of RF-EMF measuring equipment for accurate exposure assessment. These approaches encompass a range of techniques, including computational simulations, statistical models, and numerical algorithms. Their goal is to enhance measurement accuracy, reliability, and sensitivity, ultimately reducing the overall cost of the measurement process. Furthermore, the document presents computational techniques that will be employed in the project to optimize and gain a better understanding of the complex interaction between electromagnetic fields and the human body.

1.1 Mapping NextGEM Outputs

The purpose of this section is to map NextGEM's Grant Agreement (GA) commitments, both within the formal Task description and Deliverable, against the project's respective outputs and work performed.

Table 1: Adherence to NextGEM's GA Tasks and Deliverables Descriptions

TASKS	
Task Number & Title	**Respective extract from formal Task Description**
Task 3.1 - Assessment of EMF sensing technology	The task will provide an overview of the SOTA on the level of assessment of EMF sensing technologies for 5G signals in everyday life. This will help the consortium: 1) to choose off-the-shelf measurement equipment; 2) to identify niches in yet undeveloped measurement devices, like wearables for FR2 bands; 3) to set a list of requirements for the development of new, low cost, stationary, mobile and wearable sensors, either not yet existing or not existing as low-cost types; The requirements for measurement systems regarding the sensitivity and accuracy (systematic and random error) in the resulting measurement uncertainty depends on the technological SOTA and the expected level of signals as assessed in WP2, and measured in T4.4 and the potential health or biological effects (T5.1). The possible measurement uncertainty is important for getting a proper view of the possible internal and external modelling approaches (T3.2). It is also important in the requirements for developing new measurement systems for the FR2 (> 24 GHz) (T3.3) and for modelling and mapping 5G (T3.4). Technological assessment will be performed, it while will be provided a common testing ground facility for results analysis. A comprehensive literature study will be done to support formulating appropriate research questions.
DELIVERABLE	
Deliverable D3.5: EMF sensing technologies and measuring equipment - Final version (M21) This deliverable will provide input for the development of EMF sensor nodes and a basis for choosing of the shelf measurement equipment.	

1.2 Deliverable overview and report structure

Based on the objectives and work carried out under Task 3.1, the document starts with the Executive Summary followed by the introduction of the document in Section 1.

Section 2 is devoted to provide a comprehensive review of the fundamentals of EMF measurements, including the different measurement protocols, exposure guidelines and device specifications.

Section 3 provides a description of the state-of-the-art measurement equipment from high-end commercial equipment to custom-developed sensors and exposimeters. In this session, calibration procedures are also discussed.

Section 4 focuses on different use cases and calibration procedures and discusses the uncertainty budget.

Section 5 provides modelling approaches for the optimization of measurement equipment.

Section 6 is devoted to requirements and recommendations for new measurement systems.

Finally, Section 7 concludes this deliverable.

1.3 Literature base for the presented SOTA

The material presented in this deliverable is based on the information extracted from peer-reviewed scientific literature identified from an extensive search on the following search engines: Scopus, Google Scholar and Web of Science.

A selection of the following keywords has been employed, to identify the main contributions in the years 2018-2023, for the mentioned literature search:

- Frequency identification: FR1, FR2 millimetre wave, mm-wave
- Telecommunication system identification: 5G, fifth generation
- Field definition #1: exposure, human exposure, personal exposure
- Field definition #2: measurement, sense, instrument, device

Table 2 shows an example of the search result for papers which have been classified based on their citation, a set of which form the base reference used in this deliverable.

Table 2: Example showing search results for papers describing methods and test equipment for EMF exposure measurements in the FR2 band.

Search terms	Source	Papers	Cites	Cites/ye...	h	g	hl,norm	hl,annual	hA	acc10
✓ (5g OR fifth generation) AND (e...	Scopus	76	885	177.00	14	28	14	2.80	9	9
✓ (FR2 OR "millimmeter wave" OR...	Google Scholar	133	1699	339.80	19	39	10	2.00	12	17

1.4 Updates from previous Deliverable D3.1 "EMF sensing technologies and measuring equipment - Initial version"

This deliverable (D3.5) is a continuation and an update of the deliverable D3.1. Apart from the updated content in all sections, the following sections are added in this final version of the deliverable.

- The role of spectrum analysers is added in Section 3.1.2.
- Section 6 is a significant addition to this deliverable, offering comprehensive analyses for requirements and recommendations regarding the development of new measurement systems. Commencing with an emphasis on hardware design, it subsequently delves into crucial aspects of uncertainty, followed by addressing data management concerns. A dedicated subsection provides insights into the details of measurement campaigns, followed in a discussion on optimizing processes through modelling.

2 Basics of EMF measurements

This section provides basics of exposure guidelines and measurement protocols, followed by measurement device specifications and fundamentals of calibration and measurement uncertainty.

2.1 Exposure guidelines

The ICNIRP 2020 guidelines for non-ionizing radiation provide the assessment method for the exposure to external electromagnetic fields [1]. These guidelines include basic restrictions for EMF exposure, that are expressed in physical quantities that are related to health effects (i.e., temperature changes or non-thermal effects that are not yet discovered and required the deep study and investigation) of the exposed body (or parts of). These physical quantities are derived from threshold values for health effects, after applying reduction or safety factors to ascertain protection of people. The reduction factors, differentiate between exposure of the general public (factor of 50) and occupational individuals (factor of 10), the latter being aware of potential risks. The basic restrictions are 'translated' into reference levels for electric/magnetic field strength or power density.

The goal of the basic restrictions for high-frequency electromagnetic fields (100 kHz-300 GHz) is to limit the temperature increase to 1° C for the whole body, and to 5° and 2° C, for the limbs and head, respectively (local exposure).

The basic restrictions are expressed using the Specific Absorption Rate (SAR), which has a unit of W/kg and can be calculated from the electric field using Eq.1 (dielectric losses are not considered yet).

$$SAR = \frac{1}{V}\int_{sample} \frac{\sigma(r)|\boldsymbol{E}(r)|^2}{\rho(r)} dr \quad (1)$$

Where σ is the sample electrical conductivity, E is the induced electric field, ρ is the mass density of the object and V is the volume of the body considered. The SAR is a time-averaged quantity and when the considered volume is the whole body the averaging period is 30 minutes, while when local exposure is considered (i.e., 10 g of tissue) the averaging time is 6 minutes.

For local exposure and frequencies between 6 and 300 GHz, the basic restriction is expressed as absorbed power density and is equal to 100 W/m^2 for workers and 20 W/m^2 for the general public. Averaging of the absorbed power density is done over an area of 4 cm^2.

Because basic restrictions are difficult to measure, since they would require a high-precision spatial measurement of the induced field in the body, the guidelines also provide reference levels for electric and magnetic field strength and for incident plane wave power density.

The electric-field strength, power density or energy density values in the tables of the guidelines refer to RMS (Root Mean Square) values. The integration time of the RMS detector can be as high as 30 minutes for whole-body exposure. For local exposure, the average time is 6 minutes or shorter than that.

When performing EMF measurements for compliance assessment (i.e., comparison to the ICNIRP reference levels and/or other, legislative limit levels), it is important to consider the distance between the measurement setup and the radiating source.

In IEC 62232 [2], three source regions around a transmitting antenna are defined:

- source region I is defined as the reactive near field,
- source region II is the radiative near field
- source region III is the far-field region.

In the far-field region, the field has a predominantly plane-wave character and there is a fixed relationship between the electric and the magnetic field (free space impedance of 377 Ω). The distance at which the far field starts is generally considered to be equal to $2D^2/\lambda$, where D is the diameter of the antenna and λ is the wavelength. If the exposure takes place at shorter distances the fixed relationship between the electric and magnetic field is violated and both reference levels should be measured (or alternatively, retreat to the basic restrictions).

Furthermore, the assumption is made that the external field is maximally coupled to the individual. This requires the exposure to be evaluated considering all possible polarizations and propagation directions. To achieve this, the

RMS value of the electric or magnetic field strength of three co-located orthogonal sensors or antenna elements is measured (Figure 1) [2].

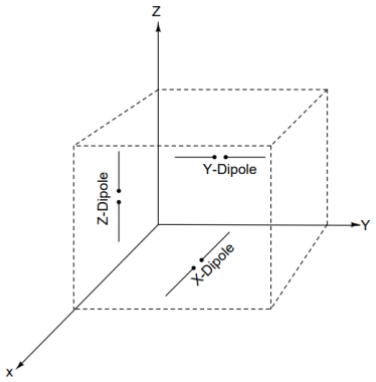

Figure 1: Example of three collocated orthogonal dipole antenna sensors.

2.2 Standardized measurement protocols

In general, government agencies take care of the supervision of the electromagnetic fields generated by users of the frequency spectrum. Within the EU, this is often done by checking compliance with the basic restrictions, set by the 1999/519/EG Council Recommendation on the limitation of exposure of the general public to electromagnetic fields (0 Hz to 300 GHz) [3] and to the Directive 2013/35/EU (workers directive) [4], both of which have been derived from the ICNIRP 1998 guidelines [5]. Although the ICNIRP 2020 guidelines [1] have been issued some time ago, they still have not been adopted by the European Council (EC). Nevertheless, the Scientific Committee on Health, Environmental and Emerging Risks (SCHEER) advised the EC to do so and many agencies already apply the latest guidelines upfront [6].

EMF measurements are done by qualified personnel, applying the European harmonized standards, EN 62232 [2] and EN 50401 [7]. Isotropic measurements shall be done with calibrated instruments according to EN 50383 [8].

Two types of EMF measurements can be carried out: broadband and frequency-selective measurements [10].

In **broadband measurements**, all emissions are integrated within a large spectrum, usually from 100 kHz to 6 GHz, which includes signals from broadcast stations (AM, FM, T-DAB, DVB-T) and mobile phone base stations (2G, 3G, 4G, 5G). Extension of the frequency range of broadband measurements is mandatory, given that 5G will be rolled-out in the future over the millimetre wave spectrum (i.e., FR2 bands). Broadband measurements are done at fixed locations and at a fixed moment in time.

Frequency-selective EMF measurements are done in addition to the broadband measurement if the latter one exceeds a fixed threshold (e.g., 0.1 W/m^2) [9]. With this type of measurement, the incident power density within a specific frequency band can be acquired. Frequency-selective measurements are done at a fixed location and at fixed moment in time.

In order to map the average incident power density to which the body is exposed, according to the ICNIRP 1998 [5] guidelines, the measured values must be averaged over a period of 6 minutes, although, in the ICNIRP 2020 [1] guidelines, a measurement duration of 30 minutes is prescribed. However, in most cases the average incident power density after 6 minutes of measurement will not differ significantly from the value averaged for 30 minutes. For practical reasons, one might restrict the measurement time to 6 minutes, unless the measured exposure exceeds a certain threshold (e.g., 5% value of the ICNIRP guidelines).

In order to perform broadband and frequency-selective EMF measurements, the following points should be considered [11]:

- Avoid own transmission sources nearby (e.g., switch mobile phones to aeroplane mode).
- To avoid assessment of both electric and magnetic field strength, measurements should be done in the far field of the source(s) of emission.
- Use a measurement device on a wooden tripod at 150 cm above street level.
- The measured field value must correspond to the 'undisturbed' field, without human body influence.
- Avoid large conducting objects or surfaces in the vicinity of the measurement device (> 0.5 m distance).
- Be aware of temporal field strength variations that depend on actual traffic.

- The measurement device should use an average or RMS detector and record the data in the preferred unit of W/m2.
- Find the local maximum RMS value of the exposure empirically by applying a quick scan in the area of interest (worst-case exposure).
- Choose a measurement bandwidth larger than the signal(s) of interest, in case of frequency-selective measurements.
- Measure and average for 6 minutes when the exposure is lower than the 5% value of the ICNIRP guidelines.
- Measure and average for 30 minutes when the exposure exceeds the 5% value of the ICNIRP guidelines.
- Measurement results are compared with the limit values, expressed as a percentage of exposure relative to the value of the ICNIRP guidelines.

Figure 2 shows illustrations of measurement equipment that is frequently used for broadband and frequency-selective EMF measurements.

Figure 2: Examples of broadband (left) and frequency-selective (right) EMF measurement equipment.

The uncertainty of the EMF measurement is estimated in compliance with methods described in EN 50383 [8] and EN 50413 [12]. The expanded uncertainty shall not exceed 4 dB with a confidence interval of 95% (expansion factor of 1.96) for frequencies up to 6 GHz. For the uncertainty calculation the method of Root Sum of the Squares (RSS) shall be used. Sources of uncertainty are calibration (antenna, cable, receiver), mismatch and repeatability. For sub-millimetre frequencies, this information will be updated in the final version of this deliverable.

2.3 Non-standardized measurement protocols

In addition to compliance testing (Section 2.2), there are various other purposes for measuring RF-EMFs, such as realistic exposure estimation [13], validation of numerical models [14], comparison of average exposure levels between different geographical areas [15], evolution of exposure levels across time [15], generation of heat maps of exposure levels in a certain area [16], assessing exposure levels by certain parts of the population [17], etc.

For many of these purposes, the measurement method and/or materials used for compliance testing are not the preferred approaches/hardware tools. This is due to (a combination of) different factors such as time consumption, cost of the measurement equipment, and size of the measurement equipment. Often, measurements are needed to either be performed at several (different) locations, or the test subject has to carry a measurement device around without intruding too much in their daily lives, or measurements need to be performed continuously for weeks at locations where devices could be damaged. Therefore, other devices have been developed in addition to high-end commercial instruments. These devices can be grouped into the following categories: a) wearables, b) smartphone apps, and c) (cheaper) sensor nodes.

These devices and the used measurement protocols introduce a higher measurement uncertainty when compared with high-end bench-top test equipment. However, they are designed to collect large amounts of data, and using statistical methods, scientifically relevant conclusions can be drawn. Below we describe the most common non-standardized measurement protocols.

Microenvironmental studies [18], where the goal is to assess personal exposure in certain geographical areas [19]. The areas under study are divided into microenvironments, i.e., small parts of a public area identified by the activity carried out in it, such as:

- Public environment (residential, commercial, industrial, etc.)
- Indoor area (offices, homes, schools, train stations, etc.)
- Public transportation environment (trains, busses, etc.)

The study defines a path through the microenvironment and performs a set of repeated measurements, potentially divided into specific timeslots, by employing wearable devices.

Currently, microenvironmental measurements are only performed in non-user scenarios, and the measured exposure is catalogued as environmental exposure. A representative measurement of the exposure requires at least 15 min of acquisition time [20].

Microenvironmental measurements can be carried out using a variety of means of transport, including drones, cars, bikes etc. Devices used in these campaigns are wearable, can measure across multiple frequency bands and are fast (typically every 3 sec across all frequency bands). Their use is limited to the assessment of environmental exposure (exposure outside of the user's control). A protocol for microenvironmental measurements in 5G NR networks was proposed in [18], including both environmental and auto-induced exposure.

Survey studies, where the goal is to assess personal exposure specific to a certain group of the population [17].

These groups are typically defined by parameters such as age, living area, type of job, etc. From each group, a number of participants are selected and are given a portable and/or wearable measurement device. Other studies have been performed where the participants installed an application on their smartphone, or replaced their smartphone with an alternative one equipped with an application, logging the transmitted power of the device and certain parameters quantifying the connectivity to the network, such as the Received Signal Strength Indicator (RSSI) [21]. The participants have to carry the measurement device with them for a number of days and keep a diary of their activities [22]. Furthermore, the measurement device often tracks GPS data [22]. The main requirements are that participants are randomly selected, representative of their group within the population, and that the sample of participants is large enough [17].

EMF filed logging from sensor networks, with the networks composed of multiple nodes (tens to hundreds of nodes typically) distributed in a (large) geographical area (typically part of a city), e.g., [23], [24].

These nodes can be placed stationary (in public places, indoors outdoors) (fixed network) or on vehicles, such as cars from the postal service [23] (mobile network). Sensor networks collect exposure data over a long period (weeks to years). With these networks, the temporal evolution of exposure levels (in specific frequency bands or overall, i.e., broadband) can be evaluated, exposure heat maps can be created, and numerical models can be validated. Due to the number of devices needed and their vulnerability to damage they are located in public places; these nodes have to be developed in a low-cost fashion.

Spot measurements, those type of measurement can be performed for compliance testing as was described in Section 2.2 but can also be used for non-standardized measurements. As an example, they can be used to validate the numerical tools used to assess the viability of a base station around sensitive places (schools, houses, etc.) [25]. Spot measurements can also be used for more fundamental scientific work such as the development of base stations or new measurement protocols [26]. In the latter case this measurement can resort to high-end laboratory equipment and is thus more labour-intensive, as will be discussed in chapter 3.

2.4 Measurement device specifications, calibration, and measurement uncertainty

As mentioned in Section 2.2 when performing EMF measurements, different devices may be used, depending on the assessment objectives and the corresponding measurement protocol (a comprehensive overview of the types of EMF measurement devices is given in Section 3). However, independently of the method or equipment used, for completeness and acceptance of the reported measurements, the presented data should always be supplemented by a description of the **uncertainty** with which the data is reported**.** Furthermore, common good practices would also include the various uncertainty sources that contribute to the achieved total uncertainty, this individual set of uncertainty sources and their (eventual) correlation takes the name of **uncertainty budget** [27]. This is especially important when the values are close to the reference levels and exposure limits issued by international organizations, such as the International Commission on Non-Ionizing Radiation Protection (ICNIRP), or

standardization bodies, such as the International Electrotechnical Commission (IEC) and the European Committee for Electrotechnical Standardization (CENELEC), or national/regional legislation.

The uncertainty of the reported response depends on specific parameters of the measurement device/setup. In this deliverable, the following specifications of the measuring setup are considered:

- **Antenna(s)**
  - Number of antennas
  - Type (monopole, dipole, patch, or other)
  - Radiation pattern
  - Polarization
  - Operating frequency band(s)
  - Antenna gain (dB)
  - Antenna aperture (m^2)
- **Detector**
  - Amplification level
  - Filter
  - Type (diode, logarithmic, true root-mean-square, or other)
  - Dynamic range (dB)
    - Sensitivity or lower detection limit (dBm, V/m, or W/m^2)
    - Upper detection limit (dBm, V/m, or W/ m^2)
- **Analog-to-Digital Converter (ADC)**
  - Sampling time (s)
  - Resolution (bit) → Resolution (dB, V/m, or W/m^2)
- **Power** supply (mains-powered, solar-powered, battery-powered, or other)
- In case of battery-powered: **autonomy** (h)
- **Output**
  - Quantity (voltage, power, power density, or electric-field strength)
  - Aggregation time (s)
  - Aggregated parameter (minimum, maximum, arithmetic average, geometric average, or other)
  - Logging interval (s)

Several (if not all) factors induce systematic errors. These errors can be resolved by application of correction factors, determined via a number of **calibration** procedures (see Section 4.3). Commercial devices are (or should be) issued with calibration certificates – meaning that correction factors have been determined and are applied when performing measurements – although [28] observed that they are issued per type of device, whereas they should be determined per the individual device.

The remaining random effects continue to cause **measurement uncertainties** (see Section 4.6), some of which are also evaluated during the calibration (and should be listed in the calibration certificates), such as uncertainties due to modulation error or resolution [2], [29]. Furthermore, uncertainties due to anisotropy, linearity and frequency response should be also considered during the calibration. In addition to these uncertainties related to the measurement equipment, the total **uncertainty budget** also contains uncertainties related to measurement circumstances (including environmental parameters, e.g., scattering, reflections, influence of nearby objects and people and measurement method) and post-processing (e.g., spatial averaging).

It is important to mention that all the different uncertainty sources do contribute to the final combined uncertainty. The goal of combining uncertainty is to calculate the total magnitude of uncertainty from a set of independent uncertainty components This process is also known as 'Summation in Quadrature' or 'Root Sum of the Squares'. Finally, the combined uncertainty is expanded (i.e., multiplied by a number greater than 1) to obtain a desired coverage factor, which determines the confidence in the data points within a certain standard deviation value. For instance, assuming a coverage factor of 1, indicates a confidence that 68% of data points lie within one standard deviation, while a coverage factor of 2 means a confidence that 95% of the data points would lie within two standard deviations.

3 State-of-the-art measurement equipment

In this section we introduce various classes of instruments suited for RF-EMF exposure and used in peer reviewed published measurement campaigns. Different classes of instrument will be described, from high-end laboratory instruments to user-developed instrument and sensors. First, a concise explanation of the operational mode of the equipment is provided for different topologies. Subsequently, a table is presented containing the essential performance parameters of each instrument topology, derived from peer-reviewed published papers. These data, together with the design consideration of lab-built devices, see Section 3.4, provides the list of requirements for the development of the new NextGEM sensor nodes in FR1 and FR2 bands to support the use cases carried out in WP7.

3.1 High-end commercial instruments

3.1.1 Frequency scanning and selective instruments

The reference class of instruments used in signal detection, demodulation and evaluation over a large frequency range and bandwidths is the Spectrum Analysers (SA). The SA is a heterodyne receiver architecture which is capable of measuring the magnitude of an input signal versus frequency within the full frequency range of the instrument.

The architecture of SAs, capable of demodulating the input signal, include attenuators, RF filtering, RF downconverter with swept Local Oscillator (LO), providing an IF which is sampled directly by an ADC, instead of a detector, and fed into a Digital Signal Processor (DSP), as can be seen in the simplified block scheme in Figure 3.

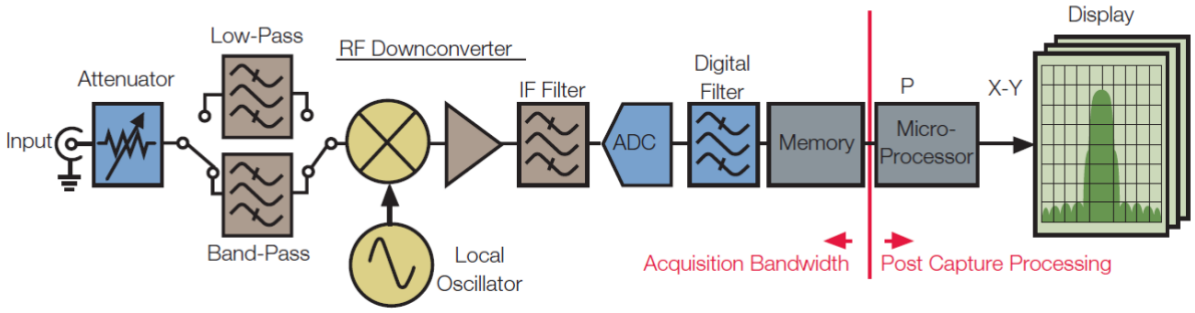

Figure 3: Fundamentals of Real-Time Spectrum Analysis [30].

Spectrum Analysers provide best-in-class performance enabling frequency sweeping coverage up to 85GHz, a sensitivity level exceeding -160 dBm/Hz and provide analysis bandwidth larger then 8GHz [31].

While the SA as an instrument is designed from test and measurement manufacturer as a multipurpose laboratory benchtop box, a similar RF front-end and DSP of the spectrum analyser is embedded by the vendors into a unit customized for in-field campaigns on RF-EMF exposure, namely the network scanners [32]. This device often incorporates multiple channels to scan different frequency bands in parallel. Moreover, network scanners can provide, via advanced software, the capability to switch between a passive scanning mode (mainly listen for periodically sent beacons) to active scanners which can actually request the access point to send a beacon and then listen for a response.

Frequency scanning and selective instruments employed in measurements of RF-EMF exposure

The assessment of RF-EMF exposure for a 5G NR base station using frequency scanning and selective instruments is reported using two methods:

- measure the instantaneous electric-field strength over the channel bandwidth for a certain time and taking the average, the so-called **time-averaged instantaneous exposure (E_{avg})**.
- measure the E-field strength per resource element of the dominant SSB beam. Then, considering the SS/PBCH block transmitting at full power an extrapolation can be determined for the **theoretical maximum exposure (E_{max})** of the base station. An initial study on estimating the parameters F_{TDC} and R which include the effect of TDD and beam sweeping, respectively in estimating the EMF has been

introduced in [33] using the N9020A SA (see deliverable D2.2 for detailed explanation of those parameters). Other measurement campaigns using the SA for FR-1 have been reported in [34]

Both methods are compared in [26], measuring E_{avg} and E_{max} have been performed using a traditional SA (R&S FSV-30) and a tri-axial probe for sub-6 GHz 5G NR.

3.1.2 Spectrum analysers

The role of spectrum analyzers is very important to conduct *in situ* measurements. The evaluation of handled spectrum analyzers such as Rohde Schwarz FSH series (ranging from 9kHz to 4/8/13.6/20 GHz), ZVH series (ranging from 100kHz/3.6/8 GHz) and FPH (ranging from 5kHz to 2(4)/6/13.6(20)/26.5(31)/44GHz) emphasize the enablement of a variety of ranges and capabilities to provide suitable on demand measurements corresponding to the needs of next generation of EMF exposures [35]. Other equivalent equipment with similar to Rohde Swartz capabilities is the Keysight FieldFox Handheld Microwave series (ranging from 30KHz to 6/14/18/26.5/32/44/50/54 GHz) [36] to get frequency coverage up to 54 GHz with precision comparable to benchtop results and make 5G field test a reality with wide analysis bandwidth up to 120 MHz. Other handheld portable devices such as Aaronia Spectran v5 real time analyzer (ranging from 9KHz to 20 GHz) are able to provide measurements and capabilities on different frequency ranges and cost [37]. Those SAs are shown in Figure 4.

Figure 4: Handheld Spectrum Analyzers (i) Rohde Swartz FPH series (ii) Keysight FieldFox series (iii) Aaronia HF series.

3.1.3 Broadband field meters and area monitors

Broadband field meters

A **broadband field meter** coupled with a tri-axial electric-field probe covering a wide frequency range (e.g., hundreds of kHz up to a hundred GHz) forms a compact handheld device to measure the total electric-field strength E or power density S within that frequency range. In most cases, the field measurement result (e.g., the average level E_{avg} during a certain averaging time and/or the minimum and/or maximum values during that time) can be directly read from a display on the field meter. Moreover, state-of-the-art broadband field meters, such as the Narda FieldMan, offer features such as a built-in distance meter, a smartphone app, and a software platform [34], [39].

Most probes, such as the Narda EF-0691 [40], have diode-based sensors, with a non-linear response that depends on the measured signal strength. In this case, the sensor behaves as a RMS detector at low levels—at the diode—and a peak detector at high levels [29]. Other probes have true Root-Mean-Square (tRMS) thermocouple sensors [34], with a true RMS response, but using this type of detector comes at a price: the sensitivity is reduced (e.g., 8 V/m [34]) and the dynamic range is restricted to 30-40 dB. Although it should be noted that for diode-based probes, the dynamic range for the RMS domain is also limited to ~40 dB.

The sensitivity of broadband probes further depends on the type and frequency range but is found to be minimally 0.2 V/m for diode-based probes measuring FR1 (such as the Narda EF-0691 and the WaveControl WPF6, both of which measure in the frequency range 100 kHz to 6 GHz). Older systems, with a typical 100 kHz - 3 GHz range, had a minimum sensitivity of 0.3 V/m [41]. The sensitivity of FR2-capable probes is found to be at least 0.7

V/m, due to their very large frequency ranges (e.g., the Narda EF 9091 [42], which measures the electric-field strength from 100 MHz to 90 GHz).

Broadband probes have also been designed **in-lab**, mostly as small dipoles loaded with a Schottky diode [43], [52] with similar characteristics as commercial probes (i.e., in terms of sensitivity, dynamic range, frequency range). Often, these probes were developed with the goal to implement them into low-cost, small, autonomous measurement devices (sensor nodes) (see Section 3.2).

Area monitors

Closely related to broadband field meters are so-called **area monitors**, such as the Narda AMB series[51] and the Wave Control (MapEM) MonitEM system [52]. Area monitors are designed for fully autonomous operation, often featuring a solar panel, internal battery, wireless connection, and automatic data transfer. Besides a processing unit with data logger, they also consist of interchangeable field probes, which are broadband or tri/quad-band (for separating mobile telephone services). Furthermore, Narda also has a selective area monitor, which monitors up to 20 individually programmable frequency bands and MapEM used to have the INSITE Box.

It should be noted that both Narda and WaveControl also have versions of their area monitors designed to be placed on cars.

The broadband probes specifically designed for area monitors are similar to the ones discussed for field meters (e.g., compare the Narda EP-1B-03 probe with the EF-0691), but the tri/quad-band ones, and also those for the selective area monitors, have a significantly improved sensitivity (in the range 0.01-0.05 V/m).

Measurement uncertainty

The datasheets of commercial equipment list the following parameters:

- Flatness of frequency response
- Linearity deviation
- Isotropic deviation
- Temperature response (not always)

Table 3: Typical uncertainty values for commercial and custom-made broadband field meters and area monitors.

	Commercial	[43], [44]	[48]	[49]
Flatness of frequency response	1 - 5 dB	14.46% (1.2 dB)	2.6 dB	1.5 - 3 dB
Linearity deviation	0.3 - 3 dB	11.13% (0.9 dB)	4.1 dB	1.5 dB
Isotropic deviation	0.3 - 3.8 dB	3.54% (0.3 dB)	1.4 dB	not provided
Temperature response	0 - 1 dB	2.27% (0.2 dB)	0.45 dB	not provided
Modulation error	not provided	10% (0.8 dB) *	not provided	not provided
Crest factor error	not provided	10% (0.8 dB) *	not provided	not provided

* Typical values: BUWAL (Schweizer Bundesamt flir Umwelt, Wald und Landschaft): Mobilfunk-Basisstationen (UMTS -FDD), Messempfehlung, Entwurfvom 17.9.2003. [43].

Estimation of correction factors is indeed mandatory for the three first factors, with calibration based on the measurement of a known electromagnetic field [29].

A comprehensive calculation of the uncertainty budget of broadband field meters was performed in [54], with expanded uncertainties ranging from 2.38 dB *(without linearity)* to 4.40 dB - adding additional uncertainty factors of 0.8 dB to 1 dB for "absolute error" and 0.5 dB - 15% (1.2 dB) for "calibration", obtained from the products' calibration certificates.

In the papers describing lab-built devices, discussion of the uncertainty ranged from "absent"[47] to "fully detailed" [43], [44]. The latter provide expanded uncertainties ranging of 1.9 dB and 2.5 dB - which seems low compared to [54]. An overview of typical uncertainty values can be found in Table 3.

3.2 Custom-developed instrument and sensors

3.2.1 SDR-based sensor nodes

Spectrum analysers (which work in the frequency domain) may be limited due to the trade-off in frequency and time resolution, which makes it difficult to distinguish between different signals sharing the same band at different instances of time, such as 5G-TDD uplink and downlink signals [55] – although this is shown to be possible in e.g. [26]. Time domain instruments such as R**eal-Rime (Spectrum) Analysers** (RT(S)As) and S**oftware-Defined Radios** (SDRs) can overcome this frequency limitation. Of the two, SDRs are compact, portable, and relatively low-cost (compared to SAs and RTAs), which could thus be used in a large-scale (sensor network) deployment.

An SDR is a programmable RF communication system (usable for both transmission and reception of RF signals) that allows physical components such as filters, attenuators and amplifiers, synchronizers, modulators and demodulators, and detectors to be implemented digitally, as close as possible to the antenna [56], [57]. This way, its behaviour relies on software (e.g., using GNU Radio) instead of hardware and its operation and characteristics can be dynamically modified [56].

Examples of SDR-based measurement nodes can be found in e.g., [56] (development of a digital FFT SA), [58] and [59] (broadband field meter), [57] (measurement node for specific frequency bands), [55], and [60] (isotropic broadband field meter).

A digital FFT spectrum analyser was developed using an SDR (24 -1760 MHz, mainly FM and DTT signals) which uses a Single Board Computer (SBC), and SDR software. Using an off-the-shelf SDR (Adalm-Pluto) for 5G NR RF-EMF exposure is tested in [57]. The original Adam Pluto SDR can cover RF analog signals between 325-3800 MHz with a bandwidth of up to 40 MHz. However, the used chipset has a frequency range of 70-6000 MHz, and hence it is possible to "trick" the Adalm-Pluto in its software to operate up to 6 GHz.

Unfortunately, uncertainty analysis is lacking in all of the aforementioned studies.

3.2.2 Hardware-based compact measurement nodes

In recent years, the advent of IoT infrastructure has made it feasible to deploy distributed (wireless) networks of cheaper, low-complexity sensing devices to monitor various environmental parameters, such as temperature, humidity, and air quality, autonomously over a long period. In order to realize accurate spatiotemporal RF-EMF exposure maps with the aid of IoT there is need for a large number of densely-distributed sensors which is not affordable with high-end expensive and relatively large devices. For that reason low-cost (e.g. lower than €300), compact and low-power deployable sensor units are being developed for specific FR1 bands to set up a continuous RF-EMF exposure monitoring system [23], [61]-[63]. A 5G-specific measurement node was developed by [57], [63], [64] measuring in the four frequency bands foreseen to be used in the Netherlands. In Figure 5 some of the lab-built low-cost RF-EMF sensor nodes are shown. The S^{3}R and WAVES sensor nodes use for each frequency band in-house designed narrowband planar half-wavelength dipole antennas, and the low-complexity dosimeter uses a printed PCB monopole antenna probe. All low-cost sensor node antennas are linearly polarized with omnidirectional radiation patterns.

The developed measurement nodes are specific to certain frequency bands (e.g., see Table 4: Frequency bands of sensor nodes for the list of low-cost sensor nodes [23], [61]-[63]). The sensors can generally measure GSM, UMTS, LTE, Wi-Fi, and 5G NR frequency bands for Downlink (DL) communications (except Wi-Fi). By designing sensor nodes usually bandpass filters are used for each band to suppress the signals from adjacent and other interfering bands. Dependent on the desired sensitivity level a Low Noise Amplifier (LNA) can be used to shift the RF power level within the dynamic range of the power detector. Two types of power detectors (the logarithmic type and the RMS type) are generally used to convert the received RF signal into a DC output voltage proportional to the power at sensor input. The log type converts the input RF power into a DC voltage proportional to the log of the input, making the output directly related to decibels. The RMS detector creates a DC output proportional to the RMS value of the signal. The dynamic range of the power detectors are varying typically between 56-70 dB for FR1 frequencies. The dc output is then sampled with an ADC and are converted to power level (dBm) by means of a look-up table in an off-the-shelf microcontroller. The power level can then be converted to E-field (V/m) by means of the antenna factor. Firstly, the power density (W/m^2) is calculated by:

$$S = \frac{4\pi P_r}{\lambda^2 G} \quad (2)$$

in which P_r is the received power (W), λ is the wavelength in free space, and G is the gain of the antenna. Then, the electric field intensity (V/m) can be calculated by:

$$S = \frac{E^2}{\eta_0} \quad (3)$$

where $\eta_0 = 120\pi$ is the free space impedance (Ω).

Personal Exposimeters (PEMs) discussed in Session 3.3 are also widely used for exposure measurements which have large measurement uncertainties and cannot be unobtrusively deployed on the human body. An on-body Personal Distributed Exposimeter (PDE), composed of multiple PEMs is proposed [65]. Each PDE module is integrated on a textile antenna feed plane with patch antennas. The PDE is configured to GSM downlink 925-960 MHz band and the used logarithmic RF power detector has a dynamic range of 80 dB. Similar to the sensor nodes, the design consists of the bandpass filter, RF power detector, ADC and a microcontroller. The PDE antenna and the exposimeter circuit are shown in Figure 6. A similar design for a drone-based measurement system for RF exposure system is used in [66].

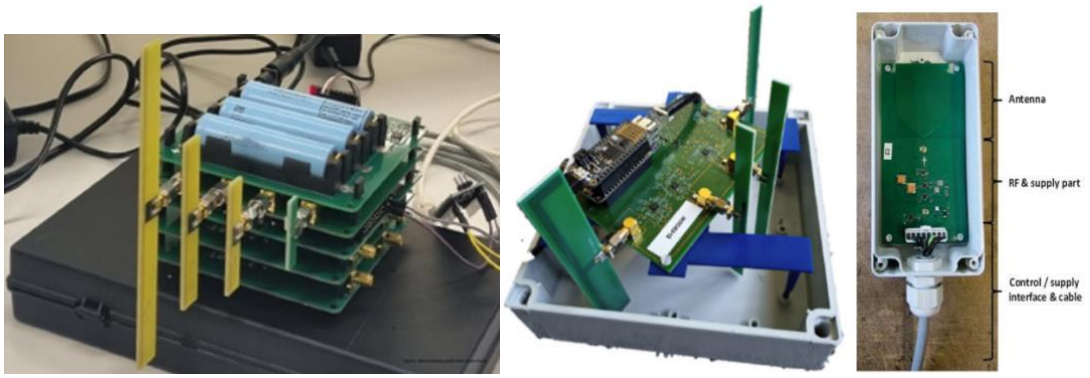

(a) (b) (c)

Figure 5: Low-cost RF-EMF sensor nodes: (a) S³R sensor node [57], (b) WAVES sensor node [57], (c) low-complexity dosimeter [61].

Table 4: Frequency bands of sensor nodes

S³R sensor node	WAVES sensor node	Low-complexity dosimeter
758-788 MHz DL	791-821 MHz DL	925-960 MHz DL
1452-1492 MHz DL	925-960 MHz DL	1805-1880 MHz DL
2110-2170 MHz DL	1805-1880 MHz DL	2110-2170 MHz DL
3450-3750 MHz DL	3550-3700 MHz DL	2400-2483.5 MHz WiFi

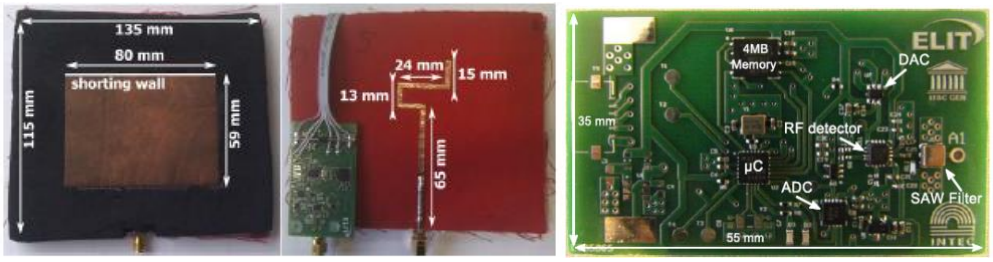

(a) (b)

Figure 6: The PDE module [65] : (a) textile patch antenna top (left) and bottom view (right) (b) top view of the exposimeter circuit.

Similarly, low-cost monitoring Wireless Sensor Network (WSN) systems for a distributed assessment of EMF exposure are proposed in [46], [48] and [50]. The WSN uses broadband probes (three orthogonal dipole antennas, three-axis dipole) each with a diode as a detector to convert the field values to a DC signal which then by means of an ADC and microcontroller converted to power or field values. The WSN is capable to operate between 200-5000 MHz [46].

A "compact exposimeter system" with "similar characteristics to a spectrum analyser, without losing the advantages of conventional exposimeters" was proposed in [66]. This system uses an array of fractal antennas and can measure the EM power in the spectrum 78-6000 GHz with a resolution bandwidth of 300 kHz in multiple narrow bands allowing the identification of different sources of electromagnetic fields. The system has a dynamic range of 90 dB with RF input power from −70 to +20 dBm.

All the proposed EMF sensors are compact, low-cost, and can be used without the need for an expert. The choices of off-the-shelf electronic components on the design of an EMF sensor are discussed in Section 3.4.

3.3 Exposimeters

Exposimeters, or Personal Exposure Meters (PEMs) are small, wearable devices that can be used by trained personel, but can also be used in studies with untrained volunteers [70]. Typically, the devices are used as dead objects, without the need (or often without the possibility) for interaction with body during the measurements. The device is set up before the measurements, and data is collected afterwards. PEMs typically measure in one or multiple radio-frequency bands (ranging from 1 MHz to 6 GHz), which are dedicated to specific technologies. This allows for the separation of exposure from different technologies (WiFi, 2-5G, etc.), and different sources (in certain technologies uplink (user devices) and downlink (base stations) use different frequency bands). Per dedicated frequency band, the electric-field strength E (V/m) or power density S (W/m²) is measured. The sampling rate is often user-defined, with the fast rate typically at 1 – 3 s. PEMs are battery-powered and designed for long measurement sessions ranging from a few hours to a few days up to about one week. The used antennas are: a monopole antenna or sets of multiple monopoles (oriented in different directions to approach isotropy). Commercial devices are available, and different labs have built their own devices for specific use cases.

3.3.1 Commercial exposimeters

Two product lines of commercial devices are most common: the ExpoM-RF series (Fields at Work), and the EME-Spy series (Microwave Vision Group) (the ESM 140 by Maschek Electronik has no new model that measures LTE or other recent technologies). The most recent iterations are the ExpoM-RF 4 [71] and the EME Spy Evolution [72] respectively. The ExpoM-RF 4 measures at up to 25 customizable centre frequencies between 50 MHz and 6 GHz with bandwidths of 35, 75, or 100 MHz. It has 60 dB dynamic range. The maximum measurable field strength can be set from 6 V/m up to 60 V/m at the cost of sensitivity. The sensitivity for 6 V/m is between 0.005 and 0.010 V/m (which varies across different frequencies). The sample interval is user-defined, with the shortest interval being 2 s for 10 bands up to 4 s for 25 bands. The device offers a spectrum analyser mode as well, as opposed to previous versions. The ExpoM-RF 3 measures in 16 fixed frequency bands (based on the occurrence of relevant technologies), with fixed sensitivities, dynamic ranges, and bandwidths [73]. Another critical difference is that this previous iteration only measured with true RMS with an integration time of 0.3 s, while the ExpoM-RF 4 measures both true RMS and envelope peak field strength within a 50 ms time interval simultaneously. How these two measurements are post-processed in one E value, is not mentioned (but might be obtained from the manufacturer). The device uses a tri-axial isotropic antenna.

According to [74], research on measurement uncertainty of PEMs is lacking (although done by e.g., [28], [75]). Major measurement uncertainties are dependent on the measurement scenario and will be discussed in 2.7. However, device-specific measurement uncertainties are often not reported by the manufacturer (neither for lab-built devices). Fields at Work mentions a -40 to -60 dB crosstalk between frequency bands for the ExpoM-RF series. No uncertainty on the isotropy of the antenna, linearity of the field strength, flatness of the frequency response etc is provided. This is the pattern for the devices discussed below as well.

The EME Spy Evolution gives users the choice to monitor up to 20 frequency bands from 80 fixed options (in bandwidth and centre frequency) between 80 MHz and 6 GHz. The dynamic range is 56 dB (up to 6 V/m), with a sensitivity of 0.02 to 0.05 V/m depending on the frequency. The sampling interval is user-defined, with a minimum of 2 s. The detector is not explicitly mentioned. The tri-axial E-field probe has an isotropic uncertainty of +/- 1.5 dB between 80 and 4000 MHz, and +/- 2.5 dB between 4 and 6 GHz. No uncertainty due to crosstalk or other factors is mentioned.

To the knowledge of the authors, there are currently no commercial PEMs available for FR2. Lastly, we should mention that both commercial devices discussed above have a GPS logger, which is not the case for most lab-built PEMs.

3.3.2 Lab-built exposimeters

The Personal Distributed Exposimeter (PDE) was developed as an answer to the measurement uncertainties inherent to measurements with commercial exposimeters due to body-shadowing. It is effectively a vest, with multiple nodes spread across in different pockets. Each node is equipped with a dual-polarized patch antenna and a diode-based RMS detector. It is modular (up to 11 frequency bands) [65], [76]. We should mention that the use-case with untrained volunteers is probably too inconvenient.

A PDE-helmet was piloted in [19]. Based on simulations, the head was identified as the location on the human body where there is the lowest variation of *E*-fields, and thus the lowest measurement uncertainty. So, 4 monopoles were distributed in a bicycle-helmet in different orientations. The device used a diode-based RMS detector. This prototype was only designed for the 900 MHz GSM band.

An exposimeter system with similar characteristics to a spectrum analyser, without losing the advantages of conventional exposimeters was proposed in [69]. This device measures the maximum received power level (using a log detector) in approximately 19000 300-kHz-wide frequency bands between 78 MHz and 6 GHz every second (46.22 μs per frequency point). An array of five fractal antennas (Fractus Antennas, Barcelona, Spain) covers the frequency range. They have a large bandwidth and are small compared to other types of commercial antennas. The system has a dynamic power measurement range of 90 dB with RF input power from −70 to +20 dBm and a 0.04 dB resolution.

There have been only two studies describing the development of a lab-built measurement device for the assessment of RF-EMF exposure at frequencies in the FR2. In [76] and [78], two different versions of a millimetre wave personal exposure meter (mm-PEM), working at 60 GHz, were designed and calibrated.

The first version consisted of a limited number of wearable antennas to be placed on a forearm [76]. The wearable antenna was a microstrip-fed four-patch single-layer antenna array initially developed for use in body area networks (BANs) in [79]. In the second study, the mm-PEM was tested specifically for exposure assessment in indoor diffuse fields [78].

In [76], the following considerations and routes for future work were identified:

- As the mm-PEM uses a power detector, the contributions due to stability issues of feed power and sensor signal should be considered in the calibration.
- At mm-waves frequency band, the calibration of the exposure meter has to be performed for the antenna(s) in the loaded chamber (i.e., with a phantom in the reverberation chamber).
- The actual exposure (i.e., S_{inc}) in a real environment should be in between both (specular [76] and diffuse [78]) estimates. The exact value in a real environment depends on the contribution of specular and diffuse fields.
- Future research includes the design of acquisition nodes (antenna and receiver electronics) for the mm-PEM to measure the IPD directly. Additionally, the calibrations will be performed on a cylindrical or spherical phantom to study the effect of body shadowing on the response of the designed mm-PEM and to design a distributed exposure meter for the mm-waves.

3.4 Design considerations for lab-built devices

Lab-built devices are predominantly used for personal exposure measurements, microenvironmental measurements (on person or vehicle), and stationary (long-term) measurements (sensor networks). In general, the lab-built devices are low-cost, compact and do not require expertise like the one needed for high-end lab devices. In this section the design considerations on the unit level will be further discussed in detail. Typically, the devices comprise a receiver antenna (sensing unit), and a PCB processing unit that houses various electronic components.

3.4.1 Antennas (sensing unit)

In order to meet the dimensions (compact) and low-cost requirements, lab-built devices typically feature simple omnidirectional antennas. In one example from [47], a broadband probe was constructed using a combination of three 30-mm long monopole antennas with a diameter of 1 mm. In [61] and [80], a printed monopole antenna was

directly integrated onto the processing Printed Circuit Board (PCB) unit for a low-complexity dosimeter design. For sensor nodes in [62] and [63], narrowband half-wavelength PCB dipole antennas were developed in-house for four different frequencies. In [69], an array of fractal linearly polarized antennas was used to cover the entire spectrum band. However, polarization mismatch can affect exposure assessment if the polarization of the EMF from the base station is not aligned with the receiver antenna. Addressing this issue, a two cross polarized antenna setup can provide accurate measurements at normal incidence in the far field where the EM field is orthogonal to the propagation direction. In case of using a single-polarized antenna, it should be rotated to ensure correct measurements for different polarizations [81]. In the comparative study of measurement nodes[57], underestimation of single-axis antennas was reported with respect to tri-axial antennas.

The PDE modules described in [65] and [76] utilized linearly polarized patch antennas. These modules were integrated onto a textile antenna feed plane that conforms to the body, with each module featuring a narrowband patch antenna. Four separate nodes of the PDE were distributed at optimal positions over the front and rear sections of the torso of a test person. The same antennas were also installed on a drone in [66].

Typically, narrowband omnidirectional antennas are selected for specific frequency bands. When opting for a broadband antenna, the radiation patterns and gain can vary across different frequencies, necessitating an extensive and sophisticated calibration procedure due to the antenna factor determining the exposed EMF values in V/m.

3.4.2 Processing unit (hardware design)

The processing PCB unit of sensor nodes generally includes bandpass filters, LNA's, RF detectors, ADC and a microcontroller. Each of these individual components will be discussed in further detail in this section.

Filters

To suppress signals from adjacent and interfering bands, bandpass filters are utilized. Two important factors come into play when selecting a bandpass filter. Firstly, the flatness of the bandpass region is crucial. A frequency band is subdivided within telecommunication providers and ripples in the passband could lead to additional errors in EMF assessment. Secondly, the stopband attenuation slope is also a significant factor in filter selection. Surface Acoustic Wave (SAW) filters were used in [62], [64], [65], [66], [76]. The SAW filter chipsets are very compact and internally matched, avoiding the need for additional impedance matching networks. In [66], for instance, a SAW filter with a Central Frequency (CF) of 315 MHz and bandwidth of 300 kHz is used where the received signal is down-converted to this CF. Meanwhile, [62], [64], [65] employed dedicated SAW filters for each considered frequency band, limiting out-of-band responses to at least 23 dB [65].

Low noise amplifiers

The dynamic range of RF detectors is limited by a minimum (sensitivity) and maximum power level. If additional losses are introduced in the design due to the use of different components, the actual dynamic range will be decreased. To address this issue, an LNA can be utilized to shift the RF power level within the dynamic range of the RF detector. However, the choice of LNA is crucial, as the gain flatness can introduce additional measurement errors in the spectrum. Additionally, the impact of noise introduced by the LNA must be thoroughly investigated. In the design of [61], the antenna is followed by an RF switch and connected to an LNA while in [63] the output of the filters is fed to LNA's to amplify the signals between 20-23 dB in order to measure lower signal levels.

RF detectors

In recent years, probes and sensors have been increasingly used based on the "dipole-diode" technology to measure electric fields, and it has become the state-of-the-art for such equipment. However, this technology has a significant drawback of having a nonlinear response that is dependent on the level of the signals being measured. At low levels, it uses RMS detection at the diode, while at high levels, it employs peak detection response. As a result, there is a possibility of significant overestimating the measured RF field. Typically, these devices consist of small antennas (dipoles) directly connected to single or multiple diodes, with an RC network used to flatten the sensor response across the frequency range of operation. For low input power, the output voltages of these devices are proportional to the square of the fields, and consequently to the power density. As the field intensity increases, the response of these devices becomes linear until it reaches saturation. Typically, these devices are sensitive to the signal's peak value, but they provide a value proportional to the effective (RMS) field strength. This technology is suitable for CW signals and not for modulated signals. Measuring a modulated signal using a diode sensor may insert an additional uncertainty that depends on the nature of the modulation and other parameters [29].

At high signal levels, the diode response changes from a square-law to a linear response which can result in spurious modulation. Consequently, when measuring pulsed signals with a low duty cycle, the sensor may indicate a higher value than the actual average level. This issue is particularly significant when measuring radar signals. The probe's

components are designed with high impedance, and the input circuits of the measurement unit have very high gain. As a result, even minor mechanical movements of the probe can cause changes in the reading of the field being measured. Due to this, it is recommended to position the probe in a stable location to minimize the effects of static exposure to fields. The diode detectors are utilized in[48], [49], [50], [57].

A more sophisticated form is the logarithmic detector, as used in [19], [46], [63] , [65], [66] and [76], which utilizes a logarithmic amplifier (log-amp). In this configuration, a cascade of detectors is employed, but the attenuators are replaced by a series of amplifiers. As the signal travels down the gain chain, it eventually reaches a level where the amplifier begins to limit. These amplifiers have precise fixed linear gain and are designed to limit at the same precise level. After the signal has gone into limiting in one of the stages, the limited signal continues down the signal chain, clipping at each stage and maintaining its peak amplitude. The number of amplifiers can be around 10. The RF voltage output of each amplifier is detected to a baseband current using diode detectors. The outputs of the detectors are then summed together to generate a piecewise linear approximation to a logarithmic function, often with an accuracy within 1 dB. The output is a DC voltage that varies over time, and its amplitude corresponds to the peak of the RF voltage amplitude. The dynamic range of this technique is limited by crosstalk between the amplifier stages within the chip, but it can be extended by using two log amps: one driven directly and the other connected to the signal path via an amplifier. Logarithmic amplifiers have an extremely fast response time, typically in the range of 10 ns, and can measure true-peak levels. As a result, they are well-suited for measuring fast transient and pulsed signal measurements, such as those found in High-Power Microwave (HPM) signals.

RF-modulated signals used in modern communication systems often have significant amplitude modulation content, which can result in a large difference between the peak power and average power of the signal. This difference is known as the Peak-to-Average Power Ratio (PAPR) and can be more than 10 dB. While logarithmic amplifiers detect the peak power of a signal, they do not always produce an accurate response. Power detectors based on peak detection can be inaccurate, particularly in applications where true power has to be detected, such as in EMF human exposure measurements and in digital communication systems power control loops. True power or RMS power detectors have been developed to address this issue. RMS detectors provide an accurate measure for the input true power level, and their response is insensitive to the input signal peak-to-average ratio. The RMS value provides the same average power as a dc voltage or current of the same level, and can be expressed in several ways, including time-dependent, peak, or average power. RMS detection is independent of PAPR and is used to measure and control signals with changing PAPR, such as signals caused by transmissions of multiple carriers at varying power levels and by variations in code-domain power in a single code-division multiple access carrier. The simplest theoretical technique for measuring RMS power is thermal detection, but it is difficult and expensive to implement in practice. Other techniques, such as using the exponential relation of a junction or squaring cells, have been implemented in true RMS detectors. These detectors can be used in parallel with log-amp detectors in a 3-D field strength probe. The sensors in [23], [61], [62], [64] utilized true RMS RF power detectors.

Microcontroller Unit (MCU) and Analog-to-Digital Convertor (ADC)

To measure the voltages produced by power detectors, an ADC is utilized. The precision of the measurement system determines the resolution of the ADC required. For instance, achieving a resolution of 0.1 dB across a 70 dB range necessitates 700 discrete points, which mandates a minimum 10-bit ADC resolution. However, it's often the case that the full input range of the ADC is not utilized. In such cases, a 12-bit ADC is better suited, however, by means of oversampling of the signal the effective resolution can be increased and provides more headroom for the ADC's effective number of bits. The noise performance can be improved by configuring the ADC's sample time based on the power detector's rise and fall times.

The choice of microcontroller depends on two main factors: vendor preference and required peripherals. Vendor preference often determines the microcontroller architecture, such as AVR (Microchip), ARM (Microchip, STMicroelectronics, NXP, etc.), or MSP (Texas Instruments). Required peripherals typically include a floating-point unit for calculations (preferably with double-point precision) and communication with the outside world, such as UART or sometimes SPI for interfacing with an SD card. Having the ADC integrated into the microcontroller reduces component count and facilitates integration due to vendor programming examples. For instance, the NXP LPC5504 is a suitable microcontroller based on these requirements. However, it does not include Ethernet, which can be resolved by using an SPI to Ethernet bridge. The LPC5504 features a 16-bit ADC with excellent performance, including built-in linearity and gain-off calibration which is utilized in [63]. For the design in [46] NI USB-6009 an external ADC is used while in [57] MSP430 MCU, in [19], [65] C8051F921 MCU, in [54] ESP32-S2 are used.

3.4.3 Software-defined radio

As mentioned above, an SDR is a programmable RF communication system that allows the physical components detailed in the previous section (filters, attenuators and amplifiers, synchronizers, (de)modulators, and detectors) to be implemented digitally, so its behaviour relies on software instead of hardware and its operation and characteristics can be dynamically modified [56].

There are many commercially available SDRs with different performance and price settings (Table 5). Most of the devices are focusing on GPS or satellite transmission bands but some also incorporate the 5G FR1 frequency bands. Using SDRs in the measurement nodes has the advantage that off-the-shelf hardware can be used which makes it relatively easy to use them in the field. Furthermore, some SDRs (such as the Adalm-Pluto) are small enough to fit in one's pocket and can be controlled from a MATLAB or Python environment [66] and are therefore ideal for a measurement node.

Table 5: Technical specifications of commercially available software-defined radios (SDRs).

SDR	Frequency range	Resolution	Sample rate (MSPS)	Bandwidth (MHz)	Open source?	Cost (€)	Chipset
Adalm-Pluto	325 MHz – 3.8 GHz (70 MHz – 6 GHz with software modification)	12 bit	61.44	20 (56 after software modification)	yes	250	AD9363
USRP E312	70 MHz – 6G Hz	12 bit		56		6000	AD9361
RTL-SDR Blog v3	500 kHz – 1766 MHz 22MHz-2.2GHz	8 bit	3.2	3.2	no	50	RTL2832U
HackRF One	1 MHz – 6 GHz	8 bit	20	20 MHz	yes	370	MAX5864
FreeSRP	70 MHz – 6 GHz	12 bit	61.44	56 MHz	yes	420	AD9364
LimeSDR	100 kHz – 3.8 GHz	12 bit	61.44	56 MHz	yes	300	LMS7002M
BladeRF x44	47 MHz – 6 GHz	12 bit	61.44			420	AD9361
AntSDR E200 (1)	325 MHz - 3.8 GHz	12 bit	61.44	20 MHz	yes	TBD	AD9363
AntSDR E200 (1)	70 MHz - 6 GHz	12 bit	61.44	56 MHz	yes	TBD	AD9361

In the following, we focus on Adalm-Pluto [57]. Detailed information on other SDRs can be found in e.g. [55],[58].

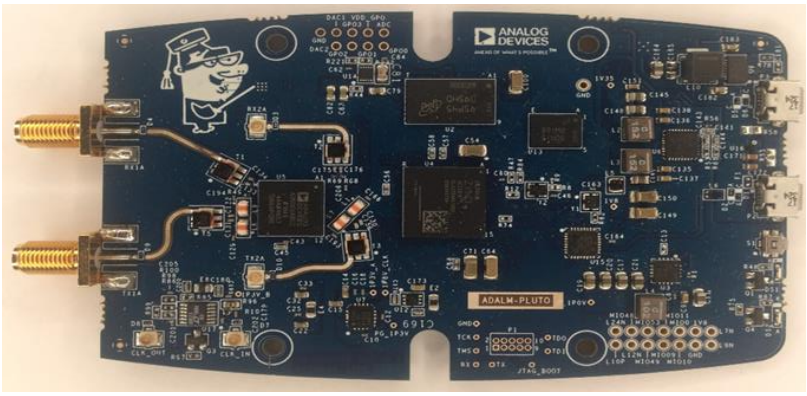

Figure 7: PCB of the Adalm-Pluto from Analogue Devices [67].

Like all SDRs, the Adalm-Pluto can be used as a transmitter (Tx) or receiver (Rx). It has an AD9363 chipset with a nominal frequency range of 325 MHz – 3.8 GHz, but, with a minor tweak, it can be extended to 70 MHz – 6 GHz. This is done by instructing the device to think it has a different (very similar) chip, with extended capabilities. The ADC resolution is 12 bits, its detection limit is -98 dBm, and the dynamic range is over 80 dB [57]. Two antennas can be connected (e.g., in [57], a dual-band JCG401 antenna (with frequency ranges 828–984 MHz and 1710–2170 MHz) and a wideband W5150 antenna (617–6000 MHz).

The Adalm-Pluto can store In-phase and Quadrature (IQ) samples ("in-phase" and "quadrature" refer to two sinusoids that have the same frequency and are 90° out of phase) or, with the software on the device itself, the IQ samples can be converted to another quantity [82]. The output will be dBFS (decibels relative to full scale). With the software, controlled gain settings up to 74.5 dB can be configured. This can be done either manually or with Automatic Gain Control (AGC). With the full-scale change due to the AGC, the device has to be calibrated with a known source to get physically meaningful quantities [55].

4 Use cases, calibration procedures and uncertainty

The various types of measurement devices described in the precious Sections can be used in different ways, each of them with a different objective in mind. The **total measurement uncertainty** depends not only on the measurement device (as described previously) but also on the measurement circumstances (methodology, environment, and sources).

4.1 Use cases

4.1.1 Stationary measurements

When an accurate assessment of the RF-EMF exposure is required (e.g., for compliance assessment), a measurement is performed at one spot at a time, lasting as long as is required by international standards (e.g., ICNIRP, FCC/IEEE) or (national) legislation. The usual equipment of choice here is a spectrum analyser, complete with an electric-field probe and often a laptop [2]. However, broadband probes may also be used for these so-called **spot measurements**, either to get a quick reading of the exposure level or for "sweeping" the area or volume to find the position of maximum exposure [2].

Stationary measurements have the lowest inherent measurement uncertainty since the measurement circumstances can be controlled to a large extent. Using a SA, most often an expanded uncertainty (95% confidence interval) of ±3 dB (including measurement circumstances) can be obtained (e.g., [83] referring to CENELEC). However, [84] estimated it to be ±3.82 dB when "evaluating the RF electromagnetic field exposure levels from cellular base stations" (so including measurement circumstances), although the dominant contributor is the calibration of the measurement device (uncertainty value of 3 dB), which they do not elaborate upon further. Overall, an expanded uncertainty of 4 dB is considered the "industry best practice" [85].

When the experimenter is carrying the measurement device - such as a broadband field meter or portable spectrum analyser (e.g., SRM-3006) in their hands - the influence of the experimenter's body can add to the uncertainty. In [84], the uncertainty value of the body influence was determined to be 0.22 dB at a distance of 1-2 m. A maximum expanded uncertainty of +3.1 / -4.9 dB is reported for the combination Narda SRM-3006 with 3502/01 electric-field probe [86] - although it is uncertain whether this includes measurement circumstances (such as carrying the device).

4.1.2 On-body measurements

When personal, **on-body exposure** assessment is required, personal exposure meters or measurement nodes (or sensors or sensor nodes) are used. These range from exposimeters carried on the hip to (a network of) measurement nodes distributed over the body [87]. On-body measurements can also be translated to in-body exposure, in terms of the specific absorption rate (SAR) [88]. Historically, on-body measurements have been used to assess the exposures in various **microenvironments**, with the devices carried by volunteers or trained experimenters during their everyday activities [18], [70].

When placing measurement devices on the body, the influence of the body may lead, on the one hand, to an underestimation of the exposure through shadowing (if the exposimeter is on the opposite side of the body from the source) and, on the other hand, to an overestimation through constructive interference with waves reflecting off the body (if the exposimeter is in the line of sight of the source) [89]. Besides the need to apply a **body correction factor** - which needs to "be determined individually and per type of microenvironment or activity and are therefore very complex to apply properly" [89], this leads to a high measurement uncertainty (standard uncertainty of 5.3 dB to 12.2 dB [89]). Indeed, to be able to compare or combine personal measurements, even from different units of the same type, systematic biases should be corrected, often by multiplicative correction factors, and measurement uncertainties should be kept to a minimum [89]. To reduce the measurement uncertainty, it was recommended to wear two PEMs on opposite sides of the body (which would lead to an approximately 3-dB reduction) [90] or to use a PEM consisting of multiple antennas/sensors/nodes distributed over the body (also called a "personal distributed exposimeter" or PDE), as proposed in [91]. Furthermore, to specifically assess RF exposure in the head, a PDE-helmet was proposed in [19].

4.1.3 Vehicle-mounted measurements

When the objective is to get a general idea of the distribution of the RF-EMF exposure in extensive geographical areas (or volumes) or to find exposure hotspots, all types of measurement devices may be carried **in or on vehicles**, such as cars [23], [89], [92]-[95] drones [66], [96], [97], and bicycles [19], [98]. This type of measurement is also known as "drive test method" and recommendations can be found in [99].

As with on-body measurements, the position of the measurement device on the vehicle can significantly influence the measurement and an additional **vehicle correction factor** needs to be determined [89], [92].

However, there are (at least) two other factors that affect the measurement result [92]:

(1) the temporal variation of the field strength caused by the signal characteristics (e.g., pulsed signals in 2G-GSM and OFDM modulated signals in 4G-LTE and 5G-NR) or by multipath fading (due to reflections from moving objects); and

(2) in most cases, the three components of the electric field are not measured simultaneously, but successively and then combined. Depending on the sample rate and the vehicle speed, the distance between the measurements of the individual components can be several meters (e.g., 3-4 m in [93]).

4.1.4 Distributed network measurements

Finally, to monitor the RF exposure over time, a **distributed network** of stationary measurement nodes (or sensors or sensor nodes) [23], [100], broadband probes [24], [101], (selective) area monitors [24], or even commercial exposimeters (although only for 24 h) [102] may be distributed over an area of any size. Aspects of remote monitoring are described in [103] - although they are outdated - and recommendations for monitoring of electromagnetic field levels are provided in [104].

Measurement equipment in a distributed sensor network can be installed in various ways: on the rooftops of buildings, on street furniture (street lamps), at a height of approximately 3–4 m from the ground level, on building facades, etc. [23]-[24]. This position (similar to on-body and vehicle-mounted measurements) can significantly influence the measurement (especially when the device is installed close by or on an object such as a wall or street lamp, which also introduces different amounts of shadowing), so for each measurement node **an installation correction factor** should be determined [23], [80]. This factor should not only include the influence of the infrastructure but also the influence of the height, since the exposure is generally assessed at a height of 1.5 m above the ground [2].

4.2 Discussion regarding use in 5G exposure assessment

At the moment of writing this deliverable, four European projects (including NextGEM) are underway in which the RF-EMF exposure in 5G networks (both FR1 and FR2) will be assessed using to-be-developed and/or state-of-the-art measurement equipment [53] and novel or recently revised measurement protocols (standardized [2] or not [18]).

Since the deployment of commercial 5G New Radio (NR) networks (started in 2019), most of the types of devices described above have been used to try and assess the EMF emitted by the new base stations. For 5G-FR1, the same equipment (*if* the range extends to 6 GHz) as for the assessment of the RF-EMF exposure in legacy networks (2G to 4G) can be used - with the exception of a 5G-enabled mobile phone (or user device or user equipment, UE), which is needed to prompt maximum exposure conditions [24] or at least assess auto-induced personal exposure [18]. For 5G-FR2, other probes (for broadband field meters and spectrum analysers) or antennas (for measurement nodes) and other hardware (e.g., harmonic mixers for spectrum analysers) are required.

In order to obtain a comprehensive assessment of the **theoretical worst-case exposures** in 5G NR networks, specialized equipment (spectrum analyser/network scanner) is required, due to the prominent stochastic nature of 5G NR wireless communications (due to "the use of massive, interactive, and agile beam forming and the reduction of the number of signals transmitted independently of the current traffic load and user behaviour" [105]. Indeed, current state-of-the-art techniques - frequency- or code-selective - are based on the extrapolation of the measurement of traffic load-independent signals (such as the SSB), which can only be assessed using this high-end measurement equipment [106]. These techniques have been demonstrated for both FR1 and FR2 (a comprehensive overview can be found in [106]). It should be noted that in the case of FR2, often directive horn antennas are used instead of isotropic probes, to increase the receiver gain and overcome the higher path loss at these high frequencies (and simultaneously minimize the influence of the UE) [81], [107], [108], [109], [110] but not always [111]. When using horn antennas, however, care should be taken to make dual-polarized measurements (either by using a dual-polarized antenna, or by tuning the single-polarized antenna) [81]; or in the case of single-axis omnidirectional antennas [111], the antenna "should be rotated to ensure correct measurements for different polarizations" [81].

However, measuring the RF-EMF in 5G networks **as is** (i.e., without extrapolation) is also done with the other types of measurement devices discussed previously.

Although it was stated in [112] that "diode-detector based probes are not suitable for signals with relatively high power and time variations" and later experimentally shown in [113] for typical 5G-FR1 signals that these probes overestimate ("by tens of percent of the electric-field strength") the amplitude of 5G signals due to their high crest factor, broadband field meters are still recommended to obtain "a reliable assessment of the current total exposure" [2], [105]. Indeed, a number of 5G-FR2 (at 26 GHz and 60 GHz) measurement campaigns have been performed with broadband field meters (with isotropic probes) [108], [114], [115], even though they are also hindered by the sensitivity of the probes (at least 0.7 V/m) and the large bandwidth of the signals [113].

Furthermore, the latest generation of commercial PEMs now also measure the 5G-FR1 bands [116]. However, since the increased importance of auto-induced exposure, however, PEMs alone are not sufficient anymore to assess personal exposure, and additional equipment such as a mobile phone has become necessary [18]. Unfortunately, there is a lack of published data at the moment and the soundness of PEMs measuring 5G-FR1 signals is unknown. Moreover, no commercial exposimeters for the 5G-FR2 band exist yet. In [117], the feasibility of PEMs for mm Waves was discussed, and in [77], [78] two different versions of a mm Wave personal exposure meter (mm-PEM), working at 60 GHz, were designed and calibrated, but they have not been used in the field yet, just as the PDE has also not been adapted to measure 5G-FR1 bands.

The 5G-FR1 bands can also be directly measured by most European measurement networks consisting of area monitors with broadband probes (which measure up to 7-8 GHz) [24] or broadband measurement nodes [24], [49] without any adaptations. However, they do suffer from the same issues as broadband field meters since the used probes also contain diode-based detectors.

And finally, the latest iterations of lab-built measurement nodes either include (some) 5G-FR1 bands [62] or are designed to measure exclusively 5G-FR1 bands [63]. It should be noted that tRMS detectors are the primary choice when designing the nodes [62]. To the authors' knowledge, no 5G-FR2-capable measurement nodes have been developed yet, either commercial or in-lab.

4.3 Calibration procedures

This chapter describes the calibration procedures for RF measurement equipment and the composition of the uncertainty budget. After relating the measurement device's raw response to standard input signals with known amplitude and frequency (Sections 6.2, 6.3.1), according to [28], the following external and internal factors can lead to an over- or underestimation of the exposure level by the RF measurement device:

- Hardware and software
  - absolute error,
  - detection of multiple signals in one band,
  - modulation / duty factor sensitivity,
  - resolution,
  - out of band response (cross talk),
  - flatness (frequency response),
  - linearity,
  - temperature and humidity sensitivity,
  - sampling interval,
  - repeatability,
  - temporal drift;
- Sensing unit
  - anisotropy (horizontal and vertical angle of incidence, and polarization);
- Influence of the body, vehicle, or installation (i.e., shadowing, reflection, and absorption, which are dependent on frequency and polarization) (see Section 4.1);
- Mechanical errors (shock or fall)

By **calibration** of the measurement device for each of these factors, **correction factors** can be determined to nullify the corresponding systematic biases (Sections 6.2, 6.3 and 6.4). However, due to the stochastic nature of both the RF signals that will be measured and of the measurement circumstances, **measurement uncertainties** remain, which are a measure for the remaining (random) differences between the real input signals and the device's responses (after adding the correction factors). These uncertainties have different distributions (e.g., normal, rectangular, triangular, or U-shaped) with different errors in the mean (e.g., calculated by dividing the semi-range by a divisor depending on the distribution). These standard uncertainties are listed in the **uncertainty budget** and then combined using the root sum squared (RSS) method to obtain the combined standard uncertainty (Section 2.4).

Methods for the estimation of the overall uncertainty budget in RF-EMF measurements can be found in e.g., [27], [43], [54], [84], [118], [119], [120] and in combination with calibration in e.g., [2], [28], [29], [12].

In principle, commercial measurement devices - which are issued with calibration certificates reporting the measurement uncertainties - should have no systematic biases left in the measurements [89], so this chapter focuses on lab-built equipment - although the techniques can of course be used to (re)calibrate commercial devices or to check the provided info.

4.3.1 Signals (CW or modulated) used for calibration

The calibration is conducted using test signals, emulating the RF signals expected to find *in-situ*. Newer generations of mobile telecommunications use OFDM-modulated signals with high and variable peak-to-average-power-ratio (PAPR) values (10-20 dB) [112]. Moreover, resources are assigned not only in frequency, but also in time, producing burst-like signals, a measure of which is called the 'duty factor' [28] or 'duty cycle' [112]. Both these factors can induce measurement errors (e.g., because the frame duration is shorter than the rise time of the detector), and calibration of the measurement system should thus involve using complex test signals [112] (e.g., test signals proposed by 3GPP and standardized by ETSI [113],[121]) even more so for measurement devices with diode-based detectors (such as most broadband probes, see above) [45].

The test signal is generated with a calibrated signal generator, at a known frequency and input power. A vector Signal Generator (VSG) is required to generate a complex test signal [28], [58], [59], [113], [122], such as proposed in [121].

4.3.2 Calibration using a direct connection

The test signal can be fed directly to the DUT's RF detector via a cable (e.g., via the DUT's SMA connector [23]. In the case the DUT has several detectors with corresponding connectors, the process is repeated for each of them.

Power response / dynamic range / linearity

Sweeping the generator's input power (in decibel milliwatt or dBm) over a large interval, e.g. [23], [58], results in a corresponding varying voltage response of the RF detector (in volt or V) under test. The voltage versus power response (considering the cable loss) is registered in a Lookup Table (LUT) on the microcontroller, which is then used to translate the voltage measured by the corresponding detector to the received power level (in dBm or in W) [29].

With this measurement, the **dynamic range** (in terms of received power level) can be determined, as well as the deviation from a perfectly linear voltage vs. power response (**linearity uncertainty**) [29].

It should be noted that a calibration framework for SDR-based nodes was proposed in [55], [66], which takes into account the automatic gain control functionality, basically resulting in a LUT with gain and correction values for each specific SDR.

Modulation response

The effect of the modulation of the input signal on the DUT's response should be assessed - e.g., by evaluating the response when using QPSK, 64 QAM, and 256 QAM-modulated signals [113]. This step can also be done over-the-air (OTA) [113], [123]. This step is especially important for diode-based detectors [29].

Frequency response

The frequency of the generated signal may also be swept to check the frequency response of the DUT without sensing unit [55], [58], [60], [122]. However, this can also be done over-the-air (OTA), e.g., [28], [48], [57], so the sensing unit is included in the assessment. (See Section 4.3.3).

Noise level

The Displayed Average Noise Level (DANL) (in dBm) is the noise generated internally by the measurement device and indicates the lowest signal power the device is theoretically able to measure. It is determined with a 50 Ω termination impedance connected to the DUT's RF input [60]. The DANL increases logarithmically with the measured channel bandwidth.

4.3.3 Over-the-air calibration

To calibrate the DUT including its sensing unit (i.e., the antennas), an Over-The-Air (OTA) calibration is performed. OTA calibration of measurement equipment can be carried out in an anechoic chamber e.g. [23], [49],

[57], [78], [66] or Gigahertz Transverse Electromagnetic (GTEM) cell e.g. [28], [57]. If neither is available, OTA calibration can also be performed at an Open Area Test Site (OATS) [43]. Furthermore, if diffuse fields are required (i.e. fields incoming from all directions, which contributions are especially important in indoor environments), calibration measurements can also/further be performed in a reverberation chamber (RC) e.g., [77], [124].

In the case of an anechoic chamber, the test signal is now fed to a calibrated transmitter antenna (Tx) in the chamber that radiates towards the DUT placed in the far field of the Tx. In the case of a GTEM cell (which itself should also have been calibrated), the cell is fed directly with the test signal generated by the signal generator [28], [113].

When it is not feasible to calibrate the device in the lab or if its intended use is significantly different than what it has been calibrated for, it may be necessary to (further) calibrate the device in the field and determine the appropriate (body, vehicle, or installation – see Section 4.1) correction factors. However, body correction factors can also be determined in a large enough anechoic chamber[77], [90], whereas both body [28] and vehicle [89] correction factors can both be determined at an OATS.

OTA calibration can be done by comparison of the DUT's response to a calculation (Method B in [29]) or a reference ("gold standard") measurement of the incident power density S_{inc} or electric-field level E_{in}, performed with a high-end measurement device (Method A in [29]; see Section 3.1) at the DUT position. This reference measurement is repeated for each test (for each signal, each polarization of the Tx, etc.).

Calibration correction factor / absolute error

For commercial devices (e.g., exposimeters [28]) or the use of calibrated antennas e.g., [122], first, a calibration correction factor should be determined, which is defined in [28] as the ratio of the "power of the input signal to the average response".

In the case of a lab-built device, per antenna, the average response (in power) is evaluated against the reference measurement of the radiated signal with a fixed magnitude and frequency. The result of this measurement is the antenna aperture (AA) (in m2), i.e., the ratio of the power received by the DUT (in watt or W) to the incident power density: AA = P/S_{inc}. However, this step can be combined with 6.3.2.2.

Anisotropy

To determine its anisotropy - i.e., the "maximum deviation from the geometric mean of the maximum response and minimum response" [29] due to the varying incident angles of the incoming EMF - the DUT should be rotated in azimuth and elevation. In the case of a single-polarized Tx (e.g., a horn antenna), it is sufficient to rotate the DUT in azimuth and repeat the test for both horizontal and vertical polarizations of the Tx [77]. For this type of calibration, the power is kept constant.

In [28], the uncertainty was calculated as the semi-range (half-width of the response distribution) divided by 1.73 (correcting for a rectangular response), in [48], the maximum deviation in response was used for the uncertainty, and in [29] it was stated that the anisotropy A should be calculated as

$$A = 10 \log\left(\frac{S_{\max}}{\sqrt{S_{\max} S_{\min}}}\right) \text{ [dB]} \quad (4)$$

with S the measured power density.

Body-worn DUT

In the case of a body-worn measurement device, this procedure should be done (to assess the combination of anisotropy and body influence) or repeated (to obtain separate contributions of anisotropy and body influence) with the DUT placed on the test subject (which is then rotated in the azimuthal plane), in order to determine the average response including the body, as well the uncertainty related to wearing the device on the body [28], [91].

Similar to the without-body assessment, by rotating the body in the azimuthal plane and repeating the measurement for two polarizations of the Tx, the average response can be determined (by averaging the measured powers and dividing it by the free-space power) as well as the corresponding confidence (or prediction) interval (e.g., 50% [90], [125] 68%, or 95% [91]).

In [28], the uncertainty related to the body correction factor (defined as "the average of the full circle of angular correction factors") is calculated as "the semi-range of the measurements over all angles of arrival divided by 1.41, correcting for a U-shaped distribution."

This calibration step could/should be repeated for every experimenter or volunteer wearing the measurement device.

Antenna aperture

In [23] (e.g., [77], [91], [125], this method was used to determine per antenna in the DUT the (effective) antenna aperture (AA) (in m^2), i.e., the ratio of the power received by the DUT (in watt or W) to the incident power density S_{inc}:

$$AA = \frac{P}{S_{\text{inc}}} \tag{5}$$

In this case, the median AA (i.e., the median of the distribution of all AA samples) was retained and the spread on the AA (also called the prediction or confidence interval (CI)) was determined, e.g., the 68% CI is calculated as the ratio of the 84th and 16th percentiles of the AA distribution:

$$R_{68} = \frac{AA_{84}}{AA_{16}} \tag{6}$$

Frequency response (flatness)

The frequency response (or flatness) is assessed by measuring the response over the width of the frequency band under test (whether the DUT measures a number of specific frequency bands (e.g., exposimeters [28] or certain measurement nodes [e.g., [57]) or it measures a wide frequency range [48]) - from the lower to the upper bound of the frequency band in steps of e.g., 1 MHz [28].

The flatness uncertainty is calculated in [28] as "the semi-range (...) divided by 1.73, correcting for a rectangular distribution." In [48], the maximum deviation was used.

Linearity

The linearity of the DUT's response is measured by changing the input power of the signal generator and thus the incident power density (e.g., in steps of 50% or 3 dB [28]).

The linearity uncertainty is calculated in [28] as "the semi-range (...) around the ideal response of the step size (e.g., 3 dB) divided by 1.73, correcting for a rectangular distribution. In [48], the maximum deviation was determined.

Repeatability (short term)

The short-term repeatability of the measurements is assessed by repeating the same measurement a number of times (e.g., 10 repetitions [28]). The resulting distribution is assumed to be normal, and the repeatability uncertainty is evaluated as the standard error of the mean of this distribution [28].

Scattering parameters

In the case of a sensor node with multiple probes, the error due to mutual coupling can be tested using a Vector Network Analyzer (VNA) [58].

4.3.4 Environmental conditions (temperature and humidity)

Calibration should be performed within a controlled environment with little or no variation in humidity and temperature [89]. Calibration certificates of commercial devices should state the environmental conditions during the calibration (e.g., the humidity of 70% and temperature of 23 °C [28]) and the potential errors (usually only for temperature) induced when environmental conditions are different.

Unfortunately, to the best of the authors knowledge, none of the calibrations of lab-built devices assessed humidity or temperature errors (this was also stated in [89]). However, it is not unreasonable to say that the effects of environmental conditions on the measurements will be more important for measurement devices made for long-term monitoring, so it is recommended to assess them during calibration (e.g., using a low-cost solution such as in [126]).

Temporal drift

In principle, the above calibration factors are only valid during the calibration measurements. Therefore, if a measurement device is used over a longer period (e.g., months or years), it is of interest to determine the temporal drift, by redoing the calibration measurements at different instances of time during its use (e.g., at the start and the

end of the measurement campaign). This results in **time-dependent correction factors** to be added (after interpolation to the correct time instance) to the measurement results [28], [48].

4.4 In-situ calibration

When it is not feasible to calibrate the device in the lab or if its intended use is significantly different than what it has been calibrated for, it may be necessary to calibrate the device in the field and determine additional correction factors:

Whereas others calibrated body-mounted measurement devices in an anechoic room (see Section 4.3.3), in [28], the **body correction factor** was determined at an open-area test site using a method similar to the one described in Section 4.3.3.

Vehicle correction factors were determined for car-mounted measurement systems in [89] and [92]. In the former, a method similar to the body correction method of [28] was applied: the response was measured by the DUT when rotating the car with respect to a Tx, and the average was compared to a reference measurement at the position of the rotational axis of the car to obtain the correction factor. Conversely, in the latter, the car was not rotated (or it wasn't mentioned) and the results for two Tx polarizations were averaged. In other studies, with vehicle-mounted measurement systems [23], [66], [93], [98], this calibration is missing.

Finally, as far as the authors know, an **installation correction factor** (which accounts for the influence of the DUT mounting position, i.e., due its mounting height and the materials surrounding it) was only determined in [23]. In this study, measurement nodes were placed on building façades (at various heights) and were calibrated through direct comparison to the reference measurement made with a high-end measurement system at ground level. Ideally, the installation correction factor should be averaged over a longer measurement time (e.g., at least 30 min) to account for small-scale fading effects.

In almost all of the studies mentioned in this section, uncertainty assessment of these correction factors is missing.

4.5 Comparison of sensor nodes

A comparison of low-cost sensor nodes both in-lab and in-situ is presented in [57] to evaluate how the sensors perform in a real-life network in the presence of known control signals and with induced traffic on nearby a user equipment. The tested sensors are hardware reliant S³R and WAVES sensor nodes (see Figure 5), and the Adalm-Pluto SDR. As a Benchmark measurement equipment, a R&S FSV30 SA with a tri-axial antenna (Clampco Sistemi AT6000) and Narda SRM3006 portable field strength analyser with a tri-axial antenna (3502/01) are used.

All sensors are firstly calibrated in a Gigahertz Transverse Electro Magnetic (GTEM) cell to determine the calibration factors including antenna gain and transmission line losses and mismatches. The GTEM generates a vertically polarized TEM wave, corresponding to the direction of the antennas on the Devices Under Test (DUTs). The signal source consists of an R&S SGMA vector signal generator that provides a 10 MHz wide Additive White Gaussian Noise (AWGN) signal to mimic the characteristics of real telecom signals. Hence, a frequency sweep was performed that allows in-band and out-of-band downlink exposure measurements by the hardware sensors. In GTEM cell SRM3006 is used as a reference (Figure 8). Eight frequencies in Table 4 belonging to S³R and WAVES sensor nodes are tested. The centre frequencies used for the SDRs are equal to the S³R group sensor. In the GTEM cell, the linearity (agreement of logarithmic slope of the power with respect to reference signal) and sensitivity (lowest sensible field value) were investigated for the three RF-EMF sensors. The field strengths that were used are: 1 V/m; 0.3 V/m; 0.1 V/m; 0.03 V/m and 0.01 V/m such that by each step approximately 10 dB difference is in power. The linearity of all sensors is clearly seen for all frequencies whereas the Waves sensor reaches its sensitivity level at 0.03 V/m value.

Figure 8: The outside and inside of a GTEM cell. Benchmark equipment (SRM3006) inserted in the GTEM cell [57].

Subsequently, contrary to the GTEM testing, only 5G exposure at 3.6 GHz was considered in-situ (in Green Village) to evaluate the performance of the sensor nodes in real life situation. The Green Village on the campus of the Delft University of Technology is an outdoor field lab for sustainable innovation [127]. As such, a 5G NR base station is primarily installed to support various types of innovative projects but may also be used for exposure assessment experiments. In in situ measurements two scenarios are considered. In the first configuration the sensors are placed in line with the base station (vertical configuration, Figure 9 a, b) and in the second configuration the sensors are positioned horizontally with respect to the line of sight of the base station (horizontal configuration, Figure 9 c, d). The sensor nodes are sequentially repositioned to have one measurement per position. A baseline measurement was performed with the FSV-30 setup. However, it must be noted that the FSV-30 remained fixed for the duration of the tests.

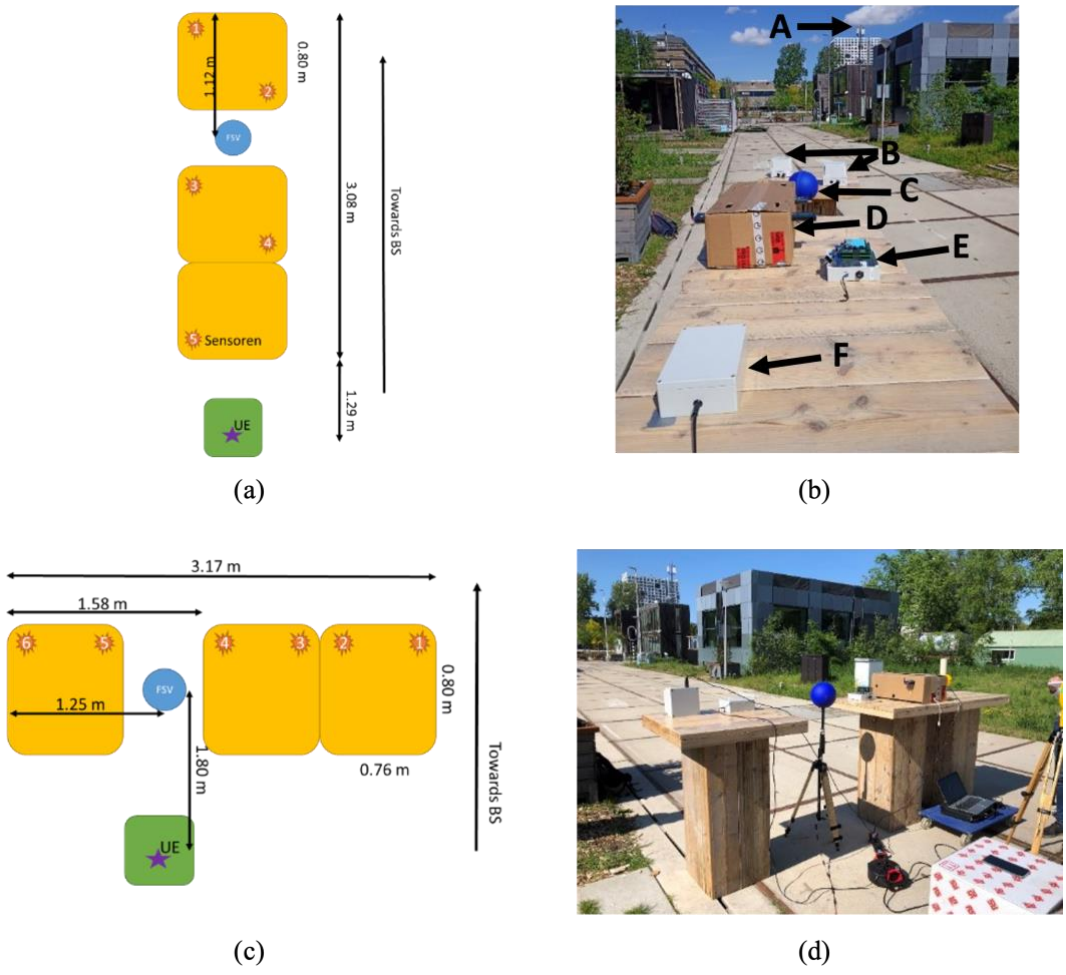

Figure 9: Overview of the in-situ setup. (a) vertical configuration, (b) real-life setup of (a). (c) horizontal configuration, (d) real-life setup of (c). A: Base station antenna; B: WAVES sensors; C: FSV; D: SDRs combined in box (not included in this work due to wrong settings of SDRs); E: S³R sensor; F: SDR sensor [57].

All the conducted measurements did use an active UE (smartphone) present in the sector, directing the beam toward the measurement setup. In-situ measurement results show a maximum deviation from 1.36 dB to 5.26 dB between sensor nodes and the baseline for different sensor positions. The sensor nodes are using a single-axis antenna whereas the reference equipment FSV SA and SRM3006 both are equipped with tri-axial antennas. An underestimation with respect to baseline was expected.

4.6 Uncertainty budget

Finally, the total measurement uncertainty ("combined uncertainty") is calculated, with the individual uncertainty contributions determined during the above calibration steps. Examples of uncertainty budget estimation can be found in [29], [43], [54], [84] and [118]. It should be noted that, although this effort was aimed at systematizing knowledge on the sources of uncertainty in EMF measurement [120], often different values and calculations are reported.

In addition to the uncertainty contributions determined during the above calibration steps, uncertainties due to measurement circumstances (including environmental parameters (e.g., scattering, reflections, influence of nearby objects and people) and measurement method) and post-processing (e.g., spatial averaging [27] can/should be evaluated.

An example of an uncertainty budget is shown in Table 6 [2].

As conventional in measurement science, sources of uncertainty are categorized based on their method of evaluation [128]. Type A evaluation of uncertainty is done using statistical analysis of a series of observations (aleatory or 'random' errors, e.g., repeatability uncertainty), whereas Type B evaluation is carried out using other, non-statistical methods ('epistemic' or 'systematic' errors).

Type A uncertainty relates to phenomena that can be evaluated by a statistical analysis of the measured quantity and in a given set of environment conditions can be related to some of the performance metrics of the measurement devices.

Type B uncertainty is instead due to the presence of systematic error and can be described as originating from standard methods and calibration procedures. For this reason, is important to note, as was discussed in [28], that in non-standardized measurement protocols four key factors influence the measurement uncertainty of wearable devices: mechanical errors, the measurement process due to hardware of software filters, the anisotropy effect, and influence of the body (shadowing, absorption, and reflection).

However, independent from their classification, all uncertainty components are expressed in terms of **standard uncertainties**, based on their associated probability distribution (e.g., normal, rectangular, U-shaped, or triangular), and summed (using a Root Sum Square (RSS), under the assumption that the individual errors are statistically independent and thus unlikely to occur simultaneously) to obtain the **combined standard uncertainty u_c** (Table 6). Then, in order to "encompass a large fraction of the distribution of values that could reasonably be attributed to the measured quantity" [84], a "coverage factor" k is added as a multiplier, and the **expanded uncertainty U** is obtained. Usually, $k = 2$, which corresponds to a 95% confidence interval (Table 6).

It should be noted that, when combining uncertainties in dB and %, the following conversion should be used [118]:

$$X\,[\mathrm{dB}] = 10\log\left(\frac{x\%}{100} + 1\right) \tag{7}$$

$$x\% = \left(10^{\frac{X\,[\mathrm{dB}]}{20}} - 1\right) \cdot 100 \tag{8}$$

Finally, in [27], [129] and [130] it is stated that exposure levels with a relative uncertainty less than ± 3 dB can be directly compared, whereas in [85] it is stated that "the target expanded uncertainty for in-situ field measurements should be 4 dB or below, which is considered industry best practice. The expanded uncertainty for the RF exposure evaluation used for in-situ field measurements should not exceed 6 dB."

Table 6: Example template for estimating the expanded uncertainty of an in-situ field strength measurement that used a frequency selective equipment [2].

Source of uncertainty (influence quantity)	Unit	Prob. distrib. type	Uncertainty or semi span a	Divisor δ	Sens. coeff. c	Standard uncertainty $u = a/\delta$	Corr. fact. CF	$c^2 \cdot u^2$
Measurement equipment								
Calibration of the meter (or spectrum analyser)	dB	normal		1,96	1			
Calibration of the antenna factor	dB	normal		1,96	1			
Calibration of the cable attenuation	dB	normal		1,96	1			
Combined frequency response of the meter/cable/antenna	dB	rect.		√3	1			
Combined linearity deviation of the meter/cable/antenna	dB	rect.		√3	1			
Isotropy of the antenna	dB	rect.		√3	1			
Combined temperature and humidity response of meter/cable/antenna	dB	rect.		√3	1			
Mismatch between antenna and meter/ spectrum analyser	dB	U-shape		√2	1			
Methodology								
Probe position in high field gradients	dB	rect.		√3	1			
Field scattering from surveyor's body	dB	rect.		√3	1			
Mutual coupling between measurement antenna or isotropic probe and object	dB	rect.		√3	1			
Meter reading error of fluctuating signals	dB	triang.		√6	1			
Source and environment								
Variation in the power of the RF source from the nominal level	dB	rect.		√3	1			
Field reflections from movable large objects near the source during measurement	dB	rect.		√3	1			
Scattering from nearby objects and the ground	dB	rect.		√3	1			
Combined correction factor, $CF_c = \sum_{i=1}^{N} CF_i$								N/A
Combined standard uncertainty, $u_c = \sqrt{\sum_{i=1}^{N} (c_i^2 \cdot u_i^2)}$								
Coverage factor for required (e.g. 95 %) confidence interval, k								
Expanded uncertainty, $U = k \cdot u_c$								

NOTE 1 The value of divisor δ for normal probability distribution is for 95 % confidence.

NOTE 2 See Annex E for guidance on the variables in this table.

NOTE 3 This table is under the assumption that the logarithmic expression of the measured quantities can be similarly treated to that of the linear expression in view of statistical properties.

5 Modelling approaches for optimization of measuring equipment

In recent decades, cellular technology has remarkably advanced, driven by the constant demand for improved utilization of the electromagnetic spectrum. This pursuit has resulted in the establishment of increasingly sophisticated standards that leverage MIMO (Multiple Input Multiple Output) techniques to exploit spatial resources within communication channels efficiently. Additionally, novel frequency bands, including the FR2 band commonly called the "millimetre wave" band, have emerged, presenting new opportunities for cellular communication systems.

However, these technological advancements also bring new challenges for developing reliable systems, designed to monitor and control RF-EMF exposure.

In this context, modelling approaches have gained significant attention as valuable tools for optimizing measuring equipment performance in RF-EMF exposure assessment. These approaches encompass a range of techniques, such as computational simulations, statistical models, and numerical algorithms, which aim to improve measurement accuracy, reliability, and sensitivity, ultimately reducing the cost of the measurement process.

The objective of this section is to identify methods that allow optimization of the performance of measurement equipment and reduce the cost of measurement, with particular attention to 5G communication systems that use new technologies compared to previous systems, such as massive MIMO antennas, and new frequencies, such as millimetre waves. Subsequently, the computational techniques will be presented that will be used during the project to help in the optimization and understanding of the complex interaction between EM fields and the human body.

5.1 Modelling approaches for equipment optimization measuring 5G base station radiated field

The realization of simulations is a well-known and widely used practice to help engineers design and optimize systems. In the framework of measurement of the field level for human exposure assessment, simulations allow for optimization of the measurement procedure and help identify the requirements for the measurement equipment by enucleating the effects of the different parameters on the systems.

Numerical simulation is particularly useful in 5G, which presents some peculiar problems compared to the previous generation of cellular systems technology [105], [131].

In particular, using antenna arrays at the base station, with several radiating elements in Massive MIMO (MaMIMO) operating mode, requires evaluating the field levels resulting from several different patterns of variable shape and pointing direction that can be alternatively used by the Base Station (BS). Moreover, the use of these radiation patterns is time-dependent, according to the number and distribution of active users in the coverage area, making it challenging to identify the most suitable measuring conditions to characterize the field levels in the environment correctly. The pattern variability mixes with the classical problems of field-level measurement systems that regard the identification of the most suitable measurement positions and the choice of the most effective measurement chain, considering the cost of equipment and time.

Because of the mentioned peculiarities of 5G systems, the most suitable approach for the realization of electromagnetic simulations is using ray-tracing/ray-launching approaches [105], [132]. These approaches can be employed to simulate indoor [133] and outdoor environments [134]. Numerical simulations allow a full analysis of the distribution of the field in the environment in actual working conditions of the systems [135]. An example of field-level simulation using ray-tracing is shown in Figure 10.

In particular, numerical simulations help in the following:

- understanding the spatial variability of the field and identifying critical areas where to perform measurements
- defining the required sensitivity level to achieve an accurate measurement
- optimizing the number of measurement points
- identifying the most appropriate instrumentation

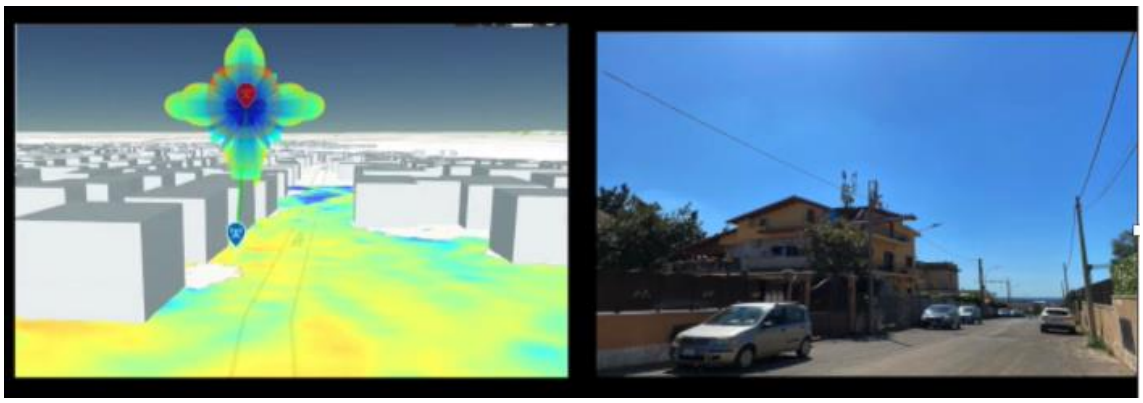

Figure 10: Numerical simulation of the field distribution using ray-tracing in false colours (left), actual environment (right).

An important feature of the numerical simulations is that they allow evaluation of the field levels resulting from using the different patterns of MaMIMO 5G antennas, as shown in Figure 11. In MaMIMO beamforming schemes, the actually employed radiation patterns depend not only on the specific channel realization but also on the number and distribution of the users within the coverage area. Consequently, the use of these radiation patterns is time-dependent, according to the number and distribution of active users in the coverage area. Regarding the above-mentioned problems, numerical simulations and analytical methods are precious tools to analyse the effect of the dynamic use of the patterns in 5G systems, allowing to optimize measurements and reducing the overall cost of the instrumentation and of the measurement itself.

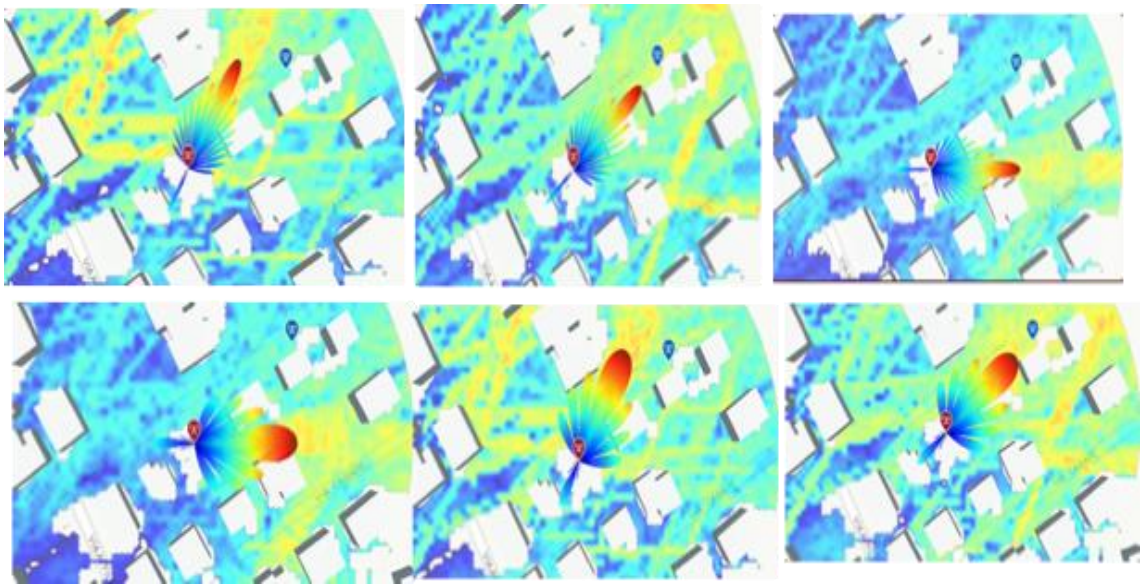

Figure 11: MaMIMO antennas used in 5G can generate different patterns with different characteristics and directions. Numerical simulation allows for estimating the field radiated by the set of patterns.

One of the main issues that could arise in evaluating the power levels is the use of radiation patterns of the antennas as they were employed in fixed-beam systems: this could lead to an overestimation of the power levels. In [136] a time-averaged approach is used to overcome this issue, and in [137], a simple method for the calculation of a power reduction factor is proposed. In [138], the analysis of the time-averaged power reported by angular-power monitoring counters is suggested as a methodology to quantify a spatial power reduction factor, while in [139], a statistical analysis is performed to achieve a similar task. Also, approaches like the one described [140] that consider a Normalized Average Power Pattern (NAPP) can be particularly beneficial in accurately evaluating the realistic power levels within the coverage area.

Simulations can also be used to improve the post-processing of measured data. In [141], the authors propose to measure the field level over a limited number of points at the street level in the city and to transmit them to an operative control centre, where the field values all over the city can be interpolated in real-time. Another possibility could be the use of surrogate models [142], which could be used for obtaining information about the field levels in areas not directly covered by the measurements campaign, or the use of artificial intelligence [143] to achieve a satisfactory reconstruction of the field levels. Finally, the realization of simulations with the Monte Carlo approach

[144], or similar ones, can help evaluate the impact of uncertainties on the measured data, eventually identifying and correcting the presence of biases in system modelling [145].

5.2 Numerical modelling of EMF exposure and human body interaction

To help in the modelling and optimization of the measurement equipment, CIMNE will provide numerical simulations of some of the experimental set-ups. For example, to calculate the optimal location of detectors on a human body we simulated with ERMES [146] the maximum electric field under different plane wave illuminations (Figure 12, Figure 13 and Figure 14):

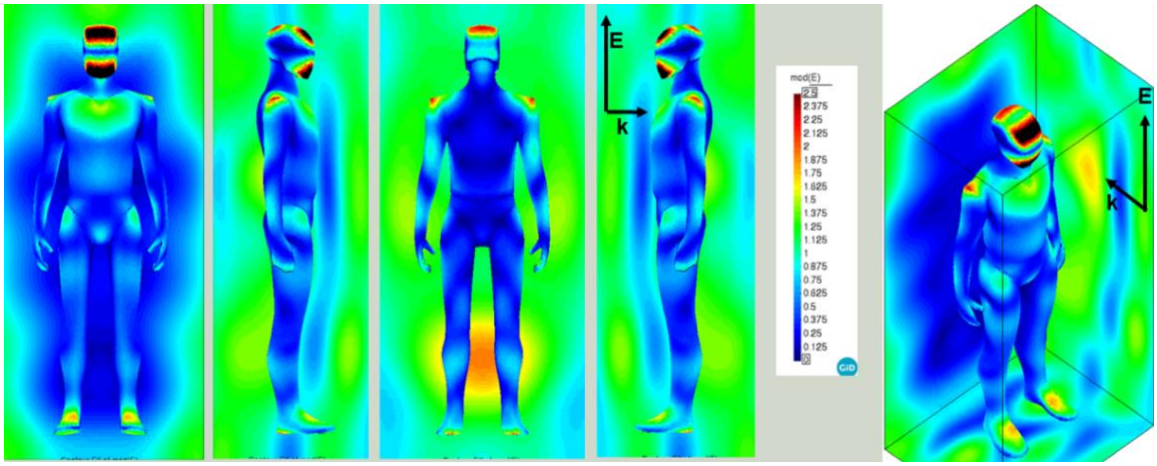

Figure 12: Plane wave illumination at 700Mz. Vertical polarization. External electric field.

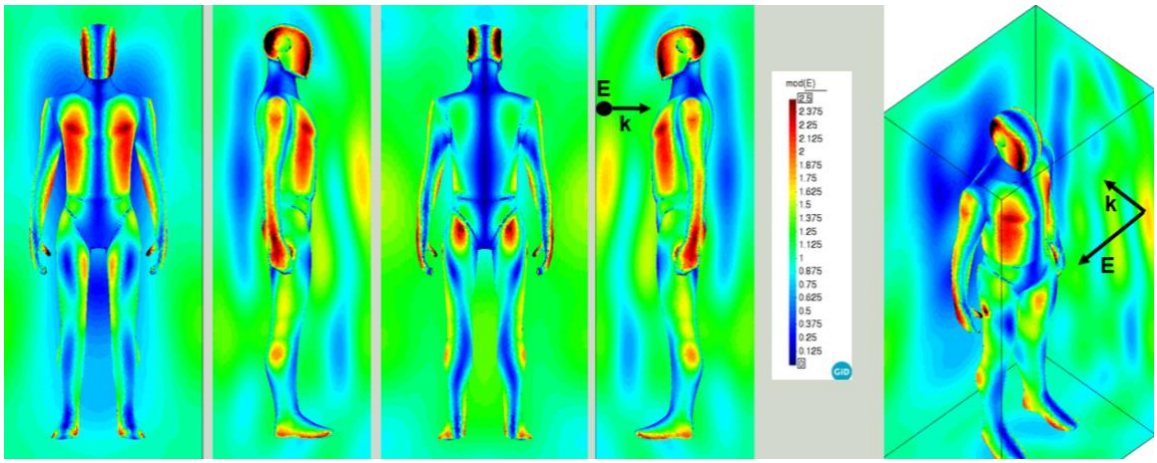

Figure 13: Plane wave illumination at 700Mz. Horizontal polarization. External electric field

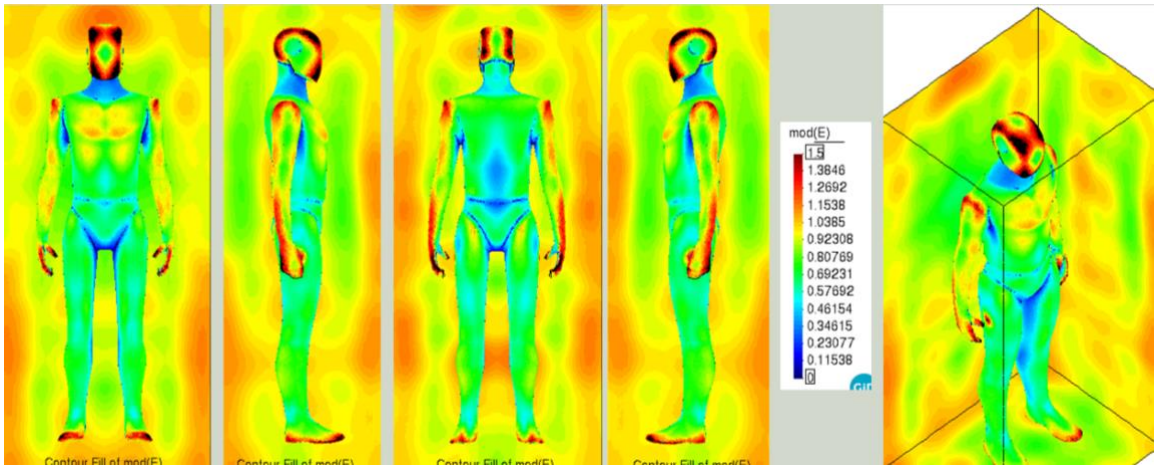

Figure 14: Average external electric field for all simulated directions and polarizations at 700 MHz.

From these figures we can conclude that the best location of the detectors for 700 MHz will be the head and shoulders for an undefined direction of the illuminating field. For specific polarizations and wave vectors we can check that particular simulation. Also, numerical simulations can help in the visualization of the fields inside the human body which are difficult to measure directly and that can be very different from the external fields due to the discontinuity of the fields when changing media. As an example, we can see in Figure 15 and Figure 16 how different the internal fields are compared with the externals shown in Figure 12 and Figure 13:

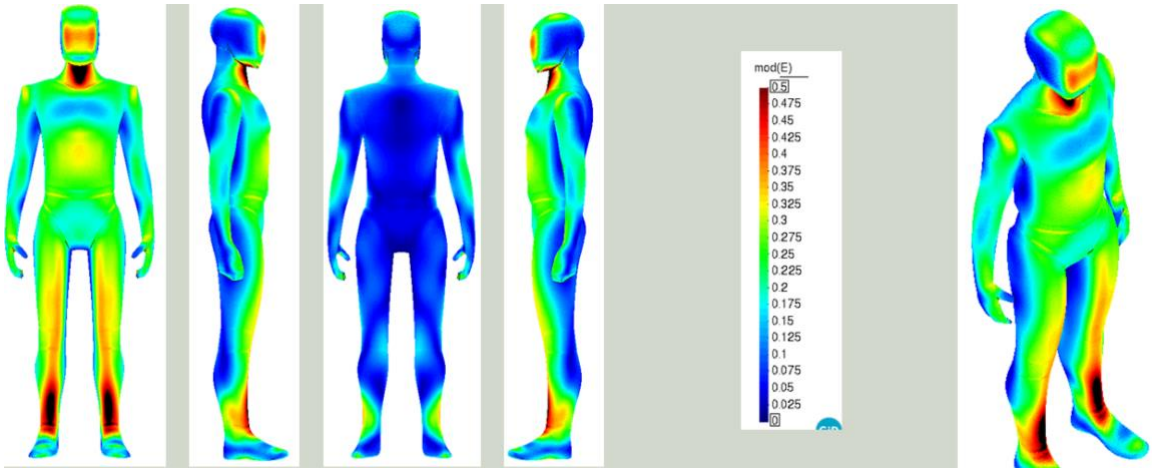

Figure 15: Internal electric field induced by the vertically polarized plane wave at 700Mz showed in Figure 12.

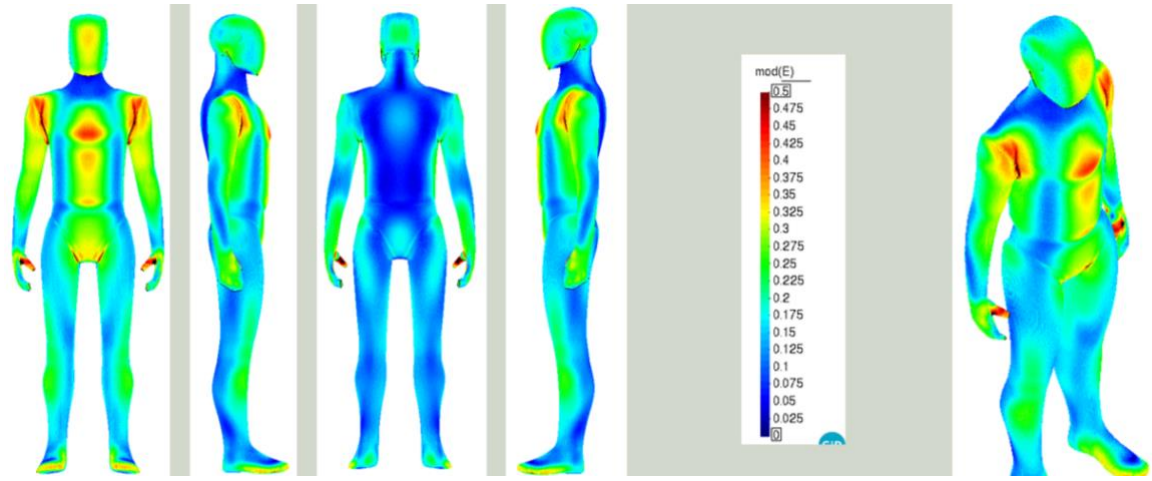

Figure 16: Internal electric field induced by the horizontally polarized plane wave at 700Mz showed in Figure 13.

More simulations, for different frequencies and geometries are expected during the project. There will be simulations focused on specific areas or vulnerable organs, computing fields, SAR and any other magnitude derived from the EM fields that will be of interest for the project.

6 Requirements & Recommendations for new measurement systems

6.1 Hardware design

The design considerations for the innovative measurement systems to be used during the NextGEM project are based on a set of requirements that depend on the specific goal(s) of the measurements (see Section 4.1).

The main questions are:

- How will the device be used?
- Which frequency band(s) (centre frequency + bandwidth) will be measured?
- What is the minimum refresh rate of the acquisition?
- What range of exposure levels will be encountered?
- What is the required level of accuracy?
- What level of autonomy (and for how long) should the device have?
- How much can the device cost?

The various choices available for antennas, filters, low-noise amplifiers, detectors, microcontroller units, and analogue-to-digital convertors have been discussed in detail in Section 3.4, as well as the available software-defined radio platforms, but this Section focuses on the recommendations for specific purposes.

6.1.1 Computing/processing unit

Although many lab-built devices have been built around a customized PCB, the use of SDRs in RF-EMF exposure assessment has seen a noticeable increase recently (e.g., [147]). With the availability of open-source (GNU Radio) or ready-to-use software packages (e.g., Maia SDR [148], these low-cost devices can be easily programmed and finetuned for specific objectives.

A customized PCB, on the other hand, comprises one or more bandpass filters, LNAs, power detectors, ADCs, and a microcontroller that have been selected upon beforehand to fit the requirements and cannot be changed afterwards, i.e., during the measurement campaign.

6.1.2 Detector

Due to the significant PAPR of modern wireless signals (> 20 dB for OFDM-modulated signals), true RMS detectors should be used in order to evaluate the correct RMS exposure levels.

6.1.3 Sampling rate

In [104], a sampling rate of at least one per second was recommended. However, ideally, the *acquisition* sampling rate of the measurement device should be high enough such that the *stored data* sample rate returns an accurate RMS exposure level at OFDM symbol [26] or Transmission Time Interval (TTI) level of the signals under test. For example, in [147], samples were obtained every 0.5 ms, as averages of 10,000 samples taken at the internal sampling rate of 20 MHz. This way, a 5G NR signal with a Subcarrier Spacing (SCS) of 30 kHz (which indeed has a TTI of 0.5 ms) can be accurately assessed.

However, if hardware, software, or storage constraints inhibit such high-speed sampling, an internal sampling time equal or less than the TTI is recommended, in order to not miss any transmissions. For the same example, an internal sampling rate of 2 kHz would then be sufficient and averaging over 1,000 samples (for an external sampling rate of 1 Hz) would smoothen the influence of the PAPR on the measurement results. In this case, it would also be informative to – next to the average and possibly minimum and maximum values – also report the ratio of samples above the noise level, i.e., the *duty cycle*. This value is important for compliance assessment in the latest- and next-generation mobile networks [2], [136][149].

6.1.4 Monoaxial, triaxial, single polarization, dual polarization?

For accurate exposure level assessment, the total electric field strength should be measured. This means that the three orthogonal field components should be measured, *ideally at the same time*. To collect simultaneous samples, multichannel ADCs are available. Also, more expensive SDRs such as USRP have this capability.

To obtain quasi-isotropy, usually three orthogonal dipoles are used (e.g., [49], [147]). However, if the measurement objective is to assess the evolution of the exposure level over time, a vertically polarized mono- [23] or dipole [57] can be sufficient (an additional correction factor to get the total field level can be obtained through a calibration measurement, if required).

6.1.5 Sensitivity

The combination of the antenna, filter, LNA, and detector determines the range of exposure levels that can be measured. The dynamic range of the detector is the limiting factor. Remember that the ICNIRP reference level for the general public for a frequency of 3.5 GHz is 10 W/m² (61.4 V/m). With a dynamic range of 60 dB (typical for a true RMS detector at this frequency), the device measurement sensitivity is at best 10 μW/m² (0.06 V/m). Thus, if it is an a-priori requirement that higher levels should be measurable (e.g., up to 50 W/m², the occupational reference level), attenuation of the received signal can be employed at the expense of a reduction of the sensitivity to ~0.14 V/m [150].

6.1.6 Time synchronization

In case the measurement device consists of multiple sensor nodes, the time stamps of the nodes should be synchronized, e.g., by equipping them with a 24.576 MHz crystal and achieving synchronization via a PC clock before starting the measurements [65], or they can have their own Real-Time Clock (RTC). However, if the nodes are each connected to a central (data storage) system (e.g., in a distributed sensor network), synchronization is more trivial.

6.1.7 Location tracking

In case location data is required, e.g., for microenvironmental or mobile measurements (described above), the inclusion of a Global Navigation Satellite System (GNSS) module is essential, whether in the measurement device itself or coupled to it. This module should sample as fast as the measurement device (i.e., the external sample rate, since the internal sample rate can be much faster). Current GNSS modules (even low-cost ones) achieve sampling times of 0.1 s or less [151]. At a sampling rate of 10 Hz, a maximum speed of 180 km/h would be allowed to stay within a 5-m distance between samples [99]. Furthermore, even though the positioning uncertainty of GNSS modules has improved (due to the availability of more satellites and the use of lower frequencies) [152], it may be necessary to map the coordinates to the (correct/most probable) route during post-processing of the data [23], especially when sampling relatively faster [151].

6.1.8 Data transfer

The easiest way to store and retrieve the measurement data is to use an on-device storage solution that can be read after the measurements (e.g., an SD card). However, if the device is designed to work autonomously or if the data is to be analysed (and visualized) on-the-go, the data should be transferrable (with or without a delay) via a wired (e.g., Ethernet, USB, or optical cable) or wireless (e.g., Wi-Fi, LoRa, Zigbee, or 4G NB-IoT) link to a central data storage server. In the case of a wireless link, the data should be transmitted in a window the device is not measuring (unless the specific transmission frequency is not part of the frequencies measured by the device) [50].

6.1.9 Power supply

The measurement system can be mains-, solar-, or battery-powered (or by a combination thereof). For fixed measurement systems, a solar and battery combination is ideal for full autonomy (e.g., Narda AMB-8059 area monitor [51]), but connection to the mains is often also possible (e.g., in [23]). For vehicle-integrated systems, power could be provided by the vehicle (e.g., via the auxiliary power outlet [23]) but a solar panel could also be installed on the vehicle, and a battery contained in the measurement system could be charged by both the vehicle and solar power. On-body sensors, on the other hand, are usually constrained to battery solutions.

It would be worth investigating energy harvesting options [153], [154], [155], [156] for increased energy sustainability [157], a factor that will be increasingly important in sensor networks [158].

6.1.10 Housing

The final important design factor is the housing or enclosure of the measurement device. On-body devices have their own design constraints (practical, unobtrusive, possibly integrated in clothing) that are more critical, but in general, measurement devices should be able to withstand the environmental conditions that are to be expected during the measurements and should thus be enclosed in housing rated at least IP56 [50] or IP66 [49]. Moreover, connectors on the outside of the enclosure should be water impermeable (IP68) [43].

6.2 Uncertainty

As discussed above, it is highly recommended – essential, in fact – to **correct** each measurement device for **systematic errors**, **assess** the remaining **random errors**, and **describe** in detail the **overall uncertainty budget**, in order to compare and aggregate measurements with different measurement systems.

Although it is recommended that the expanded uncertainty is below 4 dB [104], it is more important to collect more, well-described data (with measurement devices that are validated *in-situ* with high-end equipment to obtain the necessary correction factors).

6.3 Data management

In this subsection we describe the requirements and recommendations for the collection, security, and analysis of data for EMF sensing technologies and measuring equipment. In Section 4, different use cases and calibration procedures are described. Activities like measurements, calibration, numerical simulations, and biological studies all generate data. Traditionally we can describe data management for field surveys to, for, example detect actual exposure in everyday and occupational exposures. We can relate these measured fields to absorbed fields in the body via numerical simulations. This can then be related to biological and health effects through in vitro and in vivo studies. This describes the whole process of assessing fields incident on a (human) body to potential biological and health effects. Since the scientific world is increasingly performing interdisciplinary research, new measurements systems might be required to integrate (parts of) this process. Therefore, this data management section covers all these aspects as well.

In NextGEM specifically, we investigate all parts of this process. New measurement devices are being developed. This includes lab pilots of calibration procedures (technology readiness level TRL) 4), field tests of measurement devices (TRL 5) and field surveys to detect actual exposure in every day and occupational environments (TRL 7). We perform numerical simulations to determine the exposure in human bodies based on these field surveys. We then conduct in vitro experiments where red blood cells are being exposed, and investigate in vivo effects when humans are exposed in a lab environment. This also requires the development of instruments to produce this exposure. All these examples and more, join together in CS3 described in WP7.

6.3.1 Collection

As discussed in Section 4.2, 5G NR networks have a prominent stochastic nature. For example: exposure is typically divided in different source categories (auto-induced/environmental and uplink/downlink, and broadcasting) [18]. In contrast to legacy networks, uplink and downlink may occur in the same frequency band in 5G NR (e.g., in bands n78 (3.5 GHz) and n258 (26 GHz)). In order to split uplink and downlink exposure information, a high external sampling rate is required (at least one sample per slot, the duration of which depends on the subcarrier spacing, e.g., 0.5 ms for 30 kHz – see Section 6.1.3). This means a large amount of generated data in a short period, as well as an increased power consumption for the measurement device. In lab environments, such as for calibration or lab testing, or spot measurements, this will not pose a problem. However, in scenarios where the measurement devices have to operate autonomously for some time, such as microenvironmental measurements or in sensor networks, this might lead to limitations. However, trade-offs can be made. In a sensor network, for example, it might be more interesting to collect a high density of samples over a 10 s period each hour, than taking one sample per second.

The higher the frequency, i.e., FR2 bands, the more important localized exposure is. While it is the case that fields can travel around the human body in FR1, in FR2 the path loss is too high for that [117]. Therefore, the location of the measurement device on the body becomes more important.

6.3.2 Security

We foresee that the security of new measurements will follow the same general principles as that of current systems. If data is stored on the measurement device, Secure Digital (SD) cards provide enough safety. If data is sent back to a server, secure Wi-Fi connections should be used. If surveys or biological experiments are performed with people, only pseudonymised data (meaning that codes are attributed to volunteers, while their details are separately stored on a secured server) should be collected. GPS data from survey measurement data should be labelled with the attributed code and relevant microenvironment, and only those labels should be reported, in compliance with the European General Data Protection Regulation (GDPR). This is also described in WP1.

In NextGEM, datasets in process are saved either on the partners local premises or on the NextGEM repository, only accessible to NextGEM partners. Final datasets are shared on Zenodo[1], either directly open - or after embargo - or with restrictions. Zenodo is an open repository built and developed by researchers, to ensure that everyone can join in Open Science. All datasets uploaded on Zenodo will be linked to the required metadata for FAIR data (see deliverable D1.1 on DMP initial version). Moreover, within NextGEM, a datahub called the NextGEM

[1] https://about.zenodo.org/

Innovation & Knowledge Hub (NIKH) is being built: its primary purpose is to include all metadata, either required or additional (as set in the NextGEM DMP) linked to all outputs generated within NextGEM and the other consortia (CLUE-H) and other outputs from other databases (EMF-portal, PubMedm, etc.,). This hub has its own safety protocols, which are described in WP6.

6.3.3 Analysis

The two main topics of 6.3.1., namely the focus on localized exposure in FR2 (as used in CS3), and the high sampling rate to separate different sources, also have an effect on data analysis. First, for localized exposure, an interaction with numerical simulations is required to find the optimal location of the measurement device on the body. A sensitivity analysis would be necessary to determine how precise the sensor has to be placed. When measuring on the body, an on-body calibration of the measurement device should be performed.

To differentiate between uplink and downlink sources, a high sampling rate is required, but also a new data analysis method. Either through synchronizing the measurement results with the uplink/downlink slot allocation (which is periodic in 5G NR networks), or through a statistical analysis, where a distribution for uplink and a distribution for downlink data can be derived, and measured data can be mapped on these two distributions.

Since in 5G NR, with active base station antennas, a person's own exposure will be more strongly related to their own usage of the network than in previous generations of mobile communication, an activity-based personal exposure assessment could be implemented. In this assessment, values for (localized) exposure are assigned to certain activities (rather than just microenvironments, although activities are dependent on the microenvironment). This analysis would require a clustering algorithm based on environmental uplink and downlink exposure, auto-induced uplink and downlink exposure, microenvironment, position of the user device relative to the body, time of day, etc [18].

6.4 Measurement campaigns

6.4.1 Influence of different use and situations on measurement(s) (systems)

As discussed in Section 6.3, there is a process which aims to determine biological and potential health effects induced by incident RF-EMFs. This process includes the development and calibration of measurement devices, the design of measurement campaigns, numerical simulations to determine fields outside to inside the body, and biological experiments to relate these fields to biological effects. If, for example, one wants to know the biological effects in red blood cells at 26 GHz in humans during occupational exposure, this whole process is affected. Measurements, simulations, and biological experiments have to complement each other. This is called an 'integrated system'.

As mentioned in Section 6.3.3, auto-induced exposure is becoming a more dominant factor in 5G NR relative to legacy networks. Therefore, a measurement protocol was proposed in [18] where measurements are performed in different scenarios, ranging from a heavy user to a non-user, giving the researcher a more active role in the network. When acting as a user, on-body measurement devices will be in the near-field of the user device, and should be calibrated as such (e.g., DEVIN [159] or unnamed add-on sensor [160]).

6.4.2 In situ EMF measurement and exposure assessment for citizen awareness

As the issue of environmental burden and impact on public health has taken on a large extent since the rapid spread of mobile networks, especially for populations residing or working near the base station antennas of these networks, there has been a great concern in the public both for the effects of antennas on their health and the safety limits and safety distances from these antennas. The field measurements and network monitoring services include the signal power measurements for compliance control with national law and international regulations in cities and areas which are related to multiple network levels (natural level of EMF, network level and application level).

The protection from EMF relies on the guidelines from the International Commission on Non-Ionizing Radiation Protection (ICNIRP) [1] and the Institute of Electrical and Electronics Engineers (IEEE) [130] where most European countries adhere to these exposure limits. The 2020 updated ICNIRP guidelines consider vulnerable groups and emphasize maintaining total electromagnetic radiation below specified limits, which vary based on frequency bands. Especially for lower frequencies within the 30 MHz to 6.0 GHz range, exposures pose greater heating risks to the human body, influencing the stringency of limits for different bands.

In relation to the protection provided by the state to the citizen-passenger of the antennas, the measurements made from time to time by various authorities, for monitoring the compliance through EMF measurements, are not enough to draw safe conclusions from them. The reason is that they are not carried out for sufficient periods

of time but fragmentarily. In addition, the fluctuation of the transmitted power is technically feasible and is carried out not only during the measurement periods but also whenever required during periods of network overload due to increased demand for the provision of telecommunications services. Especially above 6 GHz, particularly in the mmWave range, EMFs are absorbed more superficially.

On the national level for each country, such as NextGEM partners' countries, public and private organizations can provide in situ measurements either through continuous monitoring or on demand by the use of spectrum analysers either handheld for on demand measurements or static outdoor equipment for continuous in situ monitoring.

6.4.2.1 In situ on demand measurements

In this direction, the need for *in situ* measurement of EMF radiation campaigns is becoming increasingly important, given the growing concern about EMF, especially from mobile telephony systems. Even though the exact implications of EMF on public health is still uncertain, it is important to continuously monitor EMF levels and check compliance to national and international limits. Even when the assigned legal limits are not exceeded, the evolution of EMF levels can provide important information, which can be later used by the scientific community or public bodies and regulators.

Although the list of handheld spectrum analysers suitable for *in situ* on demand measurements includes many devices from a number of companies, the selection of presented devices was made based on the experience and testing by the NextGEM partners from *in situ* measurements. For instance, FORTH apart from its research activities, has provided services such as consulting services and designation of studies for EMF measurements and network monitoring by using Rohde Swartz and Aaronia handheld devices. These services are related to integrated technical support and study services for the design, management and safety of mobile networks, including public access networks and corporate wireless networks, as well as the preparation of relevant studies. In this direction, FORTH has carried out a number of EMF measurements in different locations in selected areas of the city of Heraklion, villages and other cities on Crete. The main measurements were basically conducted in the bands of GSM, 3G, 4G, LTE and 5G frequencies but other measurements were also taken in the TV and FM bands, following the request from citizens and as services offered to schools for students and teachers' awareness on EMF radiation exposure.

Finally, on the national level, public organizations such as the Greece Atomic Energy Commission (EEAE), have conducted a number of *in situ* measurements for the protection of the population and the environment from high and low frequency electromagnetic fields [161]. These measures can be found also through mobile app (e-antennas.gr) where relevant stakeholders and citizens have access on EMF level updates directly through their mobile phone.

6.4.2.2 In situ continuous monitoring

With the aim of advanced monitoring and measurement, especially for mobile networks, there is the need for the deployment of continuous field measurements to control compliance with national law and international regulations. Therefore, apart from the *in situ* on demand measurements, in order to improve citizens awareness and to protect the general public, the limit values should be checked regularly and sometimes monitored with continuous field measurement in real time by using various measuring stations and systems for this purpose (e.g., see Figure 17).

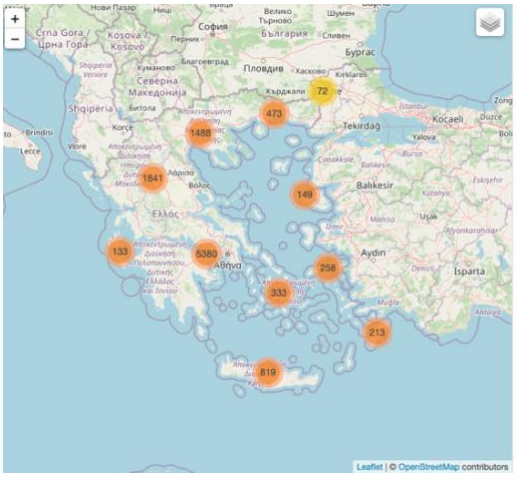

Figure 17: Collection of in situ measurement in Greece conducted by EEAE

For instance, the Serbian EMF RATEL network (see Figure 18) is a EMF sensor network that employs advanced telecommunication service-based EMF monitoring system, utilizing the Narda AMS 8061 sensor for wideband monitoring [162]. The network's focus is on the preliminary monitoring of 5G, detailing the sensor's technical aspects, acquisition process, and the analysis and dissemination of results. EMF RATEL aims to support the control and management of electromagnetic fields in upcoming smart-city ecosystems, anticipating heightened EMF radiation from various telecommunication services. However, although the deployment of 5G in the FR1 and especially in the FR2 band is projected, it is only partially implemented in certain EU countries. One contributing factor is the limited data and the availability of monitoring sensor technologies, which could enhance public acceptance by providing more comprehensive information about these systems [163].

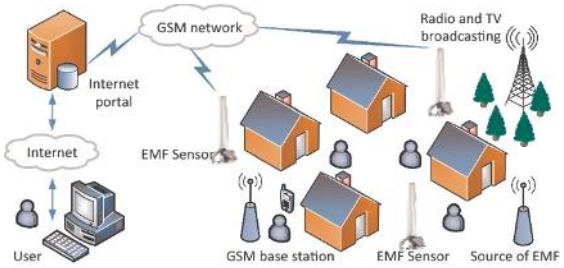

Figure 18: The concept of EMF RATEL monitoring network.

Apart from the commercial solutions for continuous EMF monitoring, there are some experimental trials based on development of systems integrating low-cost measuring devices. For instance, FORTH has developed in the past a custom solution including spectrum (Aaronia Spectran series) that could support measurements in a wide frequency range (up to 7 GHz) collected through the advanced wireless metropolitan mesh network which has been developed in the city of Heraklion (see Figure 19) [164]. Special developed software allowed the collection of measurements per spectrum area and collect measurements on various time scales to provide multi-band real time measurements. In addition, in national level, the role of such public sensor networks for citizens awareness is very important due to the given capability for online access of the measurements as taken from different locations and cities where the EMF networks are deployed [165].

Figure 19: Non-commercial deployment for continuous outdoor EMF monitoring.

Based on the above, *in situ* measurement campaigns are crucial for ensuring citizens awareness and environmental protection. The use of suitable special equipment to carry out EMF measurements and the preparation of technical studies is required to perform continuous measurements for public and private sectors and for citizens. In this direction, there is need for *in situ* measurements (on demand or continuous) to carry on especially in higher frequencies including 5G, such as in FR2 band, but also for the next generation of networks (beyond 5G, 6G) in order to comply with the latest and forthcoming of European and international guidelines.

6.5 Optimization through modelling

Currently implemented 5G cellular networks employ advanced power and antenna range management techniques, facilitating highly efficient utilization of communication channels. In this extremely dynamic context, new technological solutions are continuously introduced. This determines the existence of an extremely complex technological ecosystem characterized not only by different solutions linked to the different cell generations that currently coexist but also by different solutions within the same generation of cellular system.

The development of field measurement equipment must consider the continuous and rapid development of communication systems (see Section 5.1). A particularly challenging characteristic of 5G telecommunications systems is the use of steering beams, which, combined with complex selection strategies in choosing the users to be served, make the direction of the beam that transmits user data [142] not foreseeable a priori (Figure 20). When implemented in the system, dynamic transmitted power control represents a further challenge in measuring the field level transmitted by radio base stations.

Finally, the highly variable character of the signal in time and space will be further increased if some technologies currently under research are implemented in future cellular communication systems. In particular, the use of technologies capable of modifying the propagation environment through reflective systems that can dynamically modify the re-radiated beam [136] (Figure 21) will represent a further element of the variability of the field level in the environment.

In such a complex scenario, the simulation of the electromagnetic scenario and the measurement of the field play an important and intertwined role in helping the definition of the measurement systems in terms of the characteristics and positions of the sensors, including wearable and vehicle sensors.

Figure 20: in MaMIMO the beam is steered toward the use that requires traffic; other areas are not illuminated by the beam; this makes the evaluation of the average value of the field a not straightforward problem.

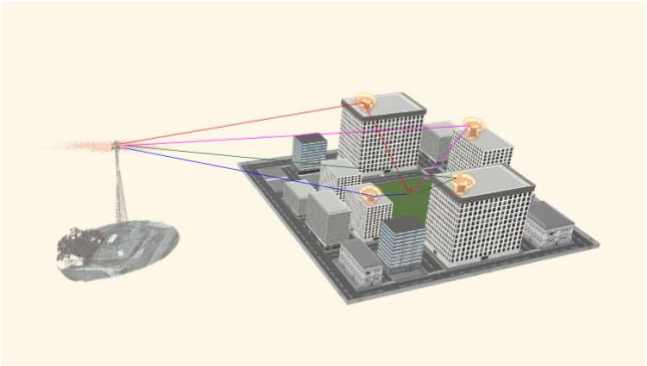

Figure 21: the active control of communication channels using controlled reflecting surfaces is one of the technologies under investigation for future communication systems.

6.5.1 How can the measurement system help the modelling/mapping?

Simulating the average level of the EMF radiated by modern telecommunications systems is not a trivial problem. It requires not only detailed knowledge of the propagation environment, but also of some details of the telecommunications system. Some of these details depend on the specific setting of the telecommunications system and are not easily accessible or are not made available by operators as they are considered sensitive data. Measurements of the signal radiated by the base station can allow the determination of such data. One example is determining whether power control is being utilized. In fact, when the power level control is active in the real system but neglected in the simulations, significant overestimates of the field levels can occur, particularly near the antenna.

Other useful information is the centre frequency and bandwidth of the signal, the specific multiplexing technology used (i.e., domain, TDD, or in the frequency domain, FDD), the type of implementation in 5G systems (i.e., 5G DDS (Dynamic Spectrum Sharing,), or 5G SA (Stand Alone) or 5G NSA (Non-Stand Alone), see Figure 22), or the numerology used in the 5G frames. In TDD, a fraction of time is used for uplink (visible as vertical green strips in the right figure), determining a lower downlink total power compared to TDD in the case of maximum-loaded downlink connection.

These instances illustrate how air signal measurements can become essential to simulations, particularly when complete information about the communications system's configuration is unavailable for accurately simulating the field level in the environment.

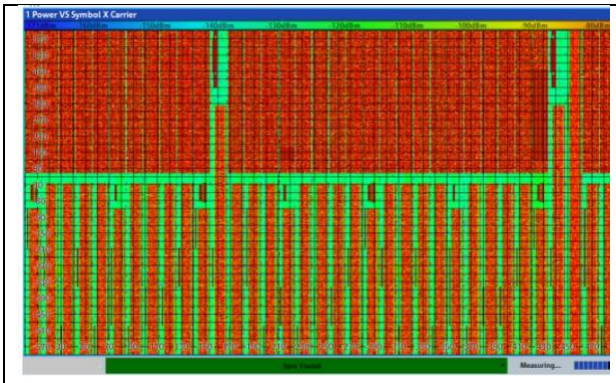

Frames radiated by a 5G-DDS base station using FDD

Frames radiated by a 5G-NSA base station using TDD

Figure 22: Frames measured on two different 5G systems

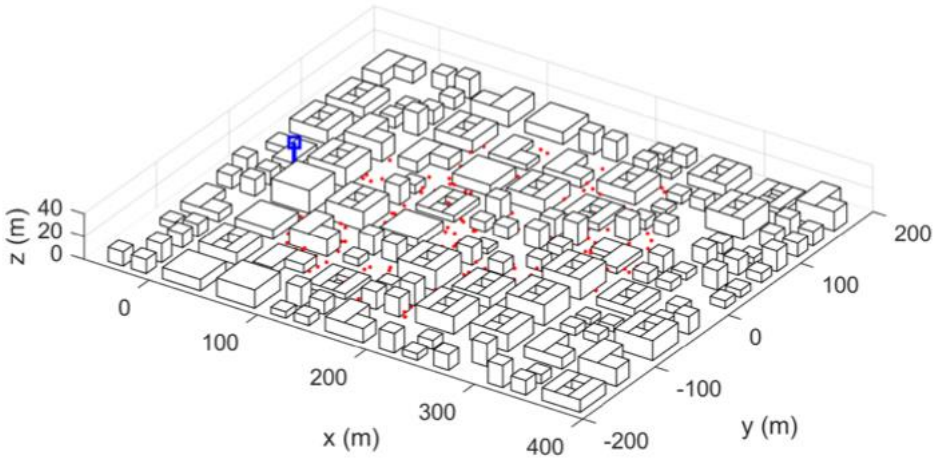

Figure 23: Numerical simulations allow the identification of critical areas in complex urban environments.

6.5.2 How can modelling/mapping optimize the measurement system?

Numerical simulation is particularly useful in defining the optimal measurement conditions for estimating the field level generated by 5G communication systems. 5G systems use MaMIMO antennas, which allow the radiated beam to be changed dynamically to optimize communication with users. The field level, therefore, varies dynamically with the number, location, and traffic demand of users (Figure 23). The numerical simulation of the field must consider the statistical aspect of communication, which is reflected in a statistical value of the field level, linked both to the number, position, and traffic request of users and to the specific set of beams that the MaMIMO antenna can generate. Using the correct values of these parameters makes it possible to obtain numerous useful information for performing measurements and evaluating the average field level from the measured data.

Numerical simulations are particularly useful for evaluating the spatial variability of the field and identifying the critical zones for measurement, determining the sensitivity necessary for precise measurements, selecting the most suitable measurement tools, and rationalizing the number of measurement points required.

These principles are equally relevant to both wearable sensors and vehicle sensors, where identifying the ideal positioning is of great importance. They are also fundamental for evaluating the scaling statistical factor (F_{PR}) of the value provided by the Maximum Power Estimation (MPE) techniques to obtain a realistic average value of the field level [137], [138].

Finally, numerical simulations are the only method to estimate the impact of technologies currently under research on the distribution of the EMF in the environment [166].

6.5.3 Can modelling/mapping optimize the measurement system positioning (on body, vehicle, infrastructure)?

Electromagnetic numerical simulations are a promising option for Wireless Body Area Network (WBAN) modelling due to their flexibility, cost-effectiveness, and ability to overcome challenges like uncertainties and inaccuracies in measurement data. There are several numerical methods suitable for simulation-based channel modelling, including full-wave and asymptotic solutions. The choice of numerical approach depends on the nature of the communication links in the wireless body network [167], [168]. Such approaches further allow for the systematic testing of various sensor placement options on the body. Researchers can explore different locations and orientations to identify positions that offer optimal signal reception and minimal interference from the human body.

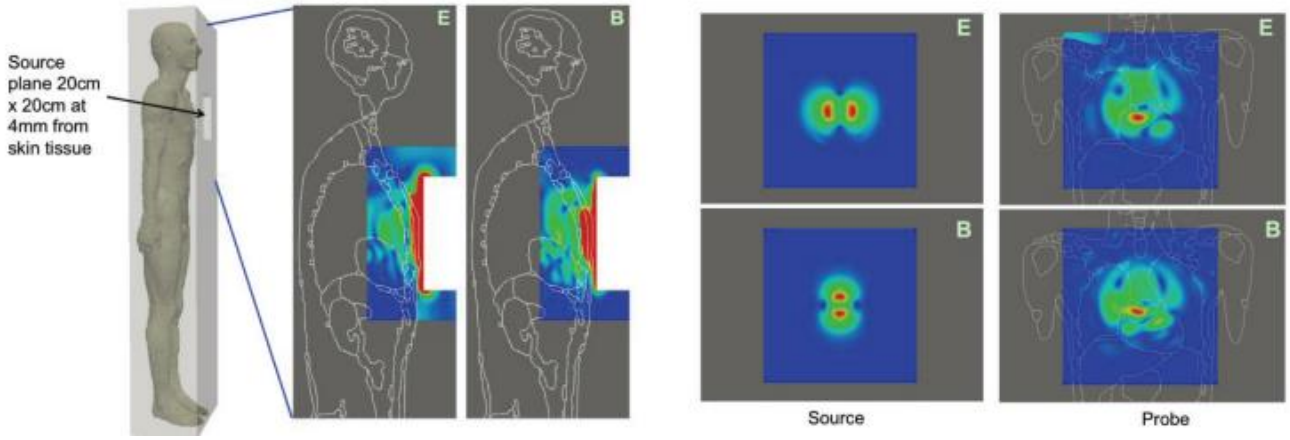

Figure 24: Example of a simulation of electromagnetic wave propagation in a human phantom (taken from [168], where they identified optimal source placement).

As with on-body measurements, the position of the measurement device on the vehicle can significantly influence the measurement, hence, electromagnetic simulations with vehicular models (such as cars, bicycles, buses, etc.) could help identify optimal sensor placement.

Finally, simulation models on the targeted area can replicate signal propagation characteristics of the 5G network [169], as well as user mobility patterns and identify areas with high user density or frequent mobility changes [170]. Using information from such simulations, measurement systems can be strategically placed on infrastructure or on vehicles to ensure comprehensive data collection and to capture dynamic network behaviour in areas with significant user movement (see Figure 25).

6.5.4 Realistic estimation of the 5G beam

As indicated in Sections 6.5.1 and 6.5.2, there is a strong synergy between the acquisition of data relating to the signal radiated by the base radio station and the numerical simulations. Numerical simulation becomes particularly interesting in the case of new-generation systems. Like those of previous generations, the structure of the signal radiated by these systems must comply with the standards set by 3GPP, which defines the air interface and all protocols and network interfaces that enable the entire mobile system. However, the implementation of the specifications is the manufacturer's choice.

A particularly challenging problem in measurements and simulations is knowing the model used by the base station in 5G links. Correct simulation of the antenna beams is of great importance not only in simulation but also in measurements, where it can help organize the measurement campaign.

Figure 25 shows a preliminary estimate of the footprint obtained by an accurate estimation of a 5G antenna beam. The simulation allows technicians to identify the field distribution, which in turn facilitates the choice of optimal locations for data collection. In this way, it is possible to reduce the number of measurements, the duration of the measurement process, and, ultimately, the overall expense involved in the measurement procedure.

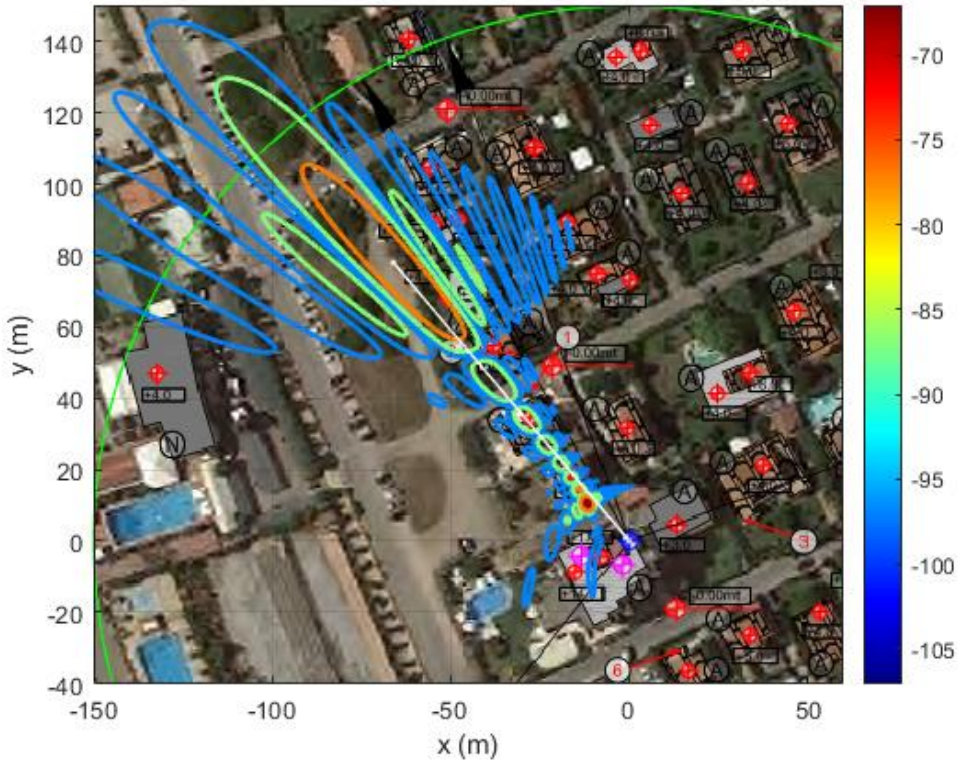

Figure 25: A preliminary simulation of the footprint of a 5G antenna beam; the simulation with a realistic estimation of the 5G beam can help to optimize the measurements.

6.5.5 Sensor location optimization in the FR1 range

As an example of use of modelling for sensor location optimization, we present in the following a summary of the results from deliverable 3.2 (see deliverable 3.2 Section 5 for more details).

The scenario assumed in this example corresponds to a far EMF source irradiating a homogenous dummy at a frequency of 0.7 GHz. The EMF source is placed in a complex environment that causes multiple reflections and illuminates the dummy with different angles and polarizations. The objective of these simulations is to obtain the optimal location for the electric field measurement devices that are going to be installed in a vest that some volunteers are going to wear while walking in the complex environment. Also, we want to correlate the external electric field measured in the vest detectors with the field inside the dummy.

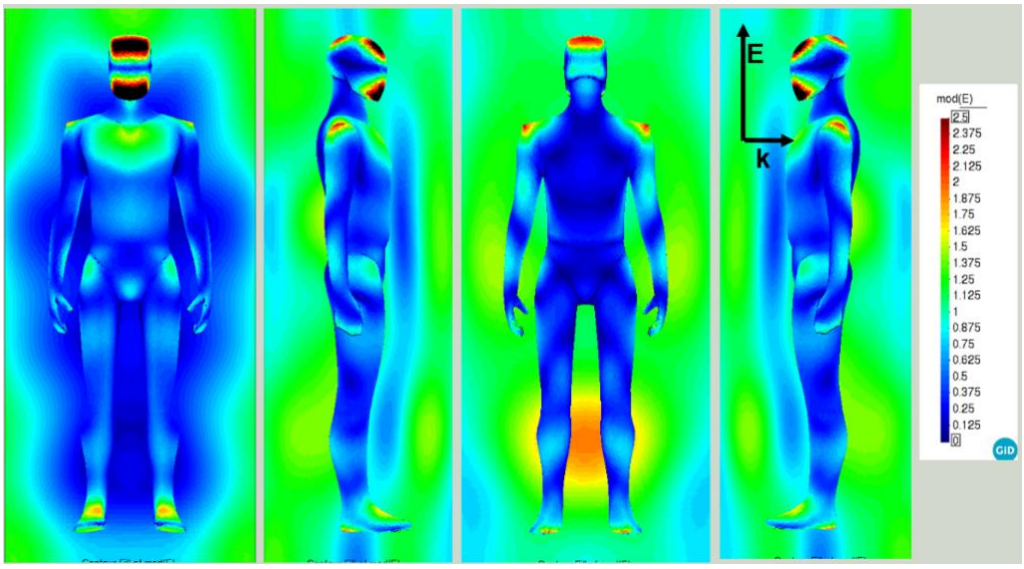

Figure 26: External electric field generated by a frontal wave vertically polarized at 0.7 GHz.

For the 0.7 GHz case we used a volumetric dummy that was irradiated with plane waves of 1 V/m of amplitude and different polarizations and wave vector directions. The fields were averaged afterwards to obtain the best locations of the detectors. In Figure 26 and Figure 27, the field is shown produced by a frontal plane wave vertically and horizontally polarized respectively. It is clearly observable how the polarization of the wave affects the field distribution in if the field is on the external surface of the dummy. The surface of the dummy has 2 values of the electric field on the same surface. One outside and other inside of the dummy. They are related by the discontinuity relations derived from the Maxwell equations. This is the general discontinuity of the fields that happens in the interface of any dielectric.

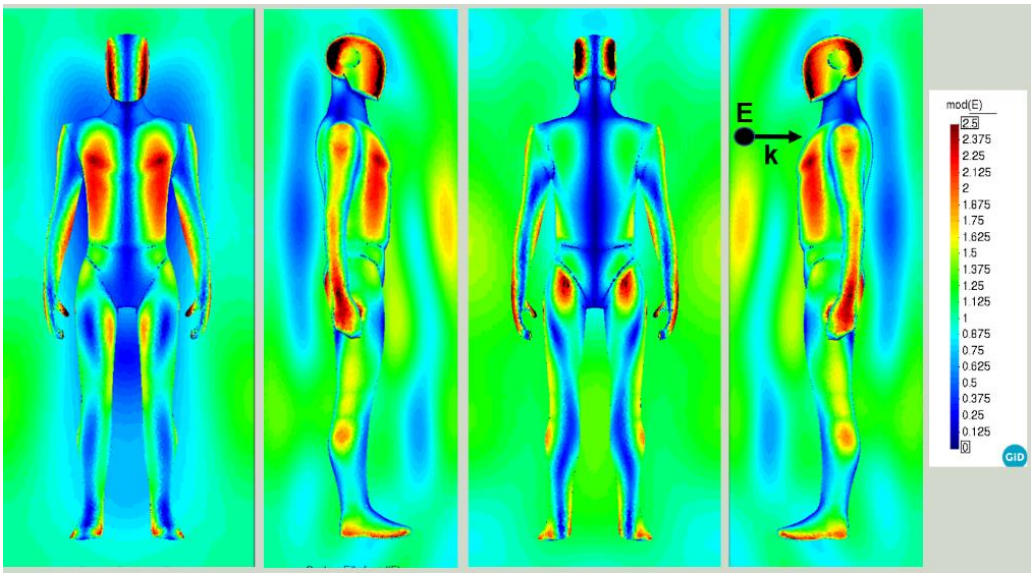

Figure 27: External electric field generated by a frontal wave horizontally polarized at 0.7 GHz.

The average over all the simulated polarizations and 5 directions is shown in Figure 28. The average is made over five different wave directions (frontal, back, left, right and top) with two polarizations each (horizontal and vertical) adding a total of ten independent simulations (incoherently added and averaged). **Figure 28** shows that the best locations for the detectors are in order: head, shoulders, arms, and chest of the dummy.

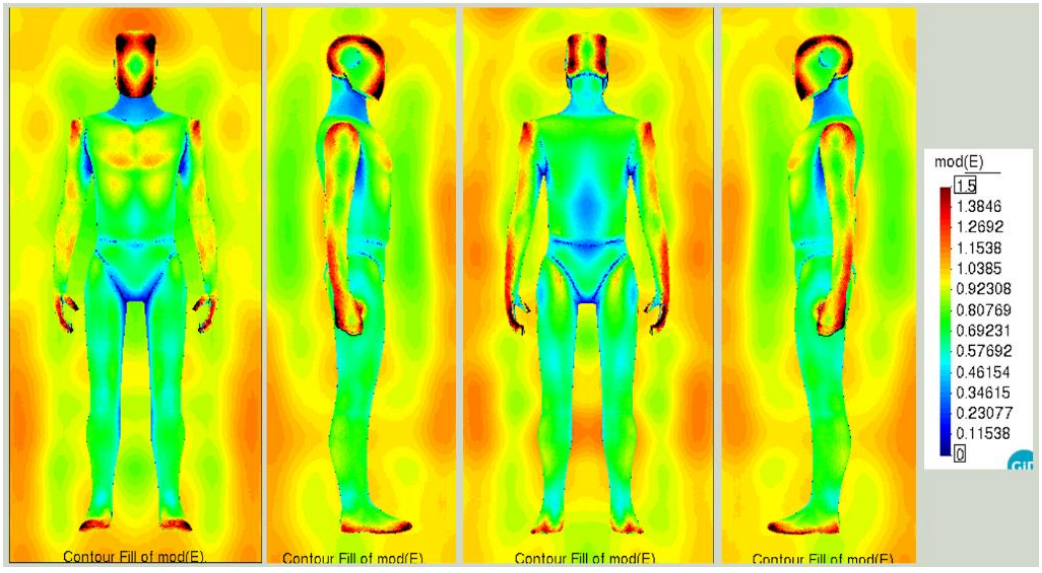

Figure 28: Average external electric field over five different wave directions (frontal, back, left, right and top) with two polarizations each (horizontal and vertical) adding a total of ten independent simulations. The fields were added incoherently and then averaged. The best locations for measuring external fields are (in order) the head, shoulders, arms and chest.

The internal electric fields were obtained for the same cases as for the external fields showed above. In Figure 28 and Figure 30 we can see the internal electric field for the vertical and horizontal polarization cases respectively.

We can appreciate on these figures the differences between the internal and external electric fields distribution shown in Figure 27 and 28. The differences are caused by the discontinuity of the fields on the materials interfaces. In Figure 31 is shown the average of the internal fields following a similar procedure as the one explained in Figure 28 (incoherently added and averaged). The maximum internal electric field are in order: neck, wrist, front head, and shins.

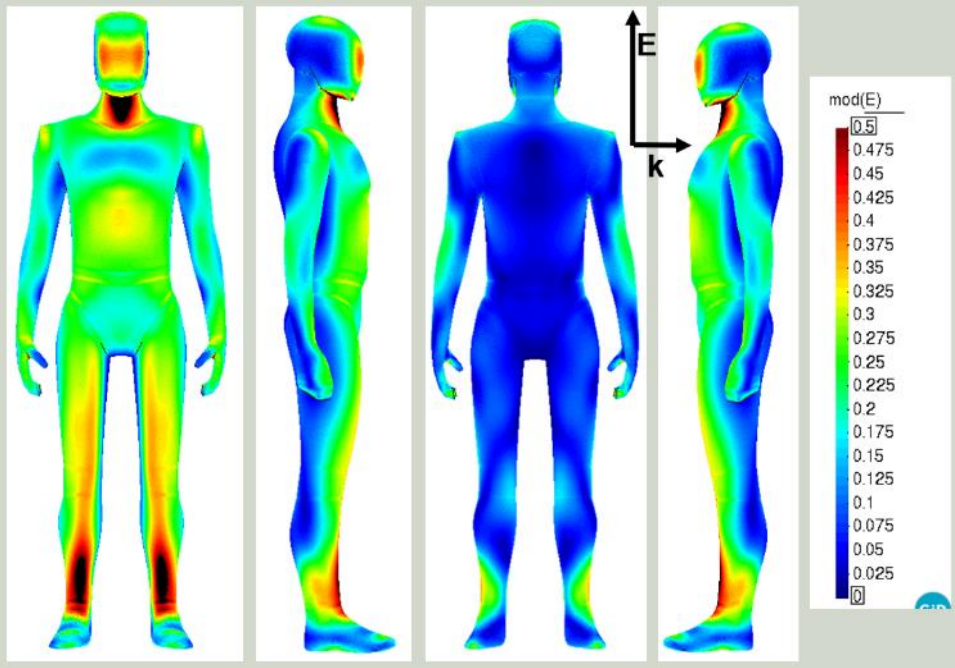

Figure 29: Internal electric field generated by a frontal wave vertically polarized at 0.7 GHz.

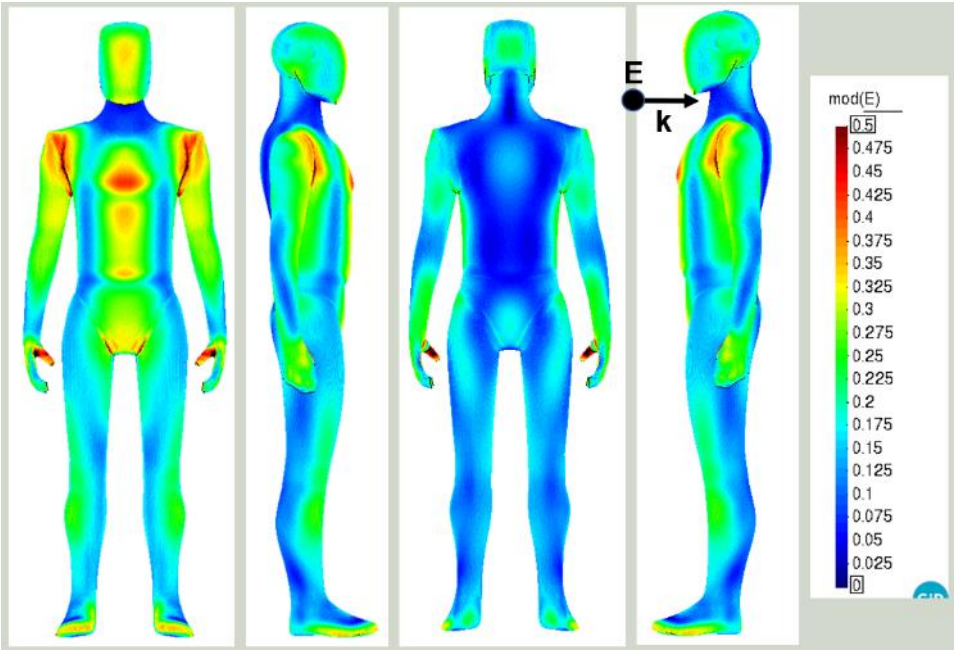

Figure 30: Internal electric field generated by a frontal wave horizontally polarized at 0.7 GHz.

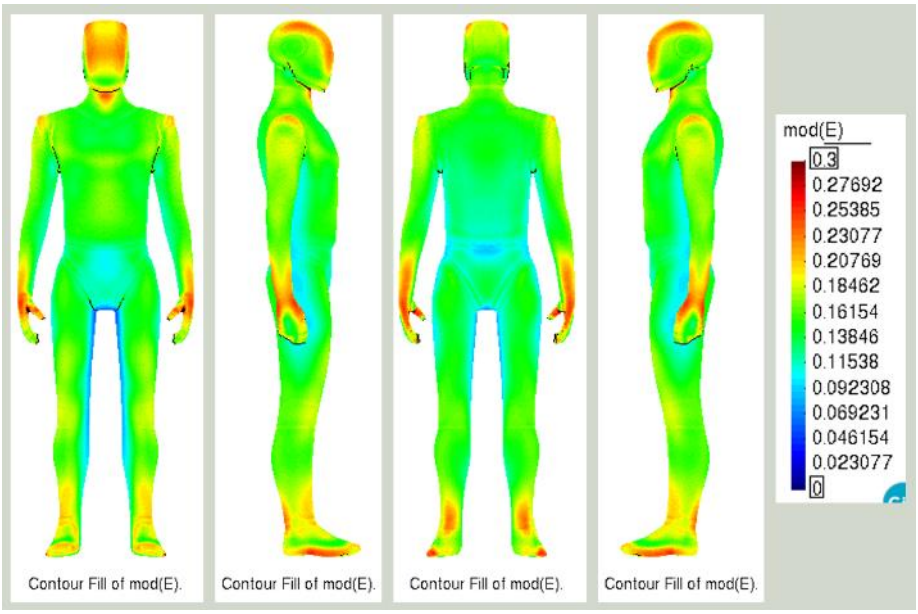

Figure 31: Average internal electric field over five different wave directions (frontal, back, left, right and top) with two polarizations each (horizontal and vertical) adding a total of ten independent simulations.

If we want a better correlation between the external field measurements and the internal magnitudes of interest in dosimetry (e.g., SAR), the best option is to measure the magnetic field on the external surface of the dummy. The magnetic field is unique and continuous on the interface, and it give us directly the internal power distribution through the relation:

$$P_S = \frac{1}{2}\boldsymbol{R_S}|\boldsymbol{H_t}|^2 \qquad (9)$$

where $\boldsymbol{R_S}$ is the surface resistance (which depends on the material properties of the first layers of the dummy) and $\boldsymbol{H_t}$ is the component of the magnetic field tangential to the dummy's surface. On the other hand, if we measure the external electric field, or the external Poynting vector, this corelation is less direct due to the discontinuity of the fields. In Figure 32 we show that the best correlation between the internal power delivered inside the dummy (internal module of the Poynting vector) and the external field measurement corresponds to the magnetic field. This is even more true when the frequency increases and the power is delivered more superficially.

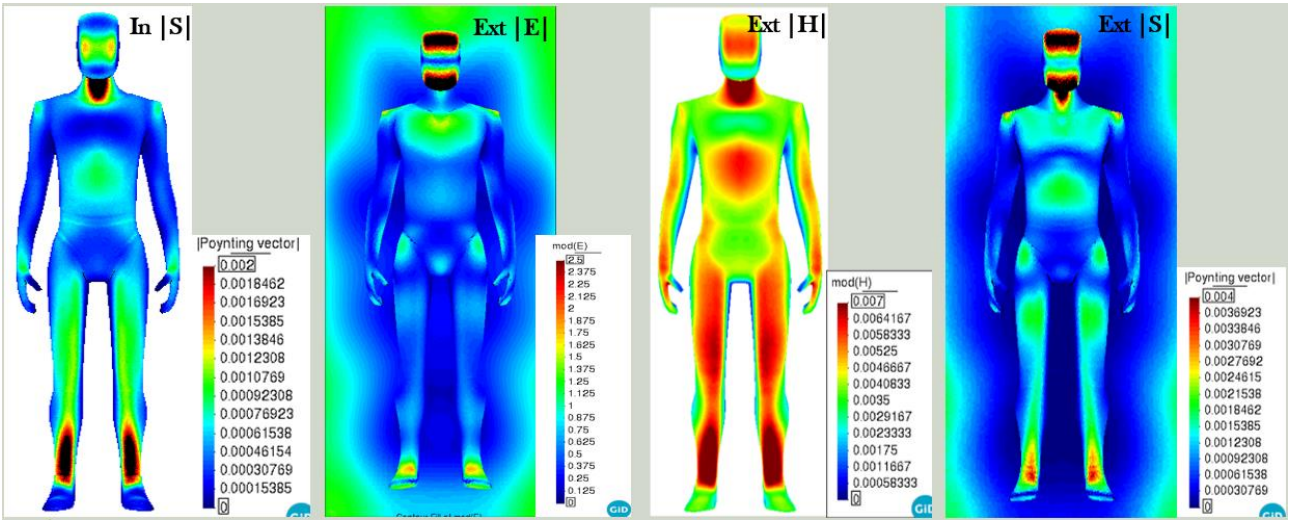

Figure 32: Correlation between the internal power delivered to the dummy and the external fields. Measuring the external tangential magnetic field and using the relation Ps = 0.5*Rs*|Ht| will give us the closest correspondence with the internal power absorbed inside the dummy.

7 Conclusions

This deliverable offers a comprehensive overview of the current state-of-the-art concerning devices used for the assessment of RF-EMF, including spectrum analysers, broadband field meters, area monitors, custom-developed instruments, and personal exposimeters, as well as of the current measurement protocols (both standardized and non-standardized). Based on the identified needs and gaps in knowledge, recommendations and requirements for future RF-EMF measurement devices are provided.

In general, there is a need for low-cost and durable measurement devices or sensors capable of collecting data at high time resolution across various frequency bands and environmental conditions. These sensors are indispensable for conducting stationary, mobile, and personal exposure assessments across larger geographical areas, time intervals, and populations than current capabilities allow. Furthermore, it is crucial to acknowledge that the specific requirements for these sensors differ based on their intended usage. For instance, on-body measurement devices need to consider the influence of the body, while vehicle-integrated sensors must account for speed and relative position, and sensors on infrastructure must address height and building materials. Additionally, there is a demand for real-time, fast-sampling solutions to understand the highly irregular temporal variations in EMF distribution within next-generation networks.

Moreover, there is a significant lack of comprehensive information regarding currently utilized custom-developed RF-EMF measurement tools, particularly regarding measuring uncertainty. Given the diversity of tools and methodologies in use, conducting a thorough comparison becomes crucial to identify the necessary statistical tools for aggregating the available measurement data.

This deliverable further elaborates the design considerations for lab-built, compact low-cost sensors on the component level. Furthermore, the importance of calibration and uncertainty analysis are emphasized to ensure accurate measurements, listing detailed steps to be followed for both issues. Additionally, essential requirements are outlined and elaborated for new measurement systems alongside specific recommendations.

Finally, besides being crucial for the design of RF measuring equipment (e.g., the antennas and PCB), numerical modelling can help understand the spatial variability of the field, identify critical areas for measurements, and optimize the number of measurement points. In addition, simulations can aid in evaluating the impact of uncertainties on measured data, identifying biases in system modelling, and visualizing the fields inside the human body that are difficult to measure directly. In summary, the use of low-cost sensors, combined with numerical modelling techniques, can significantly improve the accuracy, reliability, and cost-effectiveness of RF-EMF measurements.

References

[1] ICNIRP, Guidelines for limiting exposure to electromagnetic fields (100 kHz to 300 GHz). (2020). Health Physics, 118(5), 483–524. https://doi.org/10.1097/hp.0000000000001210

[2] IEC 62232:2022, "Determination of RF field strength, power density and SAR in the vicinity of base stations for the purpose of evaluating human exposure", IEC. (n.d.). IEC - International Electrotechnical Commission. Available at: https://webstore.iec.ch/publication/64934 [Last accessed 31 May 2023].

[3] European Union Council Recommendation 1999/519/EC on the limitation of exposure of the general public to electromagnetic fields (0 Hz to 300 GHz). Available at: https://faolex.fao.org/docs/pdf/eur40317.pdf [Last accessed 31 May 2023].

[4] Directive 2013/35/EU of the European Parliament and of the Council of 26 June 2013 on the minimum health and safety requirements regarding the exposure of workers to the risks arising from physical agents (electromagnetic fields). Available at: https://eur-lex.europa.eu/eli/dir/2013/35/oj [Last accessed 31 May 2023].

[5] ICNIRP. Guidelines for limiting exposure to time-varying electric, magnetic, and electromagnetic fields (up to 300 GHz). International Commission on Non-Ionizing Radiation Protection. (1998, April 1). PubMed. https://pubmed.ncbi.nlm.nih.gov/9525427/.

[6] SCHEER. Request for a scientific Opinion on Potential health effects of exposure to electromagnetic fields (EMF). https://health.ec.europa.eu/system/files/2021-07/scheer_q_023_0.pdf [Last accessed 13 June 2023].

[7] EN 50401:2017, Product standard to demonstrate the compliance of base station equipment with radiofrequency electromagnetic field exposure limits (110 MHz - 100 GHz), Publication date: Nov 15, 2017.

[8] EN 50383:2010/C1:2013, Basic standard for the calculation and measurement of electromagnetic field strength and SAR related to human exposure from radio base stations and fixed terminal stations for wireless telecommunication systems (110 MHz - 40 GHz). Publication date: June 1, 2013.

[9] Meerjarenplan EMV, 21 June 2021. Available at: https://www.rdi.nl/binaries/agentschap-telecom/documenten/publicaties/2020/11/meerjarenplan-emv-en-meetprotocol/meerjarenplan-emv-en-meetprotocol/Meerjarenplan+EMV+2020.pdf [Last accessed 13 June 2023].

[10] International Telecommunication Union - Radiocommunication Sector (ITU-R), Electromagnetic field measurements to assess human exposure, June 2019. https://www.itu.int/dms_pub/itu-r/opb/rep/R-REP-SM.2452-2019-PDF-E.pdf [Last accessed 31 May 2023].

[11] Meetprotocol EMV, 21 June 2021. Available at: https://www.rdi.nl/binaries/agentschap-telecom/documenten/publicaties/2020/11/meerjarenplan-emv-en-meetprotocol/meerjarenplan-emv-en-meetprotocol/Meetprotocol+EMV.pdf [Last accessed 13 June 2023].

[12] CENELEC - EN 50413. (2019). Available at: https://standards.cencenelec.eu/dyn/www/f?p=305:110:0::::FSP_ORG_ID,FSP_PROJECT,FSP_LANG_ID:1258483,77034,25&cs=185FFA4193C7637BF67C60250DF57DBB9, [Last accessed 16 June 2023].

[13] Liorni, I., Capstick, M., Van Wel, L., Wiart, J., Joseph, W., Cardis, E., Guxens, M., Vermeulen, R., & Thielens, A. (2020). Evaluation Of Specific Absorption Rate In The Far-Field, Near-To-Far Field And Near-Field Regions For Integrative Radiofrequency Exposure Assessment. Radiation Protection Dosimetry, 190(4), 459–472. https://doi.org/10.1093/rpd/ncaa127.

[14] Beekhuizen, J., Vermeulen, R., Kromhout, H., Bürgi, A., & Huss, A. (2013). Geospatial modelling of electromagnetic fields from mobile phone base stations. Science of the Total Environment, 445–446, 202–209. https://doi.org/10.1016/j.scitotenv.2012.12.020.

[15] Velghe, M., Joseph, W., Debouvere, S., Aminzadeh, R., Martens, L., & Thielens, A. (2019). Characterisation of spatial and temporal variability of RF-EMF exposure levels in urban environments in Flanders, Belgium. Environmental Research, 175, 351–366. https://doi.org/10.1016/j.envres.2019.05.027.

[16] Aerts, S., Wiart, J., Martens, L., & Joseph, W. (2018). Assessment of long-term spatio-temporal radiofrequency electromagnetic field exposure. Environmental Research, 161, 136–143. https://doi.org/10.1016/j.envres.2017.11.003.

[17] Eeftens, M., Struchen, B., Birks, L. E., Cardis, E., Estarlich, M., Fernández, M. F., Gajšek, P., Gallastegi, M., Huss, A., Kheifets, L., Meder, I. K., Olsen, J., Torrent, M., Trček, T., Valič, B., Vermeulen, R., Vrijheid, M., Van Wel, L., Guxens, M., & Röösli, M. (2018). Personal exposure to radio-frequency electromagnetic fields in Europe: Is there a generation gap? Environment International, 121, 216–226. https://doi.org/10.1016/j.envint.2018.09.002.

[18] Velghe, M., Aerts, S., Martens, L., Joseph, W., & Thielens, A. (2021). Protocol for personal RF-EMF exposure measurement studies in 5th generation telecommunication networks. Environmental Health, 20(1). https://doi.org/10.1186/s12940-021-00719-w.

[19] Thielens, A., Van Den Bossche, M., Brzozek, C., Bhatt, C. R., Abramson, M. J., Fritschi, L., Martens, L., & Joseph, W. (2018). Representativeness and repeatability of microenvironmental personal and head exposures to radio-frequency electromagnetic fields. Environmental Research, 162, 81–96. https://doi.org/10.1016/j.envres.2017.12.017.

[20] Urbinello, D., Huss, A., Beekhuizen, J., Vermeulen, R., & Röösli, M. (2014). Use of portable exposure meters for comparing mobile phone base station radiation in different types of areas in the cities of Basel and Amsterdam. Science of the Total Environment, 468–469, 1028–1033. https://doi.org/10.1016/j.scitotenv.2013.09.012.

[21] Bhatt, C. R., Redmayne, M., Abramson, M. J., Sim, M. R., Brzozek, C., Zeleke, B. M., & Fritschi, L. (2018). Estimating transmitted power density from mobile phone: an epidemiological pilot study with a software modified phone. Australasian Physical & Engineering Sciences in Medicine, 41(4), 985–991. https://doi.org/10.1007/s13246-018-0699-7.

[22] Van Wel, L., Huss, A., Bachmann, P., Zahner, M., Kromhout, H., Fröhlich, J., & Vermeulen, R. (2017). Context-sensitive ecological momentary assessments; integrating real-time exposure measurements, data-analytics and health assessment using a smartphone application. Environment International, 103, 8–12. https://doi.org/10.1016/j.envint.2017.03.016.

[23] Aerts, S., Vermeeren, G., Van Den Bossche, M., Aminzadeh, R., Verloock, L., Thielens, A., Leroux, P., Bergs, J., Braem, B., Philippron, A., Martens, L., & Joseph, W. (2022). Lessons Learned from a Distributed RF-EMF Sensor Network. Sensors, 22(5), 1715. https://doi.org/10.3390/s22051715.

[24] Iakovidis, S., Apostolidis, C., Manassas, A., & Samaras, T. (2022). Electromagnetic Fields Exposure Assessment in Europe Utilizing Publicly Available Data. Sensors, 22(21), 8481. https://doi.org/10.3390/s22218481.

[25] Ramirez-Vazquez, R., Escobar, I. C., Thielens, A., & Beléndez, A. (2020). Measurements and Analysis of Personal Exposure to Radiofrequency Electromagnetic Fields at Outdoor and Indoor School Buildings: A Case Study at a Spanish School. IEEE Access, 8, 195692–195702. https://doi.org/10.1109/access.2020.3033800.

[26] Aerts, S., Verloock, L., Van Den Bossche, M., Colombi, D., Martens, L., Tornevik, C., & Joseph, W. (2019). In-situ Measurement Methodology for the Assessment of 5G NR Massive MIMO Base Station Exposure at Sub-6 GHz Frequencies. IEEE Access, 7, 184658–184667. https://doi.org/10.1109/access.2019.2961225.

[27] Stratakis, D., Miaoudakis, A., Katsidis, C. C., Zacharopoulos, V., & Xenos, T. D. (2009). On the uncertainty estimation of electromagnetic field measurements using field sensors: a general approach. Radiation Protection Dosimetry, 133(4), 240–247. https://doi.org/10.1093/rpd/ncp050.

[28] Bolte, J. H., Van Der Zande, G., & Kamer, J. (2011). Calibration and uncertainties in personal exposure measurements of radiofrequency electromagnetic fields. Bioelectromagnetics, 32(8), 652–663. https://doi.org/10.1002/bem.20677.

[29] IEEE Std 1309™-2013 "IEEE Standard for Calibration of Electromagnetic Field Sensors and Probes (Excluding Antennas) from 9 kHz to 40 GHz" Oct. 2013.

[30] Tektronix. Fundamentals of Real-Time Spectrum Analysis [Primer] https://download.tek.com/document/37W_17249_5_HR_Letter.pdf, [Last accessed 13 June 2023].

[31] Rohde&Schwarz, R&S®FSW Signal and spectrum analyser https://www.rohde-schwarz.com/us/products/test-and-measurement/benchtop-analyzers/rs-fsw-signal-and-spectrum-analyzer_63493-11793.html, [Last accessed 13 June 2023].

[32] Rohde&Schwarz, TSMA6 Autonomous Mobile Network Scanner https://scdn.rohde-schwarz.com/ur/pws/dl_downloads/dl_common_library/dl_brochures_and_datasheets/pdf_1/TSMA6_bro_en_5215-8241-12_v1200.pdf, [Last accessed 13 June 2023].

[33] Franci, D., Coltellacci, S., Grillo, E., Pavoncello, S., Aureli, T., Cintoli, R., & Migliore, M. D. (2020). An Experimental Investigation on the Impact of Duplexing and Beamforming Techniques in Field Measurements of 5G Signals. Electronics, 9(2), 223. https://doi.org/10.3390/electronics9020223.

[34] Liu, S., Onishi, T., Taki, M., Ikuyo, M., Tobita, K., Watanabe, S., & Suzuki, Y. (2021). E-Field Strength Measurements of a 5G Base Station in 28 GHz Band for EMF Exposure Assessment. https://doi.org/10.23919/usnc-ursi51813.2021.9703567.

[35] The Rohde & Schwarz signal and spectrum analyzer portfolio, https://www.rohde-schwarz.com/us/products/test-and-measurement/signal-and-spectrum-analyzers_63665.html, [Last accessed 15 March 2024].

[36] FieldFox Handheld RF and Microwave Analyzers, https://www.keysight.com/us/en/catalog/key-34752/fieldfox-handheld-rf-microwave-analyzers.html, [Last accessed 15 March 2024].

[37] Aaronia SPECTRAN V5 X, Datasheet, https://downloads.aaronia.com/datasheets/analyzers/V5/V5-X.pdf, [Last accessed 15 March 2024].
[38] Narda, Probe EFD-5091 Datasheet, https://www.narda-sts.com/en/wideband-emf/fieldman/1/pd/pdfs/23945/eID/. [Last accessed 13 June 2023].
[39] Narda, FieldMan Datasheet, https://www.narda-sts.com/en/wideband-emf/fieldman/1/pd/pdfs/23937/eID/, [Last accessed 13 June 2023].
[40] Narda, NBM E-Field Probe EF 0691, https://www.narda-sts.com/en/wideband-emf/nbm-550/nbme-field-6-ghz/, [Last accessed 13 June 2023].
[41] Rowley, J. T., & Joyner, K. H. (2016). Observations from national Italian fixed radiofrequency monitoring network. Bioelectromagnetics, 37(2), 136–139. https://doi.org/10.1002/bem.21958.
[42] Narda, NBM E-Fied Probe EF 9091, https://www.narda-sts.com/en/wideband-emf/nbm-550/nbme-field-90-mhz/, [Last accessed 13 June 2023].
[43] Mavromatis, F., Boursianis, A. D., Samaras, T., Koukourlis, C., & Sahalos, J. N. (2009). A Broadband Monitoring System for Electromagnetic-Radiation Assessment. IEEE Antennas and Propagation Magazine, 51(1), 71–79. https://doi.org/10.1109/map.2009.4939020.
[44] Mavromatis, F., Samaras, T., Koukourlis, C. and Sahalos, J. N., (2010). A portable broadband monitoring system for electromagnetic radiation assessment, Proceedings of the Fourth European Conference on Antennas and Propagation, Barcelona, Spain, pp. 1-5.
[45] Živković, Z., Senić, D., Šarolić, A., & Vučić, A., (2011). Design and testing of a diode-based electric field probe prototype, SoftCOM 2011, 19th International Conference on Software, Telecommunications and Computer Networks, Split, Croatia, pp. 1-5.
[46] Viani, F., Donelli, M., Oliveri, G., Massa, A., & Trinchero, D. (2011). A WSN-based system for real-time electromagnetic monitoring. In *HAL (Le Centre pour la Communication Scientifique Directe)*. Le Centre pour la Communication Scientifique Directe. https://doi.org/10.1109/aps.2011.5997195
[47] Leferink, F. (2013) "Fast, Broadband, and High-Dynamic Range 3-D Field Strength Probe," IEEE Transactions on Electromagnetic Compatibility, 55(6), pp. 1015–1021. Available at: https://doi.org/10.1109/temc.2013.2256360.
[48] Viani, F., Polo, A., Donelli, M., & Giarola, E. (2016). A Relocable and Resilient Distributed Measurement System for Electromagnetic Exposure Assessment. *IEEE Sensors Journal*, *16*(11), 4595–4604. https://doi.org/10.1109/jsen.2016.2536804.
[49] Pinel, P., Tajan, P., Poiré, Y. and Ourak, Y., (2020). Observatoire des Ondes, une réponse au débat sociétal, JS URSI France. Available online: https: //ursifr-2020.sciencesconf.org/305807/document. [Last accessed 13 June 2023].
[50] Ioriatti, L., Martinelli, M. O., Viani, F., Benedetti, M., & Massa, A. (2009). Real-time distributed monitoring of electromagnetic pollution in urban environments. In *HAL (Le Centre pour la Communication Scientifique Directe)*. Le Centre pour la Communication Scientifique Directe. https://doi.org/10.1109/igarss.2009.5417724.
[51] Narda Safety Test Solutions, AMB 8059/00 version mobile (Datasheet), Available online: https://www.narda-sts.com/en/wideband-emf/amb-8059/amb-amb-805900-car-mounting-kit/pd/pdfs/23225/eID/, [Last accessed 16 June 2023].
[52] WaveControl, MapEM – RF Electromagnetic Field Level Maps (Datasheet). Avalaible online: https://www.wavecontrol.com/rfsafety/images/data-sheets/en/MapEM_Datasheet_EN.pdf, [Last accessed 16 June 2023].
[53] Milutinov, M. et al. (2012) "Multiband sensors for wireless electromagnetic field monitoring system - SEMONT," Facta Universitatis. Series Electronics and Energetics, 25(2), pp. 137–150. Available at: https://doi.org/10.2298/fuee1202137m.
[54] Oliveira, C., Sebastião, D., & Carpinteiro, G. (2006). Uncertainty of Measurement of Radiofrequency Electromagnetic Fields – Measurement Equipments, monit project, Available online: https://faqtos.pt/wp-content/uploads/2021/02/Uncertainty-of-Measurement-of-Radiofrequency-Electromagnetic-Fields-Measurement-Equipments.pdf, [Last accessed 16 June 2023].
[55] Minucci, F., Verbruggen, D., Sallouah, H., Volski, V., Vandenbosch, G., Bovet, G., & Pollin, S. (2022). Measuring 5G Electric Fields Strength With Software Defined Radios. IEEE Open Journal of the Communications Society, 3, 2258–2271. https://doi.org/10.1109/OJCOMS.2022.3222537.
[56] Rivera, I., Beltran, S. F., & Martinez-Pinon, F. (2018b). Spectrum Analyzer by Software Defined Radio. https://doi.org/10.1109/icmeae.2018.00024.
[57] Deprez, K., Colussi, L., Korkmaz, E., Aerts, S., Land, D., Littel, S., Verloock, L., Plets, D., Joseph, W., & Bolte, J. (2023). Comparison of Low-Cost 5G Electromagnetic Field Sensors. *Sensors*, *23*(6), 3312. https://doi.org/10.3390/s23063312.

[58] Bechet, A. C., Helbet, R., Bouleanu, I., Sarbu, A., Miclaus, S., & Bechet, P. (2019). Low Cost Solution Based on Software Defined Radio for the RF Exposure Assessment: A Performance Analysis. https://doi.org/10.1109/atee.2019.8724739.

[59] Robert, H., Paul, B., Simona, M., & Annamaria, S. (2021). Real Time Broadband Electromagnetic Spectrum Monitoring System based on Software Defined Radio Technology. In 2021 9th International Conference on Modern Power Systems (MPS). https://doi.org/10.1109/mps52805.2021.9492577.

[60] Sârbu, A., Migliore, M. D., Şorecău, E., Şorecău, M., Miclăuş, S., & Bechet, P. (2022). SDR-Enabled Multichannel Real-Time Measurement System for In Situ EMF Exposure Evaluation. Electronics, 11(17), 2670. https://doi.org/10.3390/electronics11172670.

[61] Díez, L. M., Anwar, S. M., De Lope, L. R., Hennaff, M. L., Toutain, Y., & Agüero, R. (2014). Design and integration of a low-complexity dosimeter into the smart city for EMF assessment. *European Conference on Networks and Communications*. https://doi.org/10.1109/eucnc.2014.6882637.

[62] K. Deprez, S. Aerts, A. Thielens, G. Vermeeren, L. Martens, and W. Joseph, (2021), Design of a Low-Cost Modular 5G RF-EMF Exposure Sensor, *in Proceedings of the Joint Annual Meeting of the Bioelectromagnetics Society and the European BioElectromagnetics Association* (BioEM 2021), Ghent, Belgium, 26–30 September 2021; pp. 421–426.

[63] Korkmaz, E.; Littel, S.; Bolte, J. (2022). Development of a low-cost sensor network for measurement of 5G-signals in the Netherlands. In Proceedings of the 1st Annual Meeting of BioEM, Nagoya, Japan, 19–24 June 2022.

[64] Korkmaz, E.; Littel, S.; Spirito, M; Bolte, J. "A Low-cost EMF Field Sensor for 5G EMF Exposure Measurements". In Proceedings of BioEM 2023, Oxford, UK, 18–23 June 2023.

[65] Vanveerdeghem, P., Van Torre, P., Thielens, A., Knockaert, J., Joseph, W., & Rogier, H. (2015). Compact Personal Distributed Wearable Exposimeter. IEEE Sensors Journal, 15(8), 4393–4401. https://doi.org/10.1109/jsen.2015.2420583

[66] F. Minucci and D. Verbruggen. "Python SDR framework, public repository." Oct. 2021. [Online]. Available at: https://gitlab.kuleuven.be/ u0117142/python-sdr-framework.

[67] ADALM-PLUTO Hardware, https://wiki.analog.com/university/tools/pluto/hacking/hardware#schematics, [Last accessed 15 March 2024].

[68] Joseph, W. et al. (2016) "Drone based measurement system for radiofrequency exposure assessment," Bioelectromagnetics, 37(3), pp. 195–199. Available at: https://doi.org/10.1002/bem.21964.

[69] González, M.A.S. et al. (2021) "Compact Exposimeter Device for the Characterization and Recording of Electromagnetic Fields from 78 MHz to 6 GHz with Several Narrow Bands (300 kHz)," Sensors, 21(21), p. 7395. Available at: https://doi.org/10.3390/s21217395.

[70] Röösli, M., Frei, P., Bolte, J. H., Neubauer, G., Cardis, E., Feychting, M., Gajšek, P., Heinrich, S., Joseph, W., Mann, S., Martens, L., Mohler, E., Parslow, R. C., Poulsen, A. H., Radon, K., Schüz, J., Thuroczy, G., Viel, J., & Vrijheid, M. (2010). Conduct of a personal radiofrequency electromagnetic field measurement study: proposed study protocol. Environmental Health, 9(1). https://doi.org/10.1186/1476-069x-9-23.

[71] ExpoM – RF 4 Configurable, Available online: https://fieldsatwork.ch/uploads/Downloads/ExpomRF4/ExpomRF4%20Fact%20Sheet%20v1.4.pdf. [Last accessed 16 June 2023].

[72] EME Spy Evolution, Available online: https://www.mvg-world.com/media/1095/download/reference, [Last accessed 16 June 2023].

[73] ExpoM – RF 3, Available online: https://fieldsatwork.ch/products/expom-rf/. [Last accessed 16 June 2023].

[74] Celaya-Echarri, M., Azpilicueta, L., Karpowicz, J., Ramos, V., López-Iturri, P., & Falcone, F. (2020). From 2G to 5G spatial modeling of personal RF-EMF exposure within urban public trams. IEEE Access, 8, 100930–100947. https://doi.org/10.1109/access.2020.2997254

[75] Blas, J., Lago, F., Fernández, P., Lorenzo, R. M., & Abril, E. J. (2007). Potential exposure assessment errors associated with body-worn RF dosimeters. Bioelectromagnetics. https://doi.org/10.1002/bem.20355.

[76] Thielens, A. et al. (2016) "A Personal, Distributed Exposimeter: Procedure for Design, Calibration, Validation, and Application," Sensors, 16(2), p. 180. Available at: https://doi.org/10.3390/s16020180.

[77] Aminzadeh, R. et al. (2017) "Personal Exposimeter for Radiation Assessment in Real Environments in the 60-GHz Band," Radiation Protection Dosimetry, 176(3), pp. 316–321. Available at: https://doi.org/10.1093/rpd/ncx012.

[78] Aminzadeh, R. et al. (2018) "A Multi-Band Body-Worn Distributed Radio-Frequency Exposure Meter: Design, On-Body Calibration and Study of Body Morphology," Sensors, 18(1), p. 272. Available at: https://doi.org/10.3390/s18010272.

[79] Chahat, N., Zhadobov, M., Coq, L. L., Alekseev, S., & Sauleau, R. (2012). Characterization of the Interactions Between a 60-GHz Antenna and the Human Body in an Off-Body Scenario. IEEE Transactions on Antennas and Propagation, 60(12), 5958–5965. https://doi.org/10.1109/tap.2012.2211326.

[80] Diez, L., Agüero, R. and Muñoz, L.V.A. (2017) "Electromagnetic Field Assessment as a Smart City Service: The SmartSantander Use-Case," Sensors, 17(6), p. 1250. Available at: https://doi.org/10.3390/s17061250.

[81] Colombi, D. et al. (2022) "Implications of ICNIRP 2020 Exposure Guidelines on the RF EMF Compliance Boundary of Base Stations," Frontiers in Communications and Networks, 3. Available at: https://doi.org/10.3389/frcmn.2022.744528.

[82] PlutoSDR/M2k boot magic explained [Analog Devices Wiki]. Available at: https://wiki.analog.com/university/tools/pluto/devs/booting (Accessed: April 21, 2023).

[83] Joseph, W. et al. (2012) "Assessment of RF Exposures from Emerging Wireless Communication Technologies in Different Environments," Health Physics, 102(2), pp. 161–172. Available at: https://doi.org/10.1097/hp.0b013e31822f8e39.

[84] Kim, B., Yun, J.-H. and Park, S.-O. (2012) "Uncertainty Estimation for Evaluating Human Exposure Levels to RF Electromagnetic Fields from Cellular Base Stations," IEEE Transactions on Electromagnetic Compatibility, 54(2), pp. 246–253. Available at: https://doi.org/10.1109/temc.2012.2182768.

[85] Telecommunication Standardization Sector of ITU, K-61. (2018). Guidance on measurement and numerical prediction of electromagnetic fields for compliance with human exposure limits for telecommunication installations. Available at: https://www.itu.int/rec/T-REC-K.61.

[86] Selective Radiation Meter SRM-3006, Datasheet. https://www.narda-sts.com/en/selective-emf/srm-3006-field-strength-analyzer/srm-3006-3006101/pd/pdfs/23164/eID/, [Last accessed 16 June 2023].

[87] Jalilian, H. et al. (2019) "Public exposure to radiofrequency electromagnetic fields in everyday microenvironments: An updated systematic review for Europe," Environmental Research, 176, p. 108517. Available at: https://doi.org/10.1016/j.envres.2019.05.048.

[88] Thielens, A. et al. (2015) "Whole-Body Averaged Specific Absorption Rate Estimation Using a Personal, Distributed Exposimeter," IEEE Antennas and Wireless Propagation Letters, 14, pp. 1534–1537. Available at: https://doi.org/10.1109/lawp.2014.2368597.

[89] Bolte, J.H. et al. (2016) "Do car-mounted mobile measurements used for radio-frequency spectrum regulation have an application for exposure assessments in epidemiological studies?" Environment International, 86, pp. 75–83. Available at: https://doi.org/10.1016/j.envint.2015.09.024.

[90] Thielens, A. et al. (2014) "On-body calibration and processing for a combination of two radio-frequency personal exposimeters," Radiation Protection Dosimetry, 163(1), pp. 58–69. Available at: https://doi.org/10.1093/rpd/ncu056.

[91] Thielens, A. et al. (2013) "Personal distributed exposimeter for radio frequency exposure assessment in real environments," Bioelectromagnetics, p. n/a. Available at: https://doi.org/10.1002/bem.21793.

[92] Estenberg, J. and Augustsson, T. (2013) "Extensive frequency selective measurements of radiofrequency fields in outdoor environments performed with a novel mobile monitoring system," Bioelectromagnetics, 35(3), pp. 227–230. Available at: https://doi.org/10.1002/bem.21830.

[93] Wang, S., Mazloum, T. and Wiart, J. (2022) "Prediction of RF-EMF Exposure by Outdoor Drive Test Measurements," Telecom, 3(3), pp. 396–406. Available at: https://doi.org/10.3390/telecom3030021.

[94] Sagar, S., Adem, S. M., Struchen, B., Loughran, S. P., Brunjes, M. E., Arangua, L., Dalvie, M. A., Croft, R. J., Jerrett, M., Moskowitz, J. M., Kuo, T., & Röösli, M. (2018). Comparison of radiofrequency electromagnetic field exposure levels in different everyday microenvironments in an international context. Environment International, 114, 297–306. https://doi.org/10.1016/j.envint.2018.02.036.

[95] Onishi, T., Esaki, K., Tobita, K., Ikuyo, M., Taki, M., & Watanabe, S. (2023). Large-Area Monitoring of Radiofrequency Electromagnetic Field Exposure Levels from Mobile Phone Base Stations and Broadcast Transmission Towers by Car-Mounted Measurements around Tokyo. Electronics, 12(8), 1835. https://doi.org/10.3390/electronics12081835.

[96] Necz, P. P., Gyulai, B., Krausz, J., & Thuróczy, G. (2021). Broadband and band-selective measurements of radiofrequency EM field with drone system around 5G base station. In Book of Abstracts. https://doi.org/10.21175/rad.abstr.book.2021.28.12.necz

[97] García-Cobos, F. J., Paniagua, J. M., Gordillo-Guerrero, A., Marabel-Calderón, C., Rufo-Pérez, M., & Jiménez, A. (2023). Personal exposimeter coupled to a drone as a system for measuring environmental electromagnetic fields. Environmental Research, 216, 114483. https://doi.org/10.1016/j.envres.2022.114483.

[98] Gonzalez-Rubio, J., Jiménez-Díaz, L. and Beléndez, A. (2016) "Comprehensive personal RF-EMF exposure map and its potential use in epidemiological studies," Environmental Research, 149, pp. 105–112. Available at: https://doi.org/10.1016/j.envres.2016.05.010.
[99] ITU-T Recommendation K.113. "Generation of radio-frequency electromagnetic field level maps," Nov. 2015. Avalaible online: https://www.itu.int/rec/T-REC-K.113/_page.print, [Last accessed 16 June 2023].
[100] Diez, L. et al. (2015) Optimal dosimeter deployment into a smart city IoT platform for wideband EMF exposure assessment. Available at: https://doi.org/10.1109/eucnc.2015.7194131.
[101] Seyfi, L. (2013) "Measurement of electromagnetic radiation with respect to the hours and days of a week at 100kHz–3GHz frequency band in a Turkish dwelling," Measurement, 46(9), pp. 3002–3009. Available at: https://doi.org/10.1016/j.measurement.2013.06.021.
[102] Vermeeren, G. et al. (2013) "Spatial and temporal RF electromagnetic field exposure of children and adults in indoor micro environments in Belgium and Greece," Progress in Biophysics & Molecular Biology, 113(2), pp. 254–263. Available at: https://doi.org/10.1016/j.pbiomolbio.2013.07.002.
[103] Suka, D.S., Simic, M. and Pejovic, P. (2015) Aspects of remote monitoring and recording system of non-ionizing electromagnetic radiation. Available at: https://doi.org/10.1109/mipro.2015.7160330.
[104] Telecommunication Standardization Sector of ITU, K-83. (2022). Monitoring of electromagnetic field levels. Available at: https://www.itu.int/rec/T-REC-K.83/en.
[105] Keller, H. (2019) "On the Assessment of Human Exposure to Electromagnetic Fields Transmitted by 5G NR Base Stations," Health Physics, 117(5), pp. 541–545. Available at: https://doi.org/10.1097/hp.0000000000001089.
[106] Fellan, A. and Schotten, H.D. (2022) Overview of the Evaluation Methods for the Maximum EMF Exposure in 5G Networks. Available at: https://doi.org/10.1109/cscn57023.2022.10050915.
[107] Liu, S. et al. (2021) E-Field Strength Measurements of a 5G Base Station in 28 GHz Band for EMF Exposure Assessment. Available at: https://doi.org/10.23919/usnc-ursi51813.2021.9703567.
[108] Wood, M. et al. (2021) 50 surveys of 5G mmWave Small Cell EME Testing, AMTA EME Symposium - September 2021. Available at: https://www.telstra.com.au/content/dam/tcom/personal/consumer-advice/pdf/telstra-50-surveys-of-5g-mmwave-small-cells-20-sept-2021.pdf, [Last accessed 16 June 2023].
[109] Chiaraviglio, L. et al. (2022) "EMF Exposure in 5G Standalone mm-Wave Deployments: What Is the Impact of Downlink Traffic?" IEEE Open Journal of the Communications Society, 3, pp. 1445–1465. Available at: https://doi.org/10.1109/ojcoms.2022.3200423.
[110] Agentschap Telecom, Rapport Veldsterktemetingen aan installaties in de 26 GHz-band, 20 Nov 2019. Available at: https://www.antennebureau.nl/straling-engezondheid/documenten/rapporten/2019/november/19/veldsterktem etingen-aan-installaties-in-de-26-ghz-band, [Last accessed 16 June 2023]
[111] Wali, S.Q. et al. (2022) "RF-EMF Exposure Measurement for 5G Over Mm-Wave Base Station With MIMO Antenna," IEEE Access, 10, pp. 9048–9058. Available at: https://doi.org/10.1109/access.2022.3143805.
[112] Letertre, T., Monebhurrun, V. and Toffano, Z. (2013) "Accurate measurement of RF exposure from emerging wireless communication systems," IOP Conference Series [Preprint]. Available at: https://doi.org/10.1088/1757-899x/44/1/012015.
[113] Adda, S. et al. (2022) "How 5G NR Signals Impact on the Response of Broadband Electric Field Probes," IEEE Transactions on Instrumentation and Measurement, p. 1. Available at: https://doi.org/10.1109/tim.2022.3227979.
[114] Agence Nationale des Fréquences, Evaluation de l'exposition du public aux ondes électromagnétiques 5G - Volet 3 intermédiaire: premiers résultats de mesures sur les pilotes 5G dans la bande 26 GHz, June 2021, Available at : https://www.anfr.fr/fileadmin/mediatheque/documents/5G/20210702-Rapport-ANFR-resultats-mesures-pilotes-5G.pdf, [Last accessed 16 June 2023].
[115] OFFCOM, (2020). Electromagnetic Field (EMF) measurements near fixed wireless equipment operating in the 60 GHz band in Liverpool., Available at: https://www.ofcom.org.uk/__data/assets/pdf_file/0016/190006/60ghz-report.pdf, [Last accessed 16 June 2023].
[116] Selmaoui, B. et al. (2021) "Exposure of South Korean Population to 5G Mobile Phone Networks (3.4–3.8 GHz)," Bioelectromagnetics, 42(5), pp. 407–414. Available at: https://doi.org/10.1002/bem.22345.
[117] Thielens, A., Martens, L. and Joseph, W. (2017) "Can body-worn devices be used for measuring personal exposure to mm waves?" Bioelectromagnetics, 38(3), pp. 239–242. Available at: https://doi.org/10.1002/bem.22036.
[118] Vulević, B. and Osmokrovic, P. (2010) "Evaluation of uncertainty in the measurement of environmental electromagnetic fields," Radiation Protection Dosimetry, 141(2), pp. 173–177. Available at: https://doi.org/10.1093/rpd/ncq158.

[119] Vulevic, B., Kovacevic, D. and Osmokrovic, P. (2012). "Expressing the Measurement Uncertainty of the NonIonizing Radiation Survey in the Vicinity of GSM Base Stations." In Progress In Electromagnetics Research Symposium Proceedings, 1169–72. KL, Malaysia.
[120] Travassos, X. L., Grubsic, S., Porath, M. C., & Souza Filho, A. L. (2021). A case study on electromagnetic field assessment and uncertainty evaluation. Journal of Physics: Conference Series, 1826(1), 012081. https://doi.org/10.1088/1742-6596/1826/1/012081.
[121] 5G; NR; Base Station (BS) Conformance Testing; Part 1: Conducted Conformance Testing, document 3GPP TS 38.141-1, Version 16.6.0, Release 16, Revision 16.6.0, Jan. 2021. Available at: https://www.etsi.org/deliver/etsi_ts/138100_138199/13814101/16.06.00_60/ts_13814101v160600p.pdf
[122] Sarbu, A. et al. (2021) Isotropic near field measurement system for new generation communication signals: Preliminary design and USRP calibration. Available at: https://doi.org/10.1109/icate49685.2021.9465022.
[123] Trinchero, D. et al. (2009) "Field Probes Performance for the Measurement of Spread-Spectrum Radio Signals," IEEE Antennas and Wireless Propagation Letters, 8, pp. 494–497. Available at: https://doi.org/10.1109/lawp.2009.2020309.
[124] Aminzadeh, R. et al. (2016) "On-body calibration and measurements using personal radiofrequency exposimeters in indoor diffuse and specular environments," Bioelectromagnetics, 37(5), pp. 298–309. Available at: https://doi.org/10.1002/bem.21975.
[125] Bhatt, C.R. et al. (2016) "Assessment of personal exposure from radiofrequency-electromagnetic fields in Australia and Belgium using on-body calibrated exposimeters," Environmental Research, 151, pp. 547–563. Available at: https://doi.org/10.1016/j.envres.2016.08.022.
[126] Rivero, R.A.G. et al. (2023) "A Low-Cost Calibration Method for Temperature, Relative Humidity, and Carbon Dioxide Sensors Used in Air Quality Monitoring Systems," Atmosphere, 14(2), p. 191. Available at: https://doi.org/10.3390/atmos14020191.
[127] Van Wijk, A. Welcome to the Green Village; IOS Press: Delft, The Netherlands, 2021; pp. 1–60. https://doi.org/10.3233/978-1-61499-284-4-I.
[128] United Kingdom Accreditation Service (UKAS), M3003 – The expression of uncertainty and confidence in measurement, ed.2, Jan 2007. Available at: https://www.ukas.com/wp-content/uploads/schedule_uploads/759162/M3003-The-Expression-of-Uncertainty-and-Confidence-in-Measurement.pdf, [Last accessed 16 June 2023].
[129] Borsero, M. et al. (2001) "Calibration and Evaluation of Uncertainty in the Measurement of Environmental Electromagnetic Fields," Radiation Protection Dosimetry, 97(4), pp. 363–368. Available at: https://doi.org/10.1093/oxfordjournals.rpd.a006690.
[130] IEEE Std C95.3™-2021 "IEEE Recommended Practice for Measurements and Computations of Electric, Magnetic, and Electromagnetic Fields with Respect to Human Exposure to Such Fields, 0 Hz to 300 GHz" Mar. 2021.
[131] Bornkessel, C. et al. (2007) "Determination of the general public exposure around GSM and UMTS base stations," Radiation Protection Dosimetry, 124(1), pp. 40–47. Available at: https://doi.org/10.1093/rpd/ncm373.
[132] Hsiao, A.-Y. et al. (2017) Ray tracing simulations for millimetre wave propagation in 5G wireless communications. Available at: https://doi.org/10.1109/apusncursinrsm.2017.8072993.
[133] Hossain, F. et al. (2019) "An Efficient 3-D Ray Tracing Method: Prediction of Indoor Radio Propagation at 28 GHz in 5G Network," Electronics, 8(3), p. 286. Available at: https://doi.org/10.3390/electronics8030286.
[134] Kim, H.-S. and Brennan, C. (2019) "Efficient Pre-processed Ray Tracing for 5G Mobile Transmitter Scenarios in Urban Microcellular Environments," IEEE Transactions on Antennas and Propagation, 67(5), pp. 3323–3333. Available at: https://doi.org/10.1109/tap.2019.2896706.
[135] Migliore, M.D. et al. (2022) "Application of the Maximum Power Extrapolation Procedure for Human Exposure Assessment to 5G Millimetre Waves: Challenges and Possible Solutions," IEEE Access, 10, pp. 103438–103446. Available at: https://doi.org/10.1109/access.2022.3210196.
[136] Thors, B. et al. (2017) "Time-Averaged Realistic Maximum Power Levels for the Assessment of Radio Frequency Exposure for 5G Radio Base Stations Using Massive MIMO," IEEE Access, 5, pp. 19711–19719. Available at: https://doi.org/10.1109/access.2017.2753459.
[137] Migliore, M.D. and Schettino, F. (2020) "Power Reduction Estimation of 5G Active Antenna Systems for Human Exposure Assessment in Realistic Scenarios," IEEE Access, 8, pp. 220095–220107. Available at: https://doi.org/10.1109/access.2020.3042002.
[138] Schiavoni, A. et al. (2022) "Methodology for Electromagnetic Field Exposure Assessment of 5G Massive MIMO Antennas Accounting for Spatial Variability of Radiated Power," IEEE Access, 10, pp. 70572–70580. Available at: https://doi.org/10.1109/access.2022.3188269.

[139] Sezgin, A. and Gündüz, D. (2018) ITG-Fb. 276: WSA 2018: 22nd International ITG Workshop on Smart Antennas March 14-16, 2018, Bochum, Germany. ITG-Fachberichte.
[140] Pinchera, D., Migliore, M.D. and Schettino, F. (2020) "Compliance Boundaries of 5G Massive MIMO Radio Base Stations: A Statistical Approach," IEEE Access, 8, pp. 182787–182800. Available at: https://doi.org/10.1109/access.2020.3028471.
[141] Ares-Pena, F.J. et al. (2016) "Simple and effective monitoring of the electromagnetic field in the smart cities arena," Radio Science [Preprint]. Available at: https://doi.org/10.1002/2016rs006045.
[142] Aerts, S. et al. (2013) "Exposure assessment of mobile phone base station radiation in an outdoor environment using sequential surrogate modelling," Bioelectromagnetics, 34(4), pp. 300–311. Available at: https://doi.org/10.1002/bem.21764.
[143] Wang, S. and Wiart, J. (2020) "Sensor-Aided EMF Exposure Assessments in an Urban Environment Using Artificial Neural Networks," International Journal of Environmental Research and Public Health, 17(9), p. 3052. Available at: https://doi.org/10.3390/ijerph17093052.
[144] Xu, B. et al. (2022) "A Monte Carlo Analysis of Actual Maximum Exposure From a 5G Millimetre-Wave Base Station Antenna for EMF Compliance Assessments," Frontiers in Public Health, 9. Available at: https://doi.org/10.3389/fpubh.2021.777759.
[145] Reniers, A. et al. (2016) Review of the accuracy and precision of mm-wave antenna simulations and measurements. Available at: https://doi.org/10.1109/eucap.2016.7481973.
[146] Otin, R. (2013) "ERMES: A nodal-based finite element code for electromagnetic simulations in frequency domain," Computer Physics Communications, 184(11), pp. 2588–2595. Available at: https://doi.org/10.1016/j.cpc.2013.06.010.
[147] A. Sârbu, M. D. Migliore, E. Şorecău, M. Şorecău, S. Miclăuş, and P. Bechet, "SDR-Enabled Multichannel Real-Time Measurement System for In Situ EMF Exposure Evaluation," Electronics, vol. 11, no. 17, p. 2670, Aug. 2022, doi: 10.3390/electronics11172670.
[148] Maia SDR, An open-source FPGA-based SDR project focusing on the ADALM Pluto, Available at: https://maia-sdr.org/, Last accessed 15 March 2024].
[149] S. Shikhantsov et al., "Ray-Tracing-Based Numerical Assessment of the Spatiotemporal Duty Cycle of 5G Massive MIMO in an Outdoor Urban Environment," Applied Sciences, vol. 10, no. 21, p. 7631, Oct. 2020, doi: 10.3390/app10217631.
[150] S. Aerts et al., "In Situ Assessment of 5G NR Massive MIMO Base Station Exposure in a Commercial Network in Bern, Switzerland," Applied Sciences, vol. 11, no. 8, p. 3592, Jan. 2021, doi: 10.3390/app11083592.
[151] R. Romero-Andrade, M. E. Trejo-Soto, J. R. Vázquez-Ontiveros, D. Hernández-Andrade, and J. L. Cabanillas-Zavala, "Sampling Rate Impact on Precise Point Positioning with a Low-Cost GNSS Receiver," Applied Sciences, vol. 11, no. 16, Art. no. 16, Jan. 2021, doi: 10.3390/app11167669.
[152] Accuracy of GNSS data, Available at: https://wiki.openstreetmap.org/wiki/Accuracy_of_GNSS_data, Last accessed 15 March 2024].
[153] T. Le, K. Mayaram, and T. Fiez, "Efficient Far-Field Radio Frequency Energy Harvesting for Passively Powered Sensor Networks," IEEE Journal of Solid-State Circuits, vol. 43, no. 5, pp. 1287–1302, May 2008, doi:10.1109/JSSC.2008.920318.
[154] L.-G. Tran, H.-K. Cha, and W.-T. Park, "RF power harvesting: a review on designing methodologies and applications," Micro and Nano Syst Lett, vol. 5, no. 1, p. 14, Dec. 2017, doi:10.1186/s40486-017-0051-0.
[155] K. Li, Q. He, J. Wang, Z. Zhou, and X. Li, "Wearable energy harvesters generating electricity from low-frequency human limb movement," Microsyst Nanoeng, vol. 4, no. 1, p. 24, Sep. 2018, doi:10.1038/s41378-018-0024-3.
[156] H. Lee and J.-S. Roh, "Charging device for wearable electromagnetic energy-harvesting textiles," Fash Text, vol. 8, no. 1, p. 5, Jan. 2021, doi:10.1186/s40691-020-00233-6.
[157] E. A. Evangelakos, D. Kandris, D. Rountos, G. Tselikis, and E. Anastasiadis, "Energy Sustainability in Wireless Sensor Networks: An Analytical Survey," JLPEA, vol. 12, no. 4, p. 65, Dec. 2022, doi:10.3390/jlpea12040065.
[158] HEXA-X, 2023. Deliverable D1.4 Hexa-X architecture for B5G/6G networks – final release, Available at: https://hexa-x.eu/wp-content/uploads/2023/07/Hexa-X-D1.4-Final.pdf, Last accessed 15 March 2024].
[159] Mazloum, T., Bories, S., Dassonville, D., & Wiart, J. (2023). Impact of Sampling Frequency on the Performance of DEVIN: A personal EM UL Exposimeter. 2023 XXXVth General Assembly and Scientific Symposium of the International Union of Radio Science (URSI GASS), 1–4. https://doi.org/10.23919/URSIGASS57860.2023.10265631.
[160] Van Bladel, H., Deprez, K., Stroobandt, B., Goegebeur, S., Aerts, S., Verloock, L., Velghe, M., Joseph, W. (2023). Design, Calibration and Validation of a Low-Cost Broadband Add-On RF-EMF Exposure Sensor

for Legacy and 5G NR Technologies. The 2nd Annual Conference of BioEM (BioEM2023), June 2023, Oxford, UK.
[161] Greek atomic energy commission, Electromagnetic field measurements, https://eeae.gr/en/
[162] Djuric, Nikola, et al. "The Wideband Approach of 5G EMF Monitoring." Towards new e-Infrastructure and e-Services for Developing Countries: 12th EAI International Conference, AFRICOMM 2020, Ebène City, Mauritius, December 2-4, 2020, Proceedings 12. Springer International Publishing, 2021.
[163] The EMF observatory. https://www.observatoiredesondes.com/en/the-emf-observatory-cities/brussels-electromagnetic-fields-exposure/, [Last accessed 25 March 2024].
[164] V. A. Siris, E. Z. Tragos, and N. E. Petroulakis: Experiences with a Metropolitan Multi-Radio Wireless Mesh Network : Design, Performance, and Application, in the IEEE Communications Magazine, July 2012.
[165] Continuous recording of EMF radiation levels in Greece https://pedion24.gr/index.php/map/, https://paratiritirioemf.eeae.gr/index.php/en/measurements/map, [Last accessed 16 March 2024].
[166] Migliore, M.D. (2023) 'Classical and quantum processing in the deep physical layer,' IEEE Access, p. 1. https://doi.org/10.1109/access.2023.3280452.
[167] M. Särestöniemi, M. Hämäläinen and J. Iinatti, "An Overview of the Electromagnetic Simulation-Based Channel Modeling Techniques for Wireless Body Area Network Applications," in IEEE Access, vol. 5, pp. 10622-10632, 2017, doi: 10.1109/ACCESS.2017.2708161.
[168] Cho-Kuen Ng, Mark Beall, Lixin Ge, Sanghoek Kim, Ottmar Klaas, Ada Poon, Electromagnetic Modeling of Human Body Using High Performance Computing, Physics Procedia, Volume 90, 2017, Pages 107-114, ISSN 1875-3892, https://doi.org/10.1016/j.phpro.2017.09.033.
[169] Tolulope T. Oladimeji, Pradeep Kumar, Nicholas O. Oyie, Propagation path loss prediction modelling in enclosed environments for 5G networks: A review, Heliyon, Volume 8, Issue 11, 2022, e11581, ISSN 2405-8440, https://doi.org/10.1016/j.heliyon.2022.e11581.
[170] W. -J. Hsu, T. Spyropoulos, K. Psounis and A. Helmy, "Modeling Spatial and Temporal Dependencies of User Mobility in Wireless Mobile Networks," in IEEE/ACM Transactions on Networking, vol. 17, no. 5, pp. 1564-1577, Oct. 2009, doi: 10.1109/TNET.2008.2011128.